Sensitivity Study for the Simulation of Heavy Rainfall events during monsoon season over Bangladesh using high resolution WRF-ARW model

M. Sc. Thesis

BY

SUMI UMME HANEY

DEPARTMENT OF PHYSICS

KHULNA UNIVERSITY OF ENGINEERING & TECHNOLOGY

KHULNA-9203, BANGLADESH

February 2017

Sensitivity Study for the Simulation of Heavy Rainfall events during monsoon season over Bangladesh using high resolution WRF-ARW model

M. Sc. Thesis

BY

SUMI UMME HANEY

ROLL NO: 1555555

SESSION: JULY-2015

A thesis submitted in partial fulfillment of the requirements for the degree of Master of Science in the Department of Physics, Khulna University of Engineering & Technology, Khulna-9203.

DEPARTMENT OF PHYSICS

KHULNA UNIVERSITY OF ENGINEERING & TECHNOLOGY

KHULNA-9203, BANGLADESH

February 2017

DECLARATION

This is to certify that the thesis work entitled "***Sensitivity Study for the Simulation of Heavy Rainfall events during monsoon season over Bangladesh using high resolution WRF-ARW model***" has been carried out by SUMI UMME HANEY in the Department of Physics, Khulna University of Engineering & Technology, Khulna, Bangladesh. The above thesis work or any part of this work has not been submitted anywhere for the award of any degree or diploma.

Signature of Supervisor — Signature of Candidate

(Professor Dr. Md. Mahbub Alam) — SUMI UMME HANEY

DEDICATED TO
MY PARENTS

Acknowledgements

With my great manner it is a pleasure for me to express my deepest sense of gratitude and indebtedness to my reverend supervisor Dr. Md. Mahbub Alam, Professor, Department of Physics, Khulna University of Engineering & Technology, Khulna, for his kind guidance and supervision and for his constant encouragement throughout the research work. His inspiration and friendly cooperation has accelerated my works.

I am indebted to Professor Dr. Shibendra Shekher Sikder, Head, Department of Physics, Khulna University of Engineering & Technology for his strong support in various ways during the entire period of my study in this department. I express my heartfelt gratitude and thanks to Professor Dr. Md. Abdullah Elias Akhter and Professor Dr. Jolly Sultana Department of Physics, Khulna University of Engineering & Technology for their inspiration and advices from the beginning of my study. I gratefully acknowledge Mr. Md. Kamrul Hasan Reza, Mr. Sujit Kumar Shil, Md. Alamgir Hossain, Assistant Professors and Mr. Sumon Halder, Sumon Deb Nath, Lecturer, Department of Physics, KUET for their cooperation regarding writing of the thesis.

My personal thankful greetings are to my good friends and well wishers for their help and cooperation. There are numerous people who could not be mentioned individually but their interesting discussions have prompted much thought on various aspects, I would also like to thank them. I would like to express my heartfelt thanks to my parents, husband, sisters and nearest relatives for their inspiration, encouragement and multifaceted supports to carry out this thesis work.

I am grateful to the KUET authority for approval of the project in the 33rd meeting of CASR, Agenda No. 33/5/10 and providing me the relevant facilities to complete this research work. The Author is grateful to National Centre for Atmospheric Research (NCAR), USA for making the WRF (WRF-ARW) model available to modeling community. The Grid Analysis and Display System software (GrADS) was used for analytical purposes and displaying Figs. Bangladesh Meteorological Department (BMD) is acknowledged for providing necessary data over Bangladesh. I am also grateful to the University Grants Commission (UGC) for financial support under the research project “Sensitivity Study for the Simulation of Heavy Rainfall events during monsoon season over Bangladesh using high resolution WRF-ARW model”.

Finally, I want to express my gratitude to almighty Creator for his mercy.

Sumi Umme Haney

CONTENTS

List of Figures

List of Tables

Acronym

ARW	:	Advanced Research WRF
AFWA	:	Air Force Weather Agency
BMD	:	Bangladesh Meteorological Department
CAM	:	Community Atmosphere Model
CGMR	:	Cloud graupel Mixing ratio
CIMR	:	Cloud Ice Mixing Ratio
CP	:	Cumulus Parameterization
CSMR	:	Cloud Snow Mixing Ratio
CWMR	:	Cloud Water Mixing Ratio
FE	:	Ferrier scheme
FNL	:	Final Reanalysis
GrADS	:	Grid Analysis and Display System
KF	:	Kain-Fritch
KS	:	Kessler
LBC	:	Lateral boundary conditions
MDM	:	Morrison double-moment
MYDM	:	Milbrandt-Yau Double-Moment 7-class
MP	:	Microphysics
NCAR	:	National Center for Atmospheric Research
NCEP	:	National Centre for Environment Prediction
NWP	:	Numerical weather prediction
PBL	:	Planetary Boundary Layer
RWMR	:	Rain Water Mixing Ratio
RH	:	Relative Humidity
SBU	:	Stony Brook University
TH	:	Thomson
WDM6	:	WRF Double-moment 6-class
WRF	:	Weather Research and Forecasting
WSM3	:	WRF Single-Moment 3-class scheme
WSM6	:	WRF Single-moment 6-class
WVMR	:	Water Vapor Mixing Ratio
YSU	:	Yonsei University Scheme
UTC	:	Universal Time Co-ordinate
NE	:	Northeastern
NW	:	Northwestern
SE	:	Southeastern
SW	:	Southwestern
N-NE	:	North-Northeastern
N-NW	:	North-Northwestern
S-SE	:	South-Southeastern
S-SW	:	South-Southwestern

ABSTRACT

In the present study, the Advanced Research WRF (ARW) v3.5.1 model have been used to simulate the heavy rainfall events in the southeastern region of Bangladesh during 23-26 June 2015, 23-26 July 2015 and 30 August – 1 September 2015. The initial and boundary conditions are drawn from the global operational analysis and forecast products of National Center for Environmental Prediction (NCEP-FNL) available at $1^o \times 1^o$ resolution. The model was configured in single domain, 6 km horizontal grid spacing with 161×183 grids in the east-west and north-south directions and 30 vertical levels. Time step of integration is set to 30 seconds for maintaining computational stability as the model uses third-order Runge-Kutta time integration scheme. For the sensitivity study of heavy rainfall events, different 12 microphysics (MP) schemes coupled with Kain-Fritsch cumulus parameterization scheme were used. The microphysics schemes are Kessler, Lin *et al*., WSM3, Ferrier, WSM6, Thomson graupel, MYDM, MDM, CAM V5.12-Moment 5 class, SBU, WDM6 and NSSL2 schemes. The amount of rainfall observed at Cox's Bazar, Teknaf, Kutubdia, Barisal, Chittagong and Sitakunda stations are 1039, 607, 602, 457, 424 and 400 mm respectively during 23-26 June 2015, at Chittagong, Kutubdia, Teknaf, Sandwip and Cox's Bazar stations are 867, 740, 690, 535 and 518 mm respectively during 23-26 July 2015 and at Sylhet, Teknaf, Chittagong, Hatiya and Sitakunda are 396, 330, 213, 200 and 198 mm respectively during 30 August to 1 September 2015. All Bangladesh station averaged rainfall suggests that among 12 MPs, TH, SBU, WSM6 and WDM6 during 23-26 June, MDM, Lin, SBU, KS and TH schemes during 23-26 July and WSM3, WDM6, CAM, MDM and MYDM schemes during 30 August to 1 September have simulated almost similar amount of rainfall as observed during the study period of 2015. The model has also simulated similar amounts of rainfall in the heavy rainfall area of 5 stations in the SE region by SBU, WDM6, Lin, TH and WSM6 schemes on 23-26 June, KS, Lin, WDM6, MDM and SBU schemes on 23-26 July and CAM, NSSL-2, MYDM and WSM3 schemes during 30 August to 1 September 2015. The maximum updraft has been identified for different MP schemes every day during 23-26 June, 23-26 July and 30 August to 1 September 2015 when heavy rainfall is observed in the SE region of Bangladesh. The maximum updraft is found as high as 20 ms^{-1} in the upper troposphere by using Lin *et al.,* WSM3, MYDM, MDM and WDM6 schemes at around 600-200, 400-100 and 600-200 hPa for the heavy rainfall events of 23-26 June, 23-26 July and 30 August to 1 September 2015 respectively.

Chapter I

Introduction

Bangladesh is a country having an area of about 147,570 sq. km situated in the northeastern part of South Asia within 88.02–92.68^{o}E and 20.57–26.63^{o}N. The land of Bangladesh is very flat: Elevation is about 1–37 m above sea level except small portions in the southeast (elevation about 200 m) which has border with Myanmar and in the northeast (elevation about 100 m) which has border with Shilling hill of India. The major source of water available either for agriculture or for human consumption is obtained from the rain that falls on the earth's surface. Rainfall in our country varies greatly in space and time. Maximum rainfall occurs in the monsoon period extending from the month of June to September (BMD, 2000). Due to high temperature of summer, the moisture - laden southwest monsoon flows over the vast expanse of the Bay of Bengal. By June this monsoon winds move all over Bangladesh and precipitation occurs heavily. The crucial months for agriculture are July and August and the fate of rained. Kharif crop largely depends upon the amount and distribution of rain especially during these two months (Bashar, 1987).

Prediction of heavy rainfall is one of the many challenging problems in meteorology, but very important for issuing timely warnings for the agencies engaged in disaster preparedness and mitigation. Widespread floods associated with heavy precipitation are common in the northeastern, southern and southeastern region of Bangladesh during monsoon season (June-September). Precipitating weather systems in combination with strong wind, hail and flooding have impact and influence on the broad range of activities. The strong moisture-laden winds from the Bay of Bengal interact with the topography, causing heavy precipitation over this region. Therefore, heavy precipitation, its timing, location and intensity, is certainly a key parameter in weather prediction and has significance on operational hydrology. Rainfall is highly variable in space and time and is strongly influenced by orographic forcing.

The Advanced Research Weather Research and Forecasting model (ARW-WRF) is the new-generation model for both weather research and forecasting (Skamarock *et al*., 2008), and is widely used for regional climate research (Leung *et al.,* 2006; Bukovsky and Karoly, 2009; Awan *et al*., 2011). Alam (2013) studied the effects of microphysics and cumulus parameterization for the prediction of heavy rainfall in post monsoon season. The study showed large variations among the different microphysical schemes. The microphysical schemes have a major impact on time and location of rainfall intensity

Cumulus parameterization (CP) schemes must estimate the rate of sub grid-scale convective precipitation, release of latent heat, and the distribution of heat, moisture, and momentum in the vertical due to convection (Kain and Fritsch, 1993). Cumulus convection modifies the large-scale temperature and moisture fields through detrainment and cumulus-induced subsidence in the environment. The detrainment causes large-scale cooling and moistening, and the cumulus-induced subsidence causes large-scale warming and drying (Arakawa and Schubert, 1974).

Bhowmik and Durai (2008) conducted research on multi-model ensemble forecasting of rainfall over Indian monsoon region. Khaladkar *et al*., (2007) studied the performance of NCMRWF Models in predicting high rainfall spells during SW-Monsoon Season. They showed that, in general, all the models predicted good rainfall activity along the west coast of India, which is consistent with the observations. Das *et al.* (2008) studied skills of different mesoscale models over Indian region during monsoon season. They made a recommendation that the WRF is able to produce best all India rainfall prediction in the day-1 forecast and, the MM5 is able to produce best all India rainfall forecasts in day-3, but ETA and RSM are able to depict the best distribution of rainfall maxima along the west coast of India. Bhanu *et al*. (2012) conducted research on simulation of heavy rainfall events during retreat phase of summer monsoon season over parts of Andhra Pradesh. They noticed that, circulation features and rainfall quantities are validated with observed rainfall of IMD and satellite derived datasets of KALPANA-1. Vitart and Molteni (2009) studied Dynamical Extended Range Prediction of early monsoon rainfall over India. They suggest that the high resolution extended range forecasts could be useful for the prediction a few weeks in advance of sub seasonal events, like the onset of the monsoon. Ranadhur *et al*. (2009) conducted research on Impacts of Satellite-Observed winds and total precipitable water on WRF Short-Range forecasts over the Indian region during the 2006 summer monsoon.

Heavy rainfall is often produced by long-lived mesoscale convective systems (MCSs) or intense mesoscale systems embedded in the mei-yu frontal cloud band (Kuo and Chen 1990; Zhang et al., 2003; Li and Chen, 1998). The presence of a southerly or southwesterly low level jet (Chen and Yu 1988) to the south side of the mei-yu front significantly helps the development of these heavy rain bearing systems (Chen et al. 2005), by providing warm and moist tropical air and strong uplifting mechanisms (Chen and Li 1995). Chowdhury (2003) investigated the relationship between the IAV of rainfall over Bangladesh and ENSO for about 40 years (1960s to 1990s). He found that although the summer monsoon rainfall in

Bangladesh showed a decreasing (increasing) tendency during strong El Ni˜no (La Ni˜na) years, the quantitative correspondence between the strength of ENSO and the summer rainfall anomaly over Bangladesh was very weak. Schumacher and Johnson (2005) investigated the structure and evolution of extreme rain events using composite radar reflectivity data, and observed two MCS organization patterns occurring frequently in the United States. Gadgil et al. (2005) expressed concerns about the ability of currently available dynamical systems to produce effective predictions of the monsoon rainfall. Every year in May–June, heavy rainfall events and associated deadly flash floods frequently cause severe property damage in South China and Taiwan. During this season, a quasi-stationary subtropical front, called the mei-yu front, occurs frequently and repeatedly (Ding, 1992).

Land in South Asia possesses complex topographical features. The interactions between the prevailing flow and the geographical features of South Asia give rise to a high rainfall area near the coastal and inland mountains. Recent satellite observations, such as those by the Tropical Rainfall Measuring Mission (TRMM)-Precipitation Radar (PR), reveal that the mean distribution of the summer monsoon rainfall is strongly influenced by the terrain distribution (e.g., Hirose et al., 2008; Romatschke and Houze, 2011; Biasutti *et al*., 2012). Narrow mountain ranges (e.g., Arakan Mountains and Meghalaya Plateau) are important in anchoring high rainfall on the windward side. The monsoon rainfall plays an important role in forming and maintaining strong monsoon circulation through the release of latent heating due to condensation (e.g., Hoskins and Rodwell, 1995; Ose, 1998; Xie *et al*., 2006).

Khaladkar *et al*., (2007) studied the performance of NCMRWF Models in predicting high rainfall spells during SW-Monsoon Season. They showed that, in general, all the models predicted good rainfall activity along the west coast of India, which is consistent with the observations. Das *et al.,* (2012) studied simulation of seasonal monsoon rainfall over the SAARC Region by dynamical downscaling using WRF Model. Their findings suggest the large scale seasonal distributions of rainfall observed by different sources are simulated fairly well by the model. Bangladesh is one of the countries of the world most vulnerable to climate change due to its least capacity to address the devastating impacts. According to the IPCC report (IPCC 2007), Bangladesh will experience 5% to 6% increase of rainfall by 2030. Small changes in the mean and standard deviation values can produce relatively large changes in the probability of extreme events (Groisman *et al*., 1999; Rodrigo, 2002; Chiew, 2006; Su *et al*., 2006).

As the primary impacts of climate change on society results from extreme events (Rodrigo, 2002), it might have severe negative consequences for Bangladesh. Significant increasing trend in extreme precipitation has been observed in last decades in the North America, Europe, Australia, Japan, and other areas (Karl and Knight, 1998; Suppiah and Hennessy, 1998; Iwashima *et al.,* 2002; Alexander et al. 2006). Kim and Lee (2006) investigated the characteristics of MCSs accompanying heavy rainfall using a single data of Weather Surveillance Radar-1998 Doppler (WSR- 88D). They demonstrated that low-level vertical wind shear plays an important role in the development of quasi-stationary and multicell storms, and that convective systems merge and stagnate due to blocking by mountain ranges in Korea. Routray *et al*., (2010) studied simulation of heavy rainfall events over Indian monsoon region using WRF-3DVAR data assimilation system. Results from the control experiments also highlight that weather and regional climate model simulations with coarse analysis have high uncertainty in simulating heavy rain events over the Indian monsoon region and assimilation approaches, such as the 3DVAR can help reduce this uncertainty. Xukai and Fumin (2015) conducted research on Changes in regional heavy rainfall events in China during 1961–2012. Some stations showed significant increasing trends in the southern part of the middle and lower reaches of the Yangtze River and the northern part of South China, while parts of North China, regions between Guangxi and Guangdong, and northern Sichuan showed decreasing trends in the accumulated intensity of regional heavy rainfall events RHREs.

Only few researches have been carried out so far to study the rainfall related extreme weather events in Bangladesh. Karmakar and Khatun (1995) and Ahmed (1989) studied the probabilistic estimates of rainfall extremes in Bangladesh during the pre-monsoon season. There studies were concentrated only on maximum rainfall events for a limited time period. The skill of the European Centre for Medium-Range Weather Forecasts (ECMWF) seasonal forecasting System3 (Anderson *et al*., 2007) has been predict the monsoon rainfall. They found that this dynamical seasonal forecasting system displays some skill in predicting the monthly-mean precipitation over India after July, but has surprisingly low skill to predict the June precipitation over India. The area around Bangladesh, where a tremendous amount of rainfall occurs in summer, predominantly exhibits sub-monthly-scale intra seasonal oscillation (ISO) but not 30–60-day ISO (Ohsawa *et al*., 2000; Murata *et al*., 2008; Fujinami *et al*., 2011). The ISO feature allows the sub-monthly-scale ISO to modulate the total seasonal rainfall and the spatial patterns of circulation and convection around Bangladesh.

In the present study, the Weather Research and Forecast (WRF-ARW V3.5.1) model has been used to simulate the different heavy rainfall events (23-26 June, 23-26 July and 30August-01 September 2015) in the monsoon (June – September) season over Bangladesh. The objectives of this study are to examine whether the high resolution WRF model is capable of simulating the observed features of heavy rainfall events. Different 12 MP schemes are considered to study these rainfall events and identify the performance of the MP schemes. The results have been compared with the observed station rainfall of Bangladesh Meteorological Department (BMD) and TRMM derived rainfall. Maximum vertical velocity has also been calculated from the model output, which indicates the maximum convection. Along the line of maximum vertical velocity reflectivity, relative humidity, vorticity, Cloud Water Mixing Ratio, Rain Water Mixing ratio, Cloud Ice mixing Ratio, Water Vapor Mixing Ratio, Cloud Gropel Mixing Ratio and Cloud snow Mixing Ratio in association with the heavy rainfall events have also been calculated and analyzed.

Chapter II

Review of Literatures

2.1. Rainfall

Rain is a type of precipitation, a product of the condensation of atmospheric water vapour that is deposited on the Earth's surface. It forms when separate drops of water fall to the Earth from clouds. Not all rain reaches the surface; some evaporates while falling through dry air. When none of it reaches the ground, it is called virga, a phenomenon often seen in hot, dry desert regions.

Rain plays a role in the hydrologic cycle in which moisture from the oceans evaporates, condenses into drops, precipitates from the sky, and eventually returns to the ocean via rivers and streams to repeat the cycle again. The water vapour from plant respiration also contributes to the moisture in the atmosphere. A major scientific explanation of how rain forms and falls is called the Bergeron process. More recent research points to the influence of Cloud condensation nuclei released as the result of biological processes.

Rainfall is typically measured using a rain gauge. It is expressed as the depth of water that collects on a flat surface, and is routinely measured with accuracy up to 0.1 mm. Rain gauges are usually placed at a uniform height above the ground, which may vary depending on the country.

Precipitation, especially rain, has a dramatic effect on agriculture. All plants need at least some water to survive; therefore rain (being the most effective means of watering) is important to agriculture. Plants need varying amounts of rainfall to survive. Agriculture of all nations at least to some extent is dependent on rain. Bangladesh's agriculture, for example, is heavily dependent on the rainfall, especially crops like rice, oilseeds and coarse grains. A delay of a few days in the arrival of the monsoon can, and does, badly affect the economy, as evidenced in the numerous droughts in Bangladesh and India. When classified according to amount of precipitation, rain can be divided into (http://my.athenet.net):

	Types		Rate (mm/hour)
i.	very light rain	when the precipitation rate is	< 0.25
ii.	light rain	when the precipitation rate is between	0.25 - 1

iii.	moderate rain	when the precipitation rate is between	1-4
iv.	heavy rain	when the precipitation rate is between	4-16
v.	very heavy rain	when the precipitation rate is between	16-50
vi.	extreme rain	when the precipitation rate is	> 50

2.2 Hydrometeors

Any product of condensation or sublimation of atmospheric vapor, whether formed in free atmosphere or at the earth's surface; also any water particles blown by the wind from the earth's surface is called hydrometeor. Hydrometeors consist of liquid or solid water particles that are either falling through or suspended in the atmosphere, blown from the surface by wind, or deposited on objects. Hydrometeors comprise all forms of precipitation, such as rain, drizzle, snow, and hail, and such elements as clouds, fog, blowing snow, dew, frost, tornadoes and waterspouts. A general term for atmospheric water in any of its forms, i.e. clouds, fog, hail, ice crystals, rain are known as hydrometeors. Any form of atmospheric water vapor, including those blown by the wind off the earth's surface also known as hydrometeors. Liquid or solid water formation that is suspended in the air includes clouds, fog, ice fog, and mist. Drizzle and rain are examples of liquid precipitation, while freezing drizzle and freezing rain are examples of freezing precipitation. Solid or frozen precipitation includes ice pellets, hail, snow, snow pellets, snow grains, and ice crystals. Water vapor that evaporates before reaching the ground is virga. Examples of liquid or solid water particles that are lifted off the earth's surface by the wind include drifting and blowing snow and blowing spray. Dew, frost, rime and glaze are examples of liquid or solid water deposits on exposed objects. A precipitation product, such as rain, snow, fog, or clouds, formed from the condensation of water vapor in the atmosphere is called hydrometeor. The typical configuration of a cloud microphysics parameterization includes three classes of hydrometeors: the source class (e.g., water vapor and cloud condensation nuclei), the cloud class (e.g., cloud water and cloud ice), and the precipitation class (e.g., rain, snow, graupel). The total budget of phase changes among hydrometeors in these three classes determines the heating rate, which feeds back to dynamical processes.

The generation of source-class materials is related to the hydrological and vegetation evaporative conditions of the atmosphere. These source-class materials are then redistributed by the large--scale dynamical processes (e.g., atmospheric transport and convergence/ divergence associated with a weather system). In state-of-the-art microphysics modeling’s,

the distributions of atmospheric aerosols and cloud condensation nuclei are not simulated (at least in a numerical weather forecast model) but are assumed to be abundant in the atmosphere and to have a uniform distribution. Water vapor is explicitly modeled and serves as the sole and deterministic source materials for the ensuing microphysical processes to occur. Whenever water vapor exceeds its saturation values (with respect to water or ice), condensation or deposition occurs.

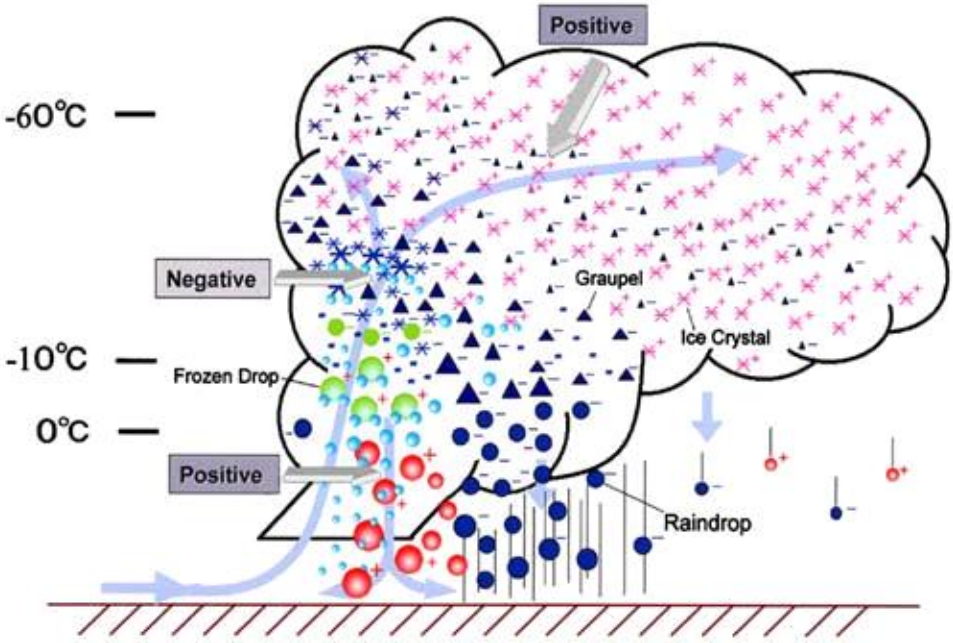

Fig. 2.1: Conceptual model of hydrometeor growth and space charge. Red circles are for raindrops originating on frozen drops. Blue circles are for raindrops, originating on graupel. Green circles are frozen drops, blue triangles are graupel, and red crosses are ice crystals. A two-step growth process is suggested by warm rain-frozen in front and graupel growth in the upper level.

Cloud water and cloud ice are the basic substances that form the cloud class, i.e., definable clouds (both in visual and physical definitions). They are the intermediate class linking the source and precipitation classes. Under a sub-saturation condition, these cloud-class materials can convert back to water vapor by evaporation or sublimation. Otherwise, they either remain in their forms as water droplets or small ice particles (for non precipitating clouds) or continuously grow and transform into the precipitation class through various growth mechanisms (for precipitating clouds) in a saturated or slightly supersaturated environment.

The precipitation fields (e.g., rain, snow, and graupel) form the final class in microphysical parameterization schemes. Either they fall out from clouds to complete the hydrological

cycle, or parts of them evaporate or sublimate to convert back to the source class during their fallout. Obviously, incorrectly parameterizing and computing the production rates of this class directly affect the accuracy of precipitation forecasts. The total budget of phase changes among hydrometeors in these three classes determines the heating rate which feeds back to dynamical processes.

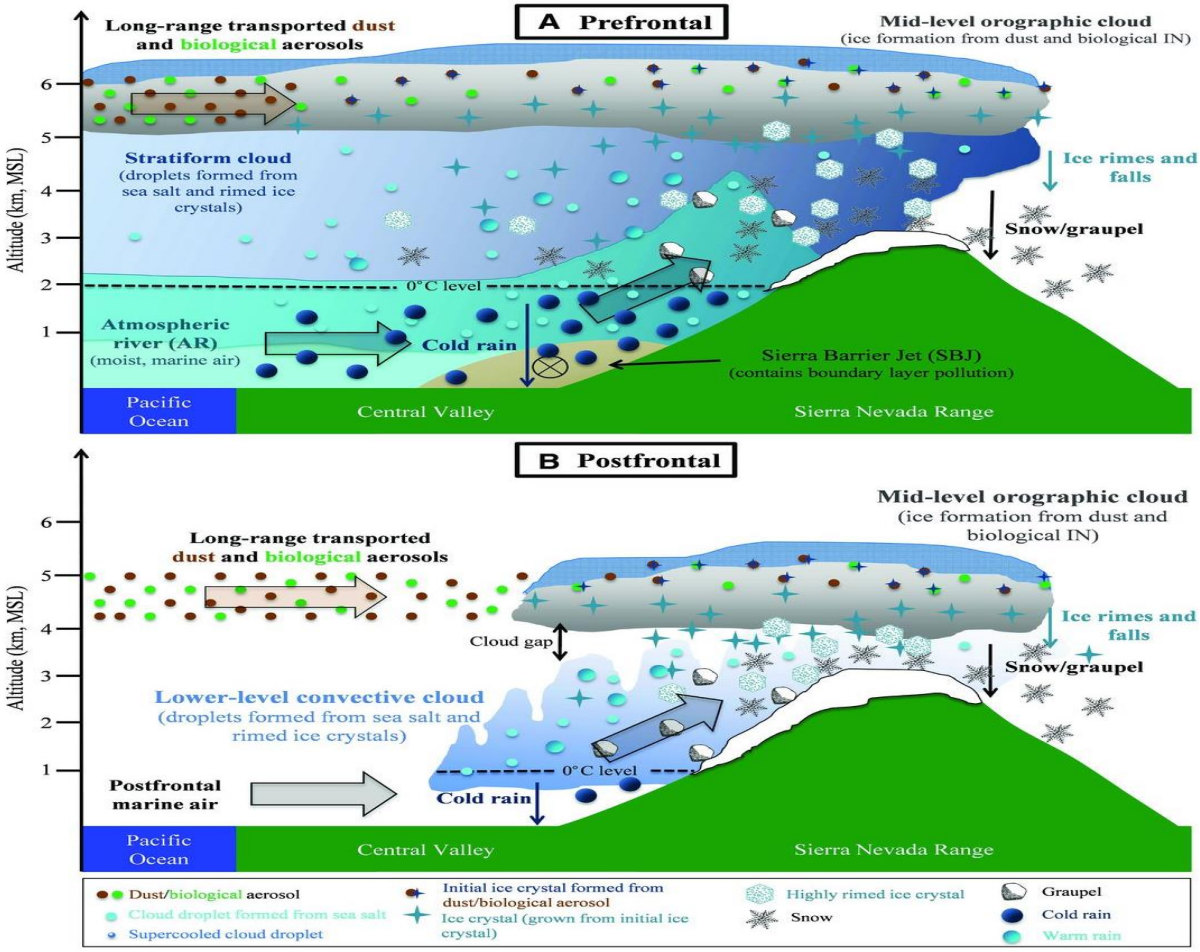

Fig. 2.2: Formation of Different Hydrometeors.

For the Kessler (1969) type of warm rain process, only three families of cloud materials are considered: water vapor, cloud water, and rain. Each of these species represents one of the functional classes discussed above. For mixed-phase clouds, a more comprehensive microphysics scheme typically includes five or six species of hydrometeors. There are both ice-phase and water-phase hydrometeors constituting the cloud and precipitation classes. McCumber *et al.* (1991) compared the performances of two- and three-class ice-phase microphysical parameterization schemes in numerical simulations. They found that the use of three ice classes produced better results in tropical squall line simulations than did two ice classes or ice-free conditions. Because the goal of this study is to analyze the currently

existing microphysical parameterization schemes (e.g., a scheme used in Penn State/NCAR MM5 model) rather than to develop a new scheme, for simplicity of presentation, a cloud scheme with water vapor and four species of hydrometeors (including two classes of water-phase and two classes of ice-phase species) is analyzed. Five families of cloud materials are: water vapor (the source class), cloud water and cloud ice (the cloud class), rain and snow (the precipitation class). In this scheme, snow can be treated as a category including all the precipitating ice. In a more complete microphysics scheme (three-class ice-phase microphysical parameterization), graupel/hail is separated from the general precipitating ice family. Again, this separation is neglected in the schemes under consideration.

In Fig. 2.1, the lines connecting two hydrometeor families represent the possible microphysical processes (conversions) between the two species. For example, water vapor can interact with all the other four species. When air is supersaturated with respect to water or ice, water vapor can condense into water-phase hydrometeors or deposit onto the ice-phase hydrometeors. When air is sub-saturated with respect to water or ice, the other four species can convert back to water vapor by evaporation or sublimation. If a conversion between two species is considered to be reversible, then eight different conversion processes would occur for water vapor. They are:

i. water vapor $\rightleftharpoons$ cloud water,

ii. vapor $\rightleftharpoons$ cloud ice,

iii. vapor $\rightleftharpoons$ rain, and

iv. vapor $\rightleftharpoons$ snow.

(Each pair of processes is not concurrent, meaning that the condition favored for one process to occur precludes the reversible process.) In nature, all these processes may exist. However, in most cloud microphysics schemes, the transformation from the source class directly to some precipitation class (excluding water vapor deposition on ice particles) is not modeled (but not vice versa); e.g., the growth of rain by consuming water vapor is essentially neglected. On the other hand, between two families of hydrometeors there may be more than one interaction mechanism transforming one species to the other. For example, cloud ice can be formed directly from water vapor by two different processes: water vapor deposition onto ice nuclei and homogeneous cloud ice initiation (e.g., at very cold temperatures).

2.2.1 Cloud Water Mixing Ratio

Water is the only naturally occurring substance that occurs in solid, liquid, and gaseous forms at the range of temperatures and pressures found in the Earth's atmosphere. This curious fact, plus the abundance of water and its importance for life, makes water one of the most important components of the atmosphere. It plays a crucial role in the weather, the transfer of energy on a wide range of scales from microclimates to the planetary, and of course is vital for the supply of moisture to plants and other living things. Atmospheric water is made visible in the form of clouds and precipitation (water droplets and ice crystals), but is also present in form of gas or vapor. Clouds are among the most fascinating phenomena in atmosphere: clouds make visible the movement of the air, and can reveal much about the state of the atmosphere. To understand them, and larger-scale weather systems, it is necessary to examine the behavior of water in the atmosphere. Clouds affect the radiation balance of the earth-atmosphere system by both reflecting a fraction of incoming solar radiation back to space (cooling the near surface) and blocking a fraction of the earth emitting long wave radiation from escaping to space (greenhouse warming). The net effect is either cooling or warming. Cloud macro-physical properties such as the amount of cloud cover, cloud top height, etc. and cloud microphysical properties such as cloud droplet size, liquid-ice phase, etc., play a key role in cloud-radiation interaction. For example, relatively shallow stratus clouds tend to cool the earth-atmosphere system (cooling dominates warming), whereas upper tropospheric thin cirrus clouds tend to warm the system (warming dominates cooling). Greenhouse warming is strongly related to high cloud amount, and cooling is more related to high cloud amount and cloud optical depth. The clouds can be composed of water droplets, ice crystals, or a mixture of the two. Water and ice clouds have distinctive appearances, so it is possible totell the difference from the ground. Ice clouds (such as cirrus) are fibrous in appearance, whereas water clouds (such as cumulus or ground fog) may vary in appearance from 'puffy' to 'misty'. Clouds are suspensions of water droplets or ice crystals. It is seen that clouds will form when the air is too cool to support the amount of water present in vapor form. In nature, clouds form in 3 basic situations: Cloud will form if a mass of air is chilled so that it can no longer support the water present as vapor. The most familiar cloud of this type is fog forming near the ground on a cold night. Because the mechanism of cooling is the loss of energy by long wave emission, this type of fog is termed radiative fog. Similarly, cloud will form if an air mass is uplifted to higher altitudes where the pressure drop causes cooling. Uplift may be due to winds blowing over high ground (orographic cloud), or by

vertical motions in the free atmosphere (convection). Cloud may also form by the mixing of two unsaturated air masses in some circumstances. This may occur because of the non-linear form of the saturation vapor pressure/temperature curve.

2.2.2 Rain Water Mixing Ratio

Water droplets or ice crystals form precipitation when they fall through the atmosphere to reach the ground. This occurs when the fall velocity of the particle is greater than up draught velocities. The likelihood that particles will form precipitation is thus a function of droplet size: small droplets will tend to be kept aloft, whereas large particles are more likely to fall to ground. Two main mechanisms have been identified to explain the growth of water droplets to form precipitation: (1) Activated nuclei or the growth of droplets by condensation from surrounding vapor; (2) Collision, or the growth of droplets by the combination of two colliding particles. For water droplets, both of these mechanisms are very slow: too slow to account for observed rates of cloud development and precipitation formation. Thus most precipitation is thought to develop as ice crystals at low temperatures, which may then defrost to form rain. This is known as the Bergeron-Findeisen mechanism, after two Norwegian meteorologists who first proposed the mechanism. Ice crystals grow more rapidly than water droplets, due to the lower saturation vapor pressure of air over ice, compared to water, but require very low temperatures. The formation of ice crystals in clouds is known as glaciations (not to be confused with terrestrial glaciation). This is probably the most important mechanism of precipitation formation in many parts of the world, even in the tropics (where low temperatures occur in high cumulus clouds). Ice crystal clouds have wispy, fibrous shapes, and allow us to see glaciations occurring in high clouds. An important type of ice clouds is known as cirrus, after the Latin word for hair. Types of precipitation include rain; snow (branching ice crystals or aggregates of crystals); sleet; hail, and graupel (conical pellets of spongy hail). The type that falls is dependent on the processes operating within clouds and the air temperature profile between there and ground (i.e. whether precipitation thaws or freezes en route to ground).

2.2.3 Cloud Ice Mixing Ratio

At low temperatures, ice crystals may form from water vapor in the atmosphere. This does not occur at $0^{o}C$, because there is a need for freezing nuclei with suitable surface characteristics, which are less common than condensation nuclei. At temperatures > $-10^{o}C$, almost no ice will form; $-10^{o}C$ to $-20^{o}C$ increasing minority of ice crystals; $-20^{o}C$ to $-30^{o}C$

increasing majority of ice crystals; < -30^{o}C mostly ice crystals. Cold air (< 0^{o} C) which contains liquid water droplets is referred to as super cooled. The water will tend to freeze as soon as it finds a suitable surface where ice crystals can grow. An example of this process is the formation of rime ice on fence posts, clothing, hair and beards when cold, misty air blows past.

Fig. 2.3: Frozen Ice

2.2.4 Cloud Snow Mixing Ratio

Snow is precipitation in the form of flakes of crystalline water ice that falls from clouds. Since snow is composed of small ice particles, it is a granular material. It has an open and therefore soft, white, and fluffy structure, unless subjected to external pressure. Snowflakes come in a variety of sizes and shapes. Types that fall in the form of a ball due to melting and refreezing, rather than a flake, are hail, ice pellets or snow grains. The process of precipitating snow is called snowfall. Snowfall tends to form within regions of upward movement of air around a type of low-pressure system known as an extra tropical cyclone.

Snow can fall pole ward of these systems' associated warm fronts and within their comma head precipitation patterns.

Fig. 2.4: Winter Snow

Where relatively warm water bodies are present, for example because of water evaporation from lakes, lake-effect snowfall becomes a concern downwind of the warm lakes within the cold cyclonic flow around the backside of extra tropical cyclones. Lake-effect snowfall can be heavy locally. Thunder snow is possible within a cyclone's comma head and within lake effect precipitation bands. In mountainous areas, heavy snow is possible where upslope flow is maximized within windward sides of the terrain at elevation, if the atmosphere is cold enough. Snowfall amount and its related liquid equivalent precipitation amount are measured using a variety of different rain gauges. Extra tropical cyclones can bring cold and dangerous conditions with heavy rain and snow with winds exceeding 119 km/h. The band of precipitation that is associated with their warm front is often extensive, forced by weak upward vertical motion of air over the frontal boundary, which condenses as it cools off and produces precipitation within an elongated band, which is wide and stratiform, meaning falling out of nimbostratus clouds. When moist air tries to dislodge an arctic air mass, overrunning snow can result within the pole ward side of the elongated precipitation band. In the Northern Hemisphere, pole ward is towards the North Pole, or north. Within the Southern Hemisphere, pole ward is towards the South Pole, or south. Large water bodies such as lakes efficiently store heat that results in significant temperature differences (larger than 13 °C)

between the water surface and the air above. Because of this temperature difference, warmth and moisture are transported upward, condensing into vertically oriented clouds that produce snow showers. The temperature decrease with height and cloud depth is directly affected by both the water temperature and the large-scale environment. The stronger the temperature decrease with height, the deeper the clouds get, and the greater the precipitation rate becomes.

Fig. 2.5: Graupel

2.2.5 Cloud Graupel Mixing Ratio

Graupel is a German word for ice pellets which are crisp, opaque and easily compressible. Graupel forms when snow in the atmosphere encounters super cooled water. In a process known as accretion, ice crystals form instantly on the outside of the snow and accumulate until the original snowflake is no longer visible or distinguishable.

Snow pellets, Soft hail, Graupel precipitation of white and opaque ice particles, which fall from a cloud and which are generally conical or rounded, with diameters attaining as much as 2 to 5 mm, but some graupel can be the size of a quarter (coin). Graupel is sometimes mistaken for hail. Graupel does not include other frozen precipitation such as snow or ice crystals with an experimental investigation of the heat and mass transfer of graupel**.** Graupel**,** heavily rimed snow, is an extreme product of this process. The coating of these ice crystals on the outside of the snow is called a rime coating. To tell the difference between graupel and

hail, simply have to touch a graupel ball. Graupel pellets typically fall apart when touched or when they hit the ground. Hail is formed when layers of ice accumulate and are very hard as a result.

2.2.6 Cloud Water Vapor Mixing Ratio

Mixing ratio (w) is the amount of water vapor that is in the air. w is the grams of vapor per kg of dry air. Structures in atmospheric (vertically) Integrated Water Vapor (IWV) strongly reflect the dynamics of the atmosphere. Cold fronts are associated with a strong gradient (from high to low values) in IWV. These structures can also be seen in water (vapor) related variables, like cloud fields. This requires detailed measurements of IWV. Ideally, of course, the complete time evolution of the two-dimensional IWV field should be known. Satellites can measure water vapor from the top of the atmosphere in the 6.7 mm water vapor absorption channel. These measurement have good spatial resolution; however, the data only represent a measure of the water vapor content of the upper troposphere above (on average) 5 km, while most of the moisture is in the lower troposphere (with about 90% in the lower 5 km). Water vapor is a very important gas in the atmosphere and can influence many things like condensation and the formation of clouds and rain, as well as how hot or cold it feels at the surface. Different regions typically contain different amounts of water vapor and this can drastically affect the climate across these regions. Water vapor is also a necessary tool in forecasting; therefore the measurement of the amount of water vapor in the air is standard for most weather observation stations (along with temperature and wind properties). The different ways in which meteorologists express water vapor amounts as well as how to measure it. The mixing ratio is the ratio of the mass of water vapor in the air over the mass of dry air. This quantity is found by reading the mixing ratio line that goes through the dew point temperature at the pressure level of interest in the thermodynamic diagram. It can be expressed as the mixing ratio divided by the saturation mixing ratio or the vapor pressure divided by the saturation vapor pressure.

2.2.7 Relative Humidity

Relative Humidity is the most commonly used measurements of moisture content in the air. The Relative Humidity is the amount of water vapor (moisture) in the air compared to the maximum amount that the air could hold at a given temperature. The relative humidity is:

$$f = \frac{\omega}{\omega_s} \times 100 = \frac{\rho_w}{\rho_{ws}} \times 100 = \frac{q}{q_s} \times 100 = \frac{e}{e_s} \times 100$$

If the relative humidity is 100%, the air is saturated. If the relative humidity is 50%, the air contains half the water vapor required for it to be saturated. If the amount of water vapor in the air increases, the relative humidity increases, and if the amount of water vapor in the air decreases, the relative humidity decreases. However, relative humidity is dependent on air temperature, too. If the water vapor content remains the same and the temperature drops, the relative humidity increases. If the water vapor content remains the same and the temperature rises, the relative humidity decreases. This is because colder air doesn't require as much moisture to become saturated as warmer air. Warm air can hold more water vapor than cool air, so a particular amount of water vapor will yield a lower relative humidity in warm air than it does in cool air. If I watch the weather in the summer, you'll notice that the relative humidity is actually higher in the morning than in the afternoon. This is because the cooler morning air is closer to saturation than the hot afternoon air, even with the same amount of water vapor. Surprisingly, there is no significant difference in daily average relative humidity between summer and winter. Since warm air is less dense than cold air, there is more room for water vapor in warm summer air as compared with cold winter air. At a given vapor pressure (or mixing ratio), relative humidity with respect to ice is higher than that with respect to water. Water is known by different names in different states. If the maximum amount of water vapor has been reached and more water is introduced into the air, an equal amount of water must transform back to liquid or solid form through condensation. At this point, the air is said to be saturated with water, and the relative humidity is 100%. On the other end of the scale, when there is no water vapor in the air, the relative humidity is 0% whatever the temperature. In other words, relative humidity always lies between 0 and 100%. As mentioned, the ability of air to hold water vapor is strongly dependent on temperature. This means that relative humidity is also strongly temperature dependent.

2.2.8 Vorticity

The vorticity is the microscopic measurement of the rotation of a small air parcel. Air parcel has vorticity when the parcel spins as it moves along its path. Although the axis of the rotation can extend in any direction, meteorologists are primarily concerned with the rotational motion about an axis that is perpendicular to the earth's surface. If it does not spin, it is said to have zero vorticity. In the Northern Hemisphere, the vorticity is positive when the parcel has a counterclockwise or cyclonic rotation. It is negative when the parcel has clockwise or anti cyclonic rotation. For turning of the atmosphere, vorticity may be imbedded in the total flow and not readily identified by a flow pattern. The rotation of the Earth imparts

vorticity to the atmosphere; absolute vorticity is the combined vorticity due to this rotation and vorticity due to circulation relative to the Earth (relative vorticity). The negative vorticity is caused by anti cyclonic turning; it is associated with downward motion of the air. The positive vorticity is caused by cyclonic turning; it is associated with upward motion of the air. Also the relative vorticity is the air relative to the Earth, disregarding the component of vorticity resulting from Earth's rotation.

The absolute vorticity ω_a is given by the curl of the absolute velocity, while the relative vorticity ω is given by the curl of the relative velocity:

$$\omega_a \equiv \overline{\nabla} \times \overline{V}_a \qquad\qquad \omega \equiv \overline{\nabla} \times \overline{V}$$

In meteorology the general concerned only with the vertical components of absolute and relative vorticity:

$$\eta = \hat{k}.\left(\overline{\nabla} \times \overline{V}_a\right), \quad \zeta = \hat{k}.\left(\overline{\nabla} \times \overline{V}\right)$$

In particular, the vertical component of relative vorticity ζ is highly correlated with synoptic scale weather disturbances. Large positive ζ tends to occur in association with cyclonic storms in the Northern Hemisphere. Furthermore, η tends to be conserved following the motion in the middle troposphere. Thus, analysis of the η field and its evolution due to advection forms the basis for the simplest dynamical forecast scheme.

2.3 Weather Research & Forecasting Model

The Weather Research and Forecasting (WRF) Model is a next-generation mesoscale numerical weather prediction system designed to serve both atmospheric research and operational forecasting needs. It features two dynamical cores, a data assimilation system, and a software architecture facilitating parallel computation and system extensibility. The model serves a wide range of meteorological applications across scales from tens of meters to thousands of kilometers. The effort to develop WRF began in the latter part of the 1990's and was a collaborative partnership principally among the National Center for Atmospheric Research (NCAR), the National Oceanic and Atmospheric Administration represented by the National Centers for Environmental Prediction (NCEP) and the Forecast Systems Laboratory (FSL) the Air Force Weather Agency (AFWA), the Naval Research Laboratory, the University of Oklahoma, and the Federal Aviation Administration (FAA). WRF offers two dynamical solvers for its computation of the atmospheric governing equations, and the variants of the model are known as WRF-ARW and WRF-NMM. The Advanced Research

WRF (ARW) is supported to the community by the NCAR Mesoscale and Micro scale Meteorology Division. The WRF-NMM solver variant was based on the Eta Model, and later Non hydrostatic Mesoscale Model, developed at NCEP. The WRF-NMM is supported to the community by the Developmental Test bed Center.

2.3.1 Microphysics schemes in WRF-ARW Model

Microphysics includes explicitly resolved water vapor, cloud and precipitation processes. The model is general enough to accommodate any number of mass mixing-ratio variables, and other quantities such as number concentrations. Four-dimensional arrays with three spatial indices and one species index are used to carry such scalars. Memory, i.e., the size of the fourth dimension in these arrays, is allocated depending on the needs of the scheme chosen, and advection of the species also applies to all those required by the microphysics option. In the current version of the ARW, microphysics is carried out at the end of the time-step as an adjustment process, and so does not provide tendencies.

The rationale for this is that condensation adjustment should be at the end of the time-step to guarantee that the final saturation balance is accurate for the updated temperature and moisture. However, it is also important to have the latent heating forcing for potential temperature during the dynamical sub-steps and this is done by saving the microphysical heating as an approximation for the next time-step as described.

2.3.1.1 Kessler Scheme

The Kessler scheme is a simple warm cloud scheme that includes water vapor, cloud water and rain. The microphysical process consists of the production, fall and evaporation of rain, the accumulation and auto conversion of cloud water and the production of cloud water from condensation. A warm-rain scheme has been used commonly in idealized cloud modeling studies. Kessler scheme is one moment scheme. The purpose of the scheme is to increase understanding of the roles of cloud conversion, accretion, evaporation, and entrainment processes in shaping the distributions of water vapor, cloud, and precipitation associated with tropical circulations. This scheme is idealized microphysics process without the consideration of ice phase and melting zone. Kessler scheme has been used widely in cloud modeling studies due to its simplicity. The equation represented the processes between cloud, vapor and rain are also much simplified compared with other scheme. Kessler scheme produced much heavier precipitation and can show unrealistic precipitation profiles in some studies (Kessler, 1969).

2.3.1.2 Lin *et al.* Scheme

A sophisticated scheme that has ice, snow and graupel processes, suitable for real-data high-resolution simulations. Lin *et al.* (1983) scheme includes six classes of hydrometeors are included: water vapor, cloud water, rain water, cloud ice, snow, and graupel. All parameterization production terms are based on Lin *et al*. (1983). This is a relatively sophisticated microphysics scheme in WRF, and it is more suitable for use in research studies. The scheme is taken from Purdue cloud model and the details can be found in Chen and Sun (2002) 2-D microphysics scheme. This is one of the first schemes to parameterize snow, graupel, and mixed-phase processes. It has been used extensively in research studies and in mesoscale NWP Model. The scheme includes ice sedimentation and time-split fall terms.

2.3.1.3 WSM 3-class scheme

The combination of ice sedimentation and other new ice-phase parameterizations follows Hong *et al*., (2004) is called the WRF single-moment microphysics scheme. It is called simple ice scheme because it is predicts three categories of hydrometers: vapor, cloud water/ice and rain/snow. It is assuming cloud water and rain for temperatures above freezing, and cloud ice and snow for temperatures below freezing. A major difference from other approaches is that a diagnostic relation is used for ice number concentration that is based on ice mass content rather than temperature. The computational procedures of WSM3 explain by Hong and Lim (2006) it is computationally efficient for the inclusion of ice processes, but lacks super cooled water and gradual melting rates.

2.3.1.4 Ferrier scheme

Ferrier scheme predicts changes in water vapor and condensate in the forms of cloud water, rain, cloud ice, and precipitation ice. Local storage arrays retain first-guess information that extract contributions of cloud water, rain, cloud ice, and precipitation ice of variable density in the form of snow, graupel, or sleet. The density of precipitation ice is expected from a local array that stores information on the total growth of ice by vapor deposition and accretion of liquid water. Sedimentation is treated by partitioning the time averaged flux of precipitation into a grid box between local storage in the box and fall out through the bottom of the box. Advection only of total condensate and vapor diagnostic cloud water, rain, & ice from storage arrays – assumes fractions of water & ice within the column are fixed during advection super cooled liquid water & ice melt (Ferrier, 1995).

2.3.1.5 WRF Single-moment 6-class (WSM6) microphysics scheme

The WRF-single-moment-6-class (WSM6) microphysics scheme has been one of the options of microphysical process in the WRF model since August 2004. This scheme predicts the mixing ratios for water vapor, cloud water, cloud ice, snow, rain, and graupel. The characteristics of the cold rain process in the WSM6 scheme follow the revised ice microphysics process (Hong *et al.*, 2004), whereas the warm rain processes are primarily based on the works of Lin *et al.* (1983) and the auto conversion process from Tropoli and Cotton (1980). The daily forecasts at NCAR have shown that the WSM6 scheme works successfully in predicting mesoscale convective systems, but it sometimes overestimates the peak intensity and underestimates the areas of anvil clouds. We attempt to improve such existing deficiencies in the WSM6 scheme by incorporating the prediction of number concentrations for warm rain species. This new method uses a large eddy simulation (LES)-based approach (Khairoutdinov and Kogan, 2000) to determine the auto conversion rates and allow for a more sophisticated coupling between cloud field and number concentrations of warm species. Double-moment prediction for the warm species in WSM6 scheme will allow more flexibility of the size distribution enabling the mean diameter to evolve in contrast to the one-moment scheme.

WSM6 scheme includes vapor, rain, snow, cloud ice, cloud water and graupel in six different arrays. A new method for representing mixed-phase particle fall speeds for the snow and graupel by assigning a single fall speed to both that is weighted by the mixing ratios, and applying that fall speed to both sedimentation and accumulation processes is introduced. Of the three WSM schemes, the WSM6 scheme is the most suitable for cloud-resolving grids, considering the efficiency and theoretical backgrounds· A new method for representing mixed-phase particle fall speeds for the snow and a scheme with ice, snow and graupel processes suitable for high-resolution simulations. The WSM6 scheme has been developed by adding additional process related to graupel to the WSM5 scheme (Hong and Lim, 2006).

2.3.1.6 Thompson Scheme

A bulk microphysical parameterization (BMP) developed for use with WRF or other mesoscale models. The snow size distribution depends on both ice water content and temperature and is represented as a sum of exponential and gamma distributions. Furthermore, snow assumes a non-spherical shape with a bulk density that varies inversely with diameter as found in observations. A new scheme with ice, snow and graupel processes

suitable for high-resolution simulations. This adds rain number concentration and updates the scheme from the one in Version 3.0 New Thompson et al. scheme in v3.1. Replacement of Thompson *et al.,* (2007) scheme that was option 8 in v3.0 6-class microphysics with graupel, ice and rain number concentrations also predicted.

2.3.1.7 Milbrandt-Yau Double-Moment 7-class scheme

The multimoment scheme of Milbrandt and Yau (2005) is ideally suited for such a study because it allows the choice between one, two, or three prognostic moments in each of the six hydrometeor categories. Milbrandt and Yau (2006) simulated a case of severe convection and found that reducing the number of moments from three to two changed the proportion of frozen and liquid precipitation at the surface. This was primarily due to the problem of excessive size sorting that exists in double-moment schemes that hold the spectral dispersion parameter constant. This problem was overcome by a triple-moment scheme. This scheme includes separate categories for hail and graupel with double-moment cloud, rain, ice, snow, graupel and hail.

2.3.1.8 Morrison Double-Moment Scheme

The Morrison scheme is similar to the Thompson scheme but has a more sophisticated treatment for frozen precipitation species. Like Thompson, the Morrison scheme predicts the mass concentration of cloud water, cloud ice, rain, snow and graupel. The physics are based on the full double-moment version described in Morrison *et al*. (2009), but the rendition implemented in WRF- ARW v.3.4.1 does not include a number concentration variable for cloud water. Thus, even though it is described as double-moment for all hydrometeors in the literature, it is treated as a single-moment cloud water scheme in this study.

2.3.1.9 Community Atmosphere Model

CAM is the atmospheric component of the NCAR Earth System Model and in its version 5 (Neale *et al.,* 2012). The Community Climate System Model (CCSM) is a coupled climate model for simulating the earth's climate system. Composed of four separate models simultaneously simulating the earth's atmosphere, ocean, land surface and sea-ice, and one central coupler component, the CCSM allows researchers to conduct fundamental research into the earth's past, present and future climate states. Cloud feedbacks, chemical interactions in clouds and aerosol indirect effects (aerosol impacts on cloud particles affecting radiation and precipitation) are critical uncertainties that should be addressed for understanding the evolution of the climate system. CAM is available at different horizontal representation (i.e.

spectral, finite volume) and at different horizontal resolutions. Since the first version, the complexity of the parameterization included has increased constantly. For example, its most recent version enables the simulation of the full cloud-aerosols indirect radiative effects, while in previous versions different schemes of aerosols prescription where available.

2.3.1.10 Stony Brook University (SBU) Microphysics

Stony Brook University scheme is a 5-class scheme with riming intensity predicted to account for the mixed-phase processes. A new approach for representing the ice microphysics is presented, which considers both temperature and riming effects on ice properties. The SBU-YLIN scheme includes five prognostic mixing ratios: water vapor, cloud ice, precipitating ice (PI), cloud liquid water, and rain. Dry snow, rimed snow, and graupel are included in the PI category through the introduction of a varying riming intensity parameter. The new scheme (SBU-YLIN) allows for physically based representation of the ice particles with temperature- and riming intensity–dependent properties, such as the mass, cross-sectional area, and fall velocity relationships. Riming intensity is diagnosed from LWC, PI mass, and temperature. One advantage of the new approach is the simplification of the scheme and the reduction of the computation time. Also, it is more physically based than many existing schemes, since it considers partially rimed particles (Lin and Colle, 2011).

2.3.1.11 WRF Double-Moment 6-class Microphysics Scheme (WDM6)

The WRF double-moment 6-class microphysics scheme (WDM6) implements a double-moment bulk micro physical parameterization of clouds and precipitation and is applicable in mesoscale and general circulation models. The WDM6 scheme enables the investigation of the aerosol effects on cloud properties and precipitation processes with the prognostic variables of cloud condensation nuclei (CCN), cloud water and rain number concentrations. WDM6 extends the WRF single-moment 6-class microphysics scheme (WSM6) by incorporating the number concentrations for cloud and rainwater along with a prognostic variable of CCN number concentration. Moreover, it predicts the mixing ratios of six water species (water vapor, cloud droplets, cloud ice, snow, rain, and graupel), similar to WSM6. Prognostic water substance variables include water vapor, clouds, rain, ice, snow, and graupel for both the WDM6 and WSM6 schemes. Additionally, the prognostic number concentrations of cloud and rain waters, together with the CCN, are considered in the WDM6 scheme. The number concentrations of ice species such as graupel, snow, and ice are diagnosed following the ice-phase microphysics of Hong *et al*. (2004).

2.3.1.12 NSSL-2 Microphysics Scheme

The scheme is a 2-moment one developed at the National Severe Storms Laboratory. It predicts the mass mixing ratio and number concentration for six hydrometeor species: cloud droplets, rain drops, ice crystals, snow, graupel, and hail *(*Mansell *et al.* 2010*)*. A unique feature is the additional prediction of average graupel particle density, which allows graupel to span the range from frozen drops to low-density graupel. Hail is produced only by wet growth of graupel to try to represent true hail rather than merely high-density ice. An option allows prediction of cloud condensation nuclei (CCN) concentration (intended for idealized simulations). The scheme also features adaptive sedimentation to allow some size sorting but prevent spurious large particles (and radar reflectivity values) that can arise from two-moment microphysics, particularly for the larger precipitation categories (graupel, hail, and rain). Size distribution shape parameters and a number of other options can be set in the code. The scheme is intended for cloud-resolving simulations (dx <= 2km) in research applications.

2.3.2 Cumulus Parameterization

These schemes are responsible for the sub-grid-scale effects of convective and/or shallow clouds. The schemes are intended to represent vertical fluxes due to unresolved up drafts and down drafts and compensating motion outside the clouds. They operate only on individual columns where the scheme is triggered and provide vertical heating and moistening profiles. Some schemes provide cloud and precipitation field tendencies in the column, and future schemes may provide momentum tendencies due to convective transport of momentum. The schemes all provide the convective component of surface rainfall. Cumulus parameterizations are theoretically only valid for coarser grid sizes, (e.g., > 10 km), where they necessary to properly release latent heat on a realistic time scale in the convective columns. Where the assumptions about the convective eddies being entirely sub-grid-scale break down for finer grid sizes, sometimes these schemes have been found to be helpful in triggering convection in 5-10 km grid applications. Generally they should not be used when the model can resolve the convective eddies itself

One of the main options which could potentially affect precipitation severely is the cumulus parameterization. It accounts for unresolved cloud formation. Depending on the grid resolution, convective clouds could be resolved by the explicit scheme, but with the resolution used here (15 km) it still seems necessary to take into account the unresolved scales. The feedback from these parameterizations to the larger–scale equations of the model

is the profile of latent heat release and moistening caused by convection. Two different schemes were used. Even though the efficiency of a given parameterization depends on the concrete event, other cumulus parameterizations have been proved to have less accuracy, e.g. the Anthes–Kuo (Ferretti *et al*., 2000) or Betts–Miller schemes (Cohen, 2002). The Kain–Fritsch scheme has demonstrated good performance on several situations and regions (Wang and Seaman, 1997; Kotroni and Lagouvardos, 2001; Cohen, 2002). In the study by Ferretti *et al*. (2000) in the Alpine region, the Grell scheme was better than the Kain–Fritsch scheme for some concrete events.

These schemes are responsible for the sub-grid-scale effects of convective and shallow clouds. The schemes are intended to represent vertical fluxes due to unresolved updrafts and downdrafts and compensating motion outside the clouds. The cumulus parameterization are theoretically only valid for coarser grid sizes, (e.g., > 10km), where they are necessary to properly release latent heat on a realistic time scale in the convective columns.

2.3.2.1 K**ain-Fritsch (KF) scheme**

In the KF scheme the condensates in the updraft are converted into precipitation when their amount exceeds threshold value. In this scheme the convection consumes the convective available potential energy in a certain time scale. The KF scheme also includes the shallow convection other than deep convection. The shallow convection creates non-perceptible condensates and the shallowness of the convection is determined by a vertical extent of the cloud layer that is known by a function of temperature at LCL of rising air parcel. The KF scheme was derived from the Fritsch–Chappell, and its fundamental framework and closure assumptions are described by Fritsch and Chappell (1980). Kain-Fritsch (1990) modified the updraft model in the scheme and later introduced numerous other changes, so that it eventually became distinctly different from the Fritsch–Chappell scheme. It was distinguished from its parent algorithm by referring to the more elaborate code as the KF scheme, beginning in the early 1990s. This is also deep and shallow convection sub-grid scheme using a mass flux approach with downdrafts and CAPE removal time scale. Updraft generates condensate and dump condensate into environment downdraft evaporates condensate at a rate that depends on RH and depth of downdraft leftover condensate accumulates at surface as precipitation

2.3.3 Planetary Boundary Layer (PBL) Parameterizations

The PBL is the layer in the lower part of the troposphere with thickness ranging from a few hundred meters to a few kilometers within which the effects of the Earth's surface are felt by the atmosphere. The PBL processes represent a consequence of interaction between the lowest layer of air and the underlying surface. The interactions can significant impact on the dynamics of the upper air flows. The influences of the small-scale eddy on large scale atmospheric circulations may be included in the model equations. Accurate depiction of meteorological conditions, especially within the PBL, is important for air pollution modeling, and PBL parameterization schemes play a critical role in simulating the boundary layer. It is a very important portion of the atmosphere to correctly model to provide accurate forecasts, e.g., air pollution forecasts (Deardorff 1972; Pleim 2007). As important as the PBL is, it has one basic property whose accurate and realistic prediction is paramount to its correct modeling: its height. After all, the height of the top of the PBL defines its upper boundary. This is critical since PBL parameterizations schemes in WRF-ARW models need to know the extent through which to mix properties such as heavy rainfall, relative humidity, outgoing long wave flux, downward long wave flux.

PBL schemes were developed to help resolve the turbulent fluxes of heat, moisture, and momentum in the boundary layer. Another important issue is the interaction between the atmosphere and the surface. The PBL schemes handle the latent and sensible heat fluxes into the atmosphere, the frictional effects with the surface and the strong sub–grid–scale mixing which takes place in the lower levels due to these processes.

2.3.3.1 Yonsei University (YSU) scheme

The Yonsei University (YSU) PBL is the next generation of the Medium Range Forecast (MRF), Non local-K scheme with explicit entrainment layer and parabolic K profile in unstable mixed layer. The YSU scheme is a bulk scheme that expresses non-local mixing by convective large eddies. Non-local mixing is achieved by adding a non-local gradient adjustment term to the local gradient. At the top of the PBL, the YSU scheme uses explicit treatment of the entrainment layer, which is proportional to the surface layer flux (Shin and Hong, 2011; Hong *et al*. 2006).

2.4 Map Projection

Commonly, a map projection is a systematic transformation of the latitudes and longitudes of locations on the surface of a sphere or an ellipsoid into locations on a plane. Map projections

are necessary for creating maps. All map projections distort the surface in some fashion. Depending on the purpose of the map, some distortions are acceptable and others are not; therefore, different map projections exist in order to preserve some properties of the sphere-like body at the expense of other properties. There is no limit to the number of possible map projections. More generally, the surfaces of planetary bodies can be mapped even if they are too irregular to be modeled well with a sphere or ellipsoid. Even more generally, projections are the subject of several pure mathematical fields, including differential geometry and projective geometry. However, map projection refers specifically to a cartographic projection.

2.4.1 Mercator projection

The Mercator projection is a cylindrical map projection presented by the Flemish geographer and cartographer Gerardus Mercator in 1569. It became the standard map projection for nautical purposes because of its ability to represent lines of constant course, known as rhumb lines loxodromes, as straight segments which conserve the angles with the meridians. While the linear scale is equal in all directions around any point, thus preserving the angles and the shapes of small objects, the Mercator projection distorts the size and shape of large objects, as the scale increases from the Equator to the poles, where it becomes infinite. Although the Mercator projection is still used commonly for navigation, due to its unique properties, cartographers agree that it is not suited to general reference world maps due to its distortion of land area. Mercator himself used the equal-area sinusoidal projection to show relative areas. As a result of these criticisms, modern atlases no longer use the Mercator projection for world maps or for areas distant from the equator, preferring other cylindrical projection or forms of equal-area projection. The Mercator projection is still commonly used for areas near the equator, however, where distortion is minimal.

2.5 Arakawa Staggered C-grids

The Arakawa grid system depicts different ways to represent and compute orthogonal physical quantities on rectangular grids used for Earth system models for meteorology and oceanography. For example, the Weather Research and Forecasting Model use the Arakawa Staggered C-Grid in its atmospheric calculations when using the ARW core. The staggered Arakawa C-grid further separates evaluation of vector quantities compared to the Arakawa B-grid e.g., instead of evaluating both east-west (u) and north-south (v) velocity components at the grid center, one might evaluate the u components at the centers of the left and right grid faces, and the v components at the centers of the upper and lower grid faces.

Chapter III

Model Description and Methodology

3.1 Model Setup

In the present study the Weather Research and Forecast (WRF-ARW Version 3.5.1) model have been used to simulate the monsoon rainfall over Bangladesh. Advance Research WRF (ARW) is a dynamic solver (Skamarock *et al.,* 2005), which is compatible with WRF system to simulate broad spectrum of meteorological phenomena. Weather Research and Forecast model consists of fully compressible non-hydrostatic equations and different prognostic variables. The model vertical coordinate is terrain following hydrostatic pressure and the horizontal grid is Arakawa C-grid staggering. The model has different microphysics options but in this research we have been used 12 microphysics schemes for the simulation of heavy rainfall events in the monsoon season. The 12 MPs are Kessler (KS), Lin et al. (Lin), WSM3-class simple ice (WSM3), Ferrier (FE), WSM6, Thompson (TH), MYDM, MDM, CAM V5.12-Moment 5 class (CAM), Stony Brook University (SBU), WDM6 and NSSL 2-moment (NSSL2) schemes. The KS scheme contains prognostic equations for cloud water and rainwater mixing ratio, Lin for cloud water, rainwater, cloud ice, snow, and graupel mixing ratio, WSM3 for cloud water and rainwater mixing ratio, FE for cloud water, rainwater and snow mixing ratio, WSM6 for cloud water, rainwater, cloud ice, snow, and graupel mixing ratio, Thompson for cloud water, rainwater, cloud ice, snow, and graupel mixing ratio, MYDM for cloud water, rainwater, cloud ice, snow, graupel and hail mixing ratio, MDM for cloud water, rainwater, cloud ice, snow, and graupel mixing ratio, SBU for cloud water, rainwater, cloud ice and snow mixing ratio, WDM6 for cloud water, rainwater, cloud ice, snow, and graupel mixing ratio and NSSL-2 for cloud water, rainwater, cloud ice, snow, graupel and hail mixing ratio. The model has integrated by using initial and lateral boundary conditions (LBCs) from NCEP-FNL analysis at six hourly intervals. Surface layer is treated using Monin-Obukhov and planetary boundary layer (PBL) is treated with Yonsei University scheme. Dudhia (1989) scheme has been used for short wave radiation and Rapid Radiative Transfer Model (RRTM) for long wave (Mlawer *et al.* 1997). Kain-Fritsch (KF) (1993) cumulus parameterization (CP) scheme has been used for simulating the monsoon rainfall.

Table 1: WRF Model and Domain Configurations

Dynamics	Non-hydrostatic
Number of domain	1
Central points of the domain	Central Lat.: 22.80°N, Central Lon.: 90.70°E
Horizontal grid distance	6 km
Integration time step	30 s
Number of grid points	X-direction 161 points, Y-direction 183 points
Map projection	Mercator
Horizontal grid distribution	Arakawa C-grid
Nesting	One way
Vertical co-ordinate	Terrain-following hydrostatic-pressure co-ordinate (30 sigma levels up to 100 hPa)
Time integration	3rd order Runge-Kutta
Spatial differencing scheme	6th order centered differencing
Initial conditions	Three-dimensional real-data (FNL: 1° × 1°)
Lateral boundary condition	Specified options for real-data
Top boundary condition	Gravity wave absorbing (diffusion or Rayleigh damping)
Bottom boundary condition	Physical or free-slip
Diffusion and Damping	Simple Diffusion
Microphysics	(1) Kessler (2) Lin *et al*. (3) WSM3-class simple ice (4) Ferrier (5) WSM6-class graupel (6) Thomson graupel (7) Milbrandt-Yau Double-Moment 7-class (8) Morrison Double-Moment (9) CAM V5.12-Moment 5 class (10) Stony Brook University (11) WDM6-class & (12) NSSL 2-moment schemes
Radiation scheme	Dudhia (1989) for short wave radiation/ RRTM long wave Mlawer *et al.* (1997)
Surface layer	Monin-Obukhov similarity theory scheme (Hong and Pan, 1996)
Land surface parameterization	5 Layer Thermal diffusion scheme (Ek *et al*., 2003)
Cumulus parameterization schemes	Kain-Fritsch (KF) scheme, (Kain and Fritsch, 1990, 1993; Kain, 2004)
PBL parameterization	Yonsei University Scheme (YSU) (Hong *et al*., 2006)

3.2 Model Domain and Configuration

The model has been configured in single domain, 6 km horizontal grid spacing with 161×183 grids in the east-west and north-south directions and 30 vertical levels. Time step of integration is set to 30 seconds for maintaining computational stability as the model uses third-order Runge-Kutta time integration scheme. The model domain is given in Fig. 3.1. The detail of the model and domain configuration is given in Table 1:

Fig. 1: WRF Model Domain for the prediction of heavy rainfall in Bangladesh

3.3 Data and Methodology

Final Reanalysis (FNL) data (1^{o}x1^{o}) collected from National Centre for Environment Prediction (NCEP) is used as initial and lateral boundary Conditions (LBCs) which is updated at six hours interval i.e. the model is initialized with 0000, 0600, 1200 and 1800 UTC initial field of corresponding date. The NCEP FNL data will be interpolated to the model horizontal and vertical grids. There are many MP and CP schemes in WRF-ARW Model.

Table 2: Heavy rainfall events and their observed rainfall in the SE region of Bangladesh

Events	Heavy Rainfall observed at different stations				
	Chittagong	Cox's Bazzar	Teknaf	Kutubdia	
23-26 June 2015	424	1039	607	602	Sitakunda, 400
23-26 July 2015	867	518	690	740	Sandwip, 535
30 August – 1 September 2015	213	Sylhet, 396	330	Hatiya, 200	Sitakunda, 198

In this research we have used twelve different MP schemes and Kain-Fritsch cumulus parameterization scheme. Tropical Rainfall Measuring Mission (TRMM)-3B42RT 3-hourly rainfall data sets were downloaded from their website (http://lake.nascom. nasa.gov) while 3-hourly rain gauge data of 33 meteorological stations have been collected from Bangladesh Meteorological Department (BMD) all over Bangladesh. There is limited no. of meteorological observation stations in the northeastern and southwestern regions of Bangladesh. For this reason we have added 8 more points in the Bangladesh to see the exact rainfall pattern in Bangladesh Map. There are extracted convective and non-convective rainfall data from WRF Model output at 33 BMD station points with additional 8 points in the northeastern and southwestern regions of Bangladesh. We have also extracted TRMM rainfall data from above mentioned 41 points during the monsoon season of those three events. From WRF Model run we made 3 hourly outputs during the study period. This 3 hourly rainfall data converted into daily rainfall data of 23-26 June, 23-26 July and 30 August-01 September 2015. For collecting 24, 48 and 72 hour model rainfall data the WRF model has been run with those days with initial condition starting from 0000 UTC of 23 June to 0000 UTC of 26 June 2015, 0000 UTC of 23 July to 0000 UTC of 26 July 2015 and 0000 UTC of 30 August to 0000 UTC of 1 September 2015. The model is generated 24 hours as 1^{st} day of model run, 48 hours as 2^{nd} day of model run and 72 hours as 3^{rd} day of model run. Txt format data from ctl file of WRF model output has been found using Grid Analysis and Display System (GrADS). These txt data have been converted into Microsoft Excel format and then plotted using SURFER Software. The daily rainfall data of three different rain periods have been plotted of June, July and August using 24, 48 and 72-hour lead time prediction for 2015. There are analyzed area average rainfall and space and time dependent rainfall in the heavy rainfall occurred regions for three events.

There is also calculated maximum vertical velocity from the model output, which indicates the maximum convection. Along the line of maximum vertical velocity Reflectivity, Relative Humidity, Vorticity, Cloud Water Mixing Ratio, Rain Water Mixing Ratio, Cloud Ice Mixing Ratio, Water Vapor Mixing Ratio, Cloud Graupel Mixing Ratio and Cloud Snow Mixing Ratio have also been calculated.

Chapter IV

Results & Discussions

In this research Analysis has been made on 24, 48 and 72 hour predicted rainfall for 33 meteorological stations of Bangladesh but analysis of only 24 hour predicted rainfall is presented. There are also presented and compared time variation of station rainfall in the heavy rainfall area in the following subsection. The vorticity, vertical velocity, reflectivity, relative humidity, cloud water mixing ratio (CWMR), rain water mixing ratio (RWMR) have been presented along the line of maximum convection. There are also analyzed area averaged CWMR, RWMR, water vapor mixing ratio (WVMR), cloud ice mixing ratio (CIMR), cloud snow mixing ratio (CSMR) and cloud graupel mixing ratio (CGMR) and presented in the following subsection.

4.1 Heavy rainfall during 23 – 26 June 2015

4.1.1 Observed, TRMM and Model Simulated Rainfall on 23 June 2015

The observed and TRMM rainfall over Bangladesh during 23-26 June 2015 is presented in Fig. 2(a-h). The heavy rainfall is observed on 23 June (Fig. 2a) in the S-SE region and light rainfall is found in the central to W-NW, NE and SW regions of Bangladesh. Maximum rainfall observed at Sitakunda, Patuakhali, Rangamati, Chittagong, Hatiya and Sandwip are 182, 150, 149, 142, 112 and 104 mm respectively. TRMM derived light rainfall all over the country on 23June (Fig. 2e). Maximum rainfall is seen at Rangamati, Sitakunda, Cox's Bazar, Teknaf and Kutubdia and the rainfall amounts are 46, 46, 33, 31 and 31 mm respectively. It is seen that the distribution pattern of TRMM and observed rainfall are almost similar but TRMM derived rainfall is much lower than that of observed rainfall.

The rainfall simulated using different MP schemes on 23 June 2015 are presented in Fig. 3(a-l). The Kessler scheme has simulated heavy rainfall (Fig. 3a) in the S-SE regions, light rain fall in other regions of Bangladesh. Maximum rainfall is simulated at Sitakunda, Chittagong, Teknaf, Cox Bazar, Kutubdia and Sandwip regions having146, 143, 140, 132, 131 and 114 mm respectively. The Lin *et al.* scheme has simulated heavy rainfall (Fig. 3b) in the S-SE and northern regions of the country on that day and light rainfall is simulated at other regions. Maximum rainfall simulated at Sitakunda, Teknaf, Chittagong, Sandwip, Kutubdia and Rangamati regions are 149, 140, 139, 132, 130 and 104 mm respectively and actual maximum is seen at Hatiya, which indicates that the model simulated maximum rainfall is shifted from Hatiya towards east.

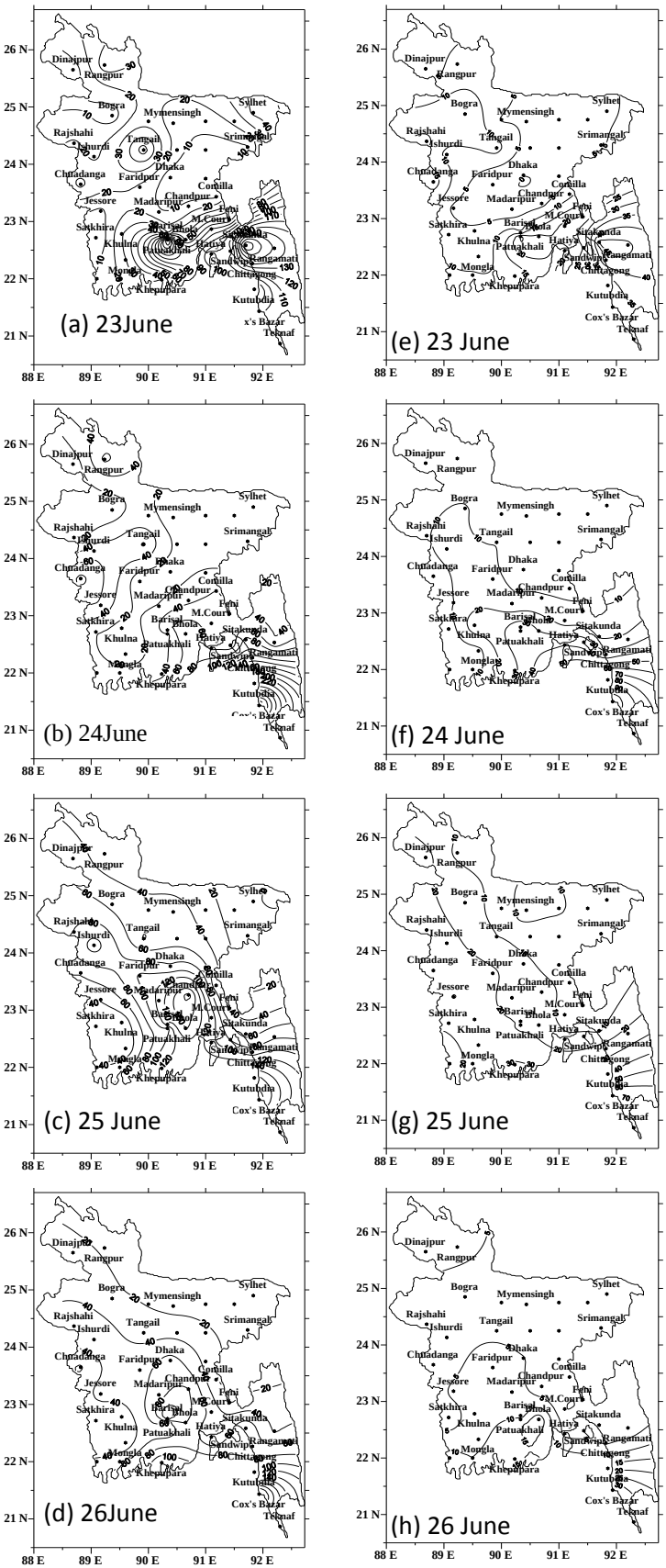

Fig. 2: Distribution of (a-d) Observed and (e-h) TRMM rainfall during 23-26 June 2015 all over Bangladesh.

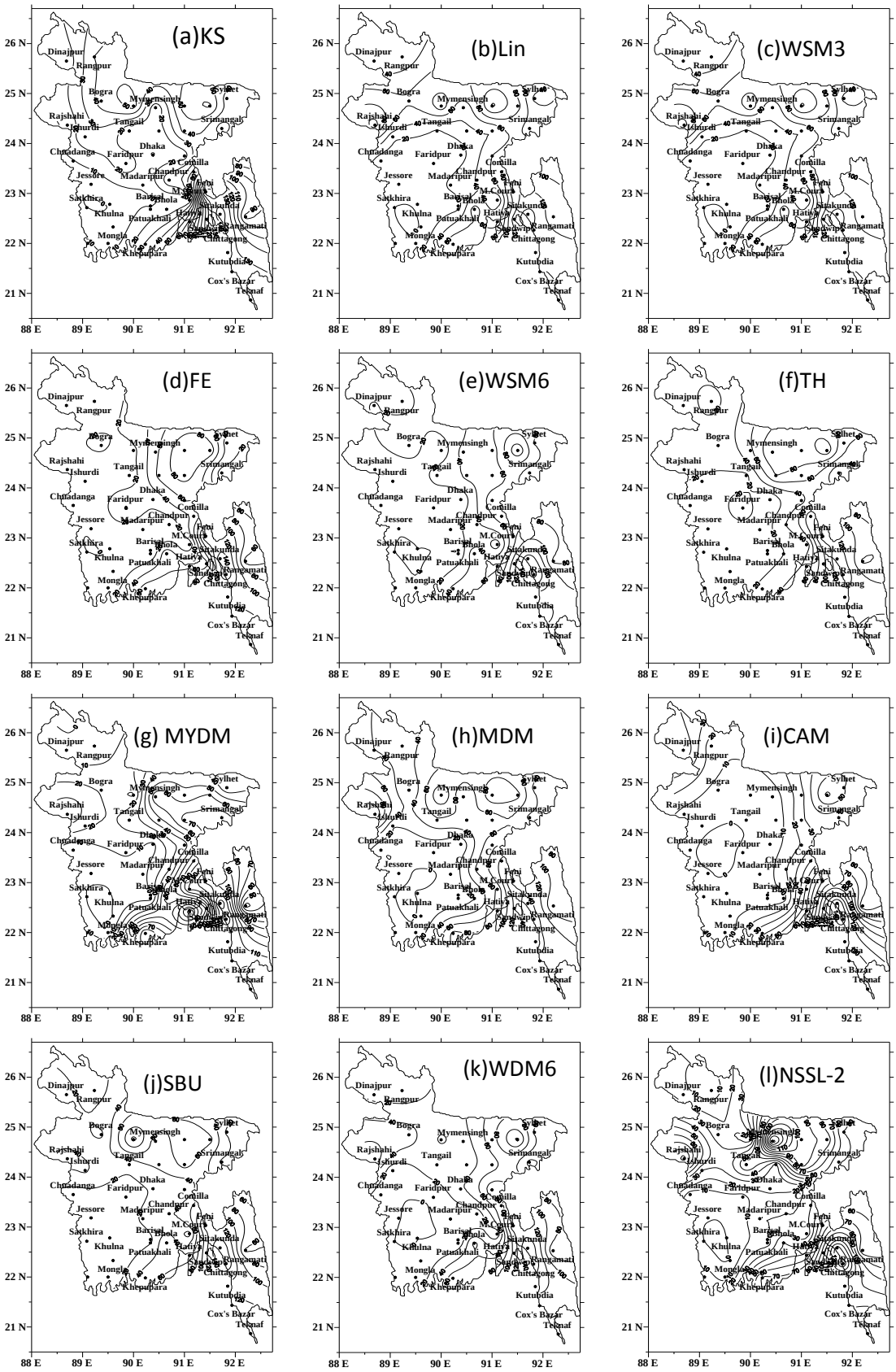

Fig.3: Distribution of 24 hour model simulated rainfall using different MPs on 23 June 2015 all over Bangladesh.

WSM3 has simulated heavy rainfall in the E-SE and northern regions and light rainfall is simulated from centre to W-SW region (Fig. 3c). Maximum rainfall simulated at Chittagong, Sitakunda, Teknaf, Kutubdia and Cox's Bazar are 145, 141, 134, 133 and 126 mm respectively. The model simulated maximum rainfall pattern is matched with the observed rainfall pattern. Ferrier, WSM6 and Thompson schemes have simulated heavy rainfall in the S-SE and NE regions and light rainfall in other regions of the country as shown in Fig. 3(d-f)). Maximum rainfall of 158, 157, 144, 135 and 133 mm are simulated by FE and 135, 131, 134, 141 and 108 mm by Thompson scheme at Chittagong, Sitakunda, Feni, Teknaf and Cox's Bazar respectively, which is matched with the observed maximum rainfall position but maximum rainfall position is shifted from Hatiya towards E-NE region i.e. Feni region. Maximum rainfall of 169, 155, 140, 112 and 109 mm are simulated by WSM6 at Chittagong, Sitakunda, Teknaf, Sandwip and Kutubdia. The model simulated maximum rainfall in the SE region is matched with the observed rainfall and minimum rainfall is also matched all through the country. MYDM and MDM schemes have simulated heavy rainfall in the S-SE and northern regions and light rainfall in other regions of the country (Fig. 3g & h). Maximum rainfall amounts of 143, 143, 140, 117, 112 and 110 mm are simulated by MYDM and the amounts of 142, 153, 149, 146, 151 and 138 mm are simulated by MDM scheme at Teknaf, Chittagong, Sitakunda, Kutubdia, Feni and Cox's Bazar respectively, which are matched with the observed maximum rainfall position.

CAM, SBU and WDM6 schemes have simulated heavy rainfall in the S-SE and NE regions and light rainfall in other regions of the country as shown in Fig. 3(i-k). Maximum rainfall amounts of 146, 137, 136, 129 and 111 mm are simulated by CAM and the amounts 159, 140, 125, 112 and 118 mm by SBU and 155, 140, 102, 133 and 105 mm by WDM6 at Chittagong, Teknaf, Cox's Bazar, Kutubdia and Sandwip respectively, which are matched with the observed maximum rainfall position. The model simulated maximum rainfall position is matched with the observed rainfall position in the SE region. NSSL-2 scheme has been simulated heavy rainfall in the S-SE and northern regions and light rainfall in the centre to NW and SW regions as shown in Fig. 3(l). Maximum rainfall amounts simulated at Mymensingh, Chittagong, Sitakunda, Teknaf and Cox's Bazar are 159, 149, 135, 129 and 108 mm respectively.

The model simulated maximum rainfall for different microphysics schemes is matched with the observed rainfall in the SE region and observed heavy rainfall position is shifted from Hatiya towards Feni region.

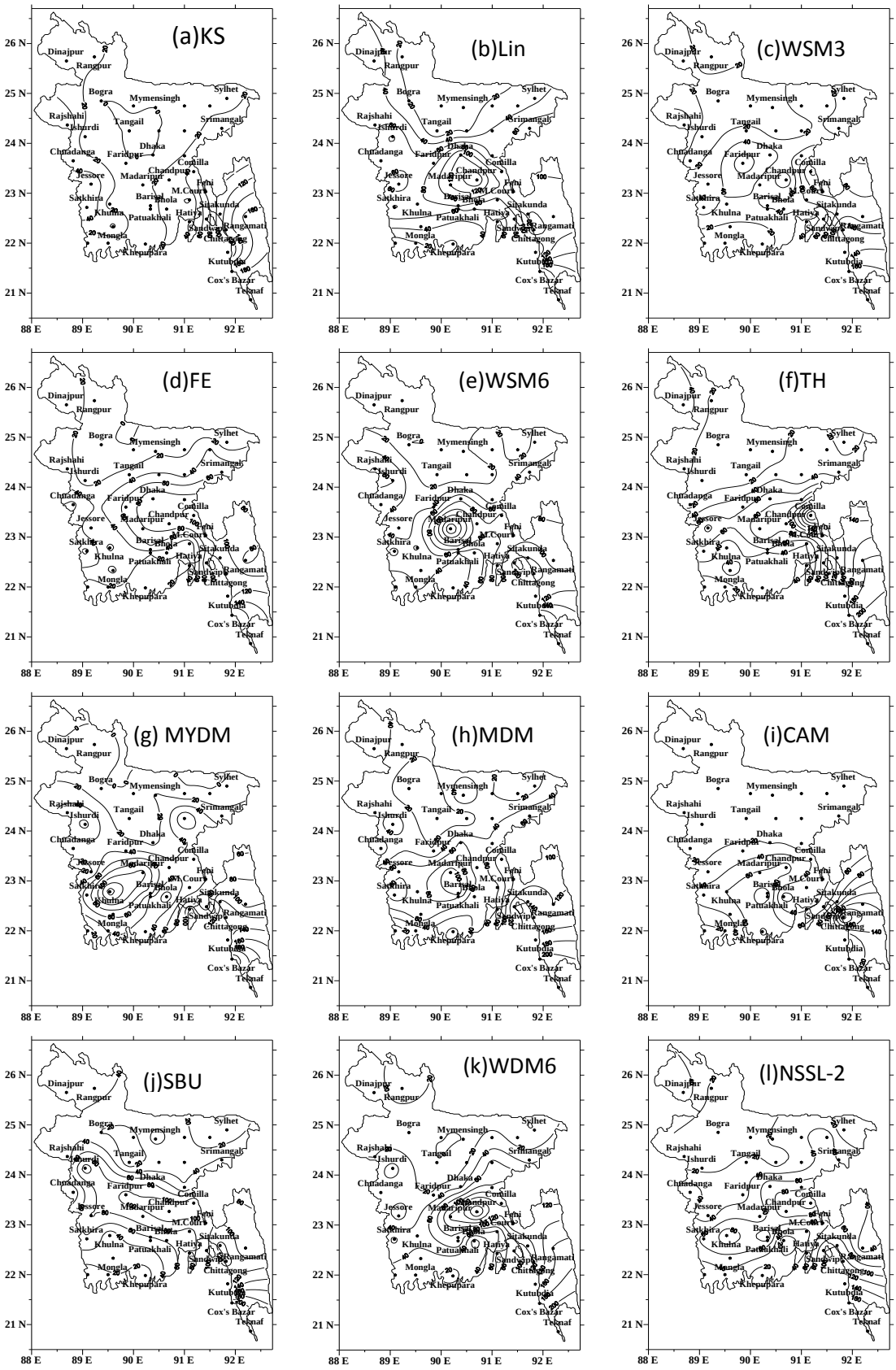

Fig.4: Distribution of 24 hour model simulated rainfall using different MPs on 24 June 2015 all over Bangladesh.

4.1.2 Observed, TRMM and Model Simulated Rainfall for 24 June 2015

The heavy rainfall is observed on 24 June in the SE region (Fig. 2b) and light rainfall is found in all other regions of Bangladesh. Significant amount of rainfall is observed at Cox's Bazar, Kutubdia, Teknaf and Chittagong and the amounts are 367, 241, 177 and 128 mm respectively on 24 June 2015. Maximum TRMM rainfall (Fig. 2f) is seen at Cox's Bazar, Kutubdia and Teknaf with the values of 109, 82 and 82 mm respectively. It is seen that the distribution pattern of TRMM and observed rainfall are similar but TRMM rainfall is much lower than that of observed rainfall.

The rainfall amounts simulated using 12 different MPs on 24 June 2015 are presented in Fig. 4(a-l). The Kessler and WSM3 schemes have simulated heavy rainfall in the S-SE regions and light rainfall in other regions of the country (Fig. 4a & c). Maximum rainfall amounts of 204, 178, 130 and 111 mm are simulated by KS and the amounts of 175, 170, 142 and 83 mm are simulated by WSM3 scheme at Teknaf, Chittagong, Cox's Bazar and Sitakunda respectively, which match with the observed maximum rainfall position. Lin *et al*. scheme has simulated heavy rainfall (Fig. 4b) in the central and SE region and light rainfall in the SW, NW and NE regions of Bangladesh. Maximum rainfall is simulated at Cox's Bazar, Teknaf, Chandpur, Chittagong and Sitakunda regions having 200, 168, 160, 137 and 120 mm respectively. The simulated position of maximum heavy rainfall in the SE region is found to match with the observed rainfall. The FE, WSM6 and TH schemes have simulated heavy rainfall in the central and S-SE regions and light rainfall in other regions of the country (Fig. 4(d-f)). Maximum rainfall amounts of 189, 137, 122, 108 and 104 mm are simulated by FE and the amounts 195, 213, 135, 122 and 157 mm by TH scheme at Cox's Bazar, Teknaf, Chittagong, Sitakunda and Feni respectively, the positions of which are matched with the observed maximum rainfall position. Maximum rainfall is simulated by WSM6 scheme at Madaripur, Cox's Bazar, Teknaf, Chittagong and Sandwip regions and the amounts are 186, 185, 151, 140 and 125 mm respectively. The simulated position of maximum rainfall in the SE region is matched with the observed rainfall. The MYDM scheme has simulated heavy rainfall (Fig. 4g) in the SE and SW regions of the country on that day. Maximum rainfall is simulated at Cox's Bazar, Teknaf, Khulna, Chittagong, Kutubdia and Sitakunda regions where the amounts of rainfall are 245, 167, 154, 141, 134 and 124 mm respectively and the simulated heavy rainfall distribution pattern is similar to the observed maximum rainfall in the SE region. MDM and WDM6 schemes (Fig. 4 (h & k)) have simulated heavy rainfall in the central and SE regions and light rainfall in other regions of the country. Maximum rainfall

amounts are 217, 210, 162, 146, 139 and 119 mm simulated by MDM and the amounts 234, 182, 145, 112, 109 and 162 mm are simulated by WDM6 scheme at Teknaf, Cox's Bazar, Kutubdia, Chittagong, Sitakunda and Rangamati respectively, the simulated rainfall position being matched with the observed maximum rainfall position. CAM, SBU and NSSL-2 schemes have simulated heavy rainfall in the SE regions and light rainfall in other regions of the country (Fig. 4(i, j & l)). Maximum rainfall amounts of 211, 131, 106 and 76 mm are simulated by CAM, the amounts of 128, 204, 220 and 100 mm by SBU scheme and the amounts of 109, 179, 173 and 134 mm by NSSL-2 at Chittagong, Teknaf, Cox's Bazar, and Kutubdia respectively, the position of heavy rainfall is similar to the observed maximum rainfall position. The model simulated maximum rainfall and its position for different microphysics schemes are found to match with the observed rainfall in the SE region and observed heavy rainfall position.

4.1.3 Observed, TRMM and Model Simulated Rainfall on 25 June 2015

The heavy rainfall is observed on 25 June in the central to south and SE region (Fig. 2c) and light rainfall in all other regions of the country. The amounts of rainfall observed are188, 210, 197, 177, 163 and 135 mm at Chandpur, Cox's Bazar, Kutubdia, Hatiya, Bhola and Barisal respectively. On that day TRMM (Fig. 2g) derived light rainfall all over the country. Maximum TRMM rainfall amounts seen at Cox's Bazar, Teknaf and Kutubdia are 71, 82 and 37 mm respectively. It is seen that the distribution pattern of TRMM and observed rainfall are similar but TRMM derived rainfall is much lower than that of observed rainfall.

The model simulated rainfall amounts using different MP schemes on 25 June 2015 are presented in Fig. 5(a-l). The Kessler scheme has simulated heavy rainfall (Fig. 5a) in the S-SE, east and SW regions and light rainfall in the central to W-NW regions of Bangladesh. Significant amounts of rainfall simulated at Teknaf, Bhola, Satkhira, Chittagong and Cox's Bazar regions are 165, 164, 157, 125 and 116 mm respectively. The model simulated maximum rainfall is matched with the observed rainfall at Bhola but maximum rainfall in the Chandpur station is shifted towards Comilla region. Lin et al. and WSM3 schemes have simulated heavy rainfall in the central and SE regions and light rainfall in other regions of the country (Fig. 5(b-c)). Maximum rainfall amounts of 281, 182, 133, 131 and 126 mm are simulated by Lin et al. and the amounts of 256, 169, 112, 134 and 76 mm by WSM3 scheme at Teknaf, Cox's Bazar, Chittagong, Dhaka and Bhola respectively.

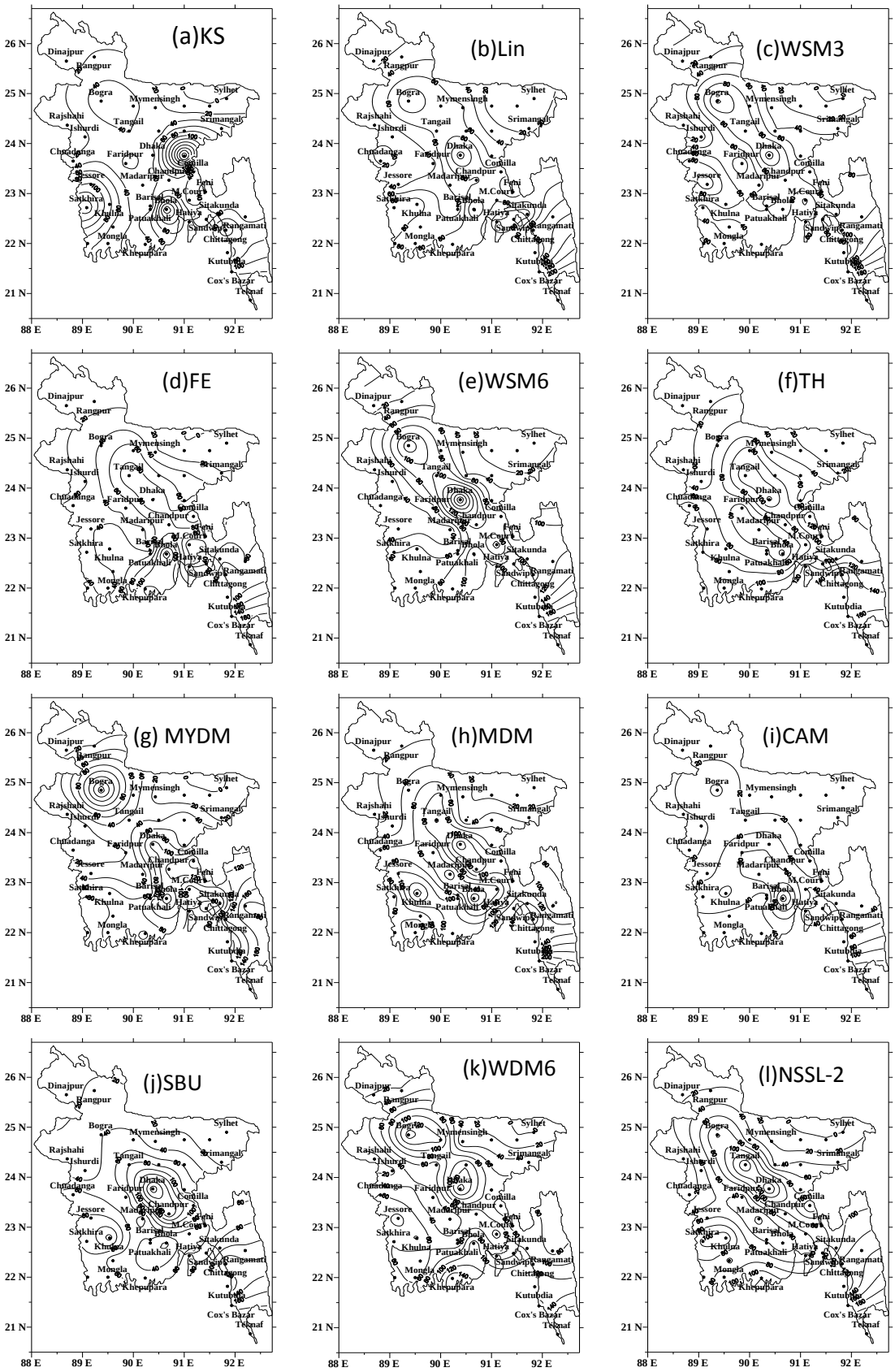

Fig.5: Distribution of model simulated rainfall for 24 hour prediction using different MPs coupling with KF scheme on 25 June 2015 all over Bangladesh.

The model simulated maximum rainfall is matched with the observed rainfall at Bhola but maximum rainfall at Chandpur is shifted towards Comilla region. The FE scheme has simulated heavy rainfall (Fig. 5d) in the central to S-SE regions and light rainfall in the other regions of Bangladesh.

Maximum rainfall is simulated at Teknaf, Bhola, Cox's Bazar, Khepupara and Dhaka regions and the amounts are 234, 161, 148, 123 and 103 mm respectively. WSM6, MYDM, WDM6 and NSSL-2 schemes have simulated heavy rainfall in the NW, central and S-SE regions and light rainfall in other regions of the country (Fig. 5(e, g, k & l)). Maximum rainfall amounts of270, 223, 176, 135 and 123 mm has been simulated by WSM6 and the amounts of 210, 111, 105, 174 and 160 mm by MYDM scheme at Teknaf, Dhaka, Cox's Bazar, Bogra and Bhola respectively. The model simulated maximum rainfall is matched with the observed rainfall at Bhola. Maximum rainfall amounts simulated are 224, 151, 109, 109, 83 and 74 mm 265, 165, 174, 128, 117 and 133 by WDM6 and NSSL-2 schemes at Teknaf, Chittagong, Dhaka, Cox's Bazar, Khulna and Rangamati respectively. The model simulated maximum rainfall does not match with the observed rainfall except Cox's Bazar. TH and MDM schemes have simulated heavy rainfall in the central, S-SE and SW regions and light rainfall in other regions of the country (Fig. 5(f & h)). Maximum rainfall amounts of 212, 182, 153, 126 and 116 mm have been simulated by Thompson and the amounts of 257, 180, 229, 157 and 117 mm by MDM scheme at Teknaf, Chittagong, Cox's Bazar, Dhaka and Khepupara regions respectively. The model simulated maximum rainfall does not match with the observed rainfall except Cox's Bazar. The CAM scheme has simulated heavy rainfall (Fig. 5i) in the SE regions of Bangladesh. Maximum rainfall amounts simulated at Teknaf, Bhola and Cox's Bazar are 170, 138 and 112 and 122 mm respectively and the distribution pattern of heavy rainfall is matched with the observed maximum rainfall.SBU scheme (Fig. 5j) has simulated maximum rainfall in the central, SE and SW regions and the amounts are 219, 196, 172, 142, 130 and 106 mm respectively at Teknaf, Chittagong, Dhaka, Cox's Bazar, Khulna and Rangamati respectively.

The model simulated maximum rainfall position and amount has been matched with the observed rainfall position and amount. All MPs have simulated maximum rainfall in the central to SE regions but observed rainfall is found in the SE region. The model simulated maximum rainfall is matched with the observed rainfall at Bhola but maximum rainfall at Chandpur has been shifted towards SE region i.e. Chittagong.

4.1.4 Observed, TRMM and Model Simulated Rainfall on26June 2015

The heavy rainfall has been observed by Bangladesh Meteorological Department (BMD) in the S-SE region (Fig. 2d) and light rainfall is seen in all other regions of the country on 26 June. The amounts of rainfall observed are 263, 232, 126 and 121 mm at Cox's Bazar, Teknaf, Barisal and Khepupara respectively. On that day, TRMM (Fig. 2h) derived light rainfall all over the country with little higher values in the SE region. The TRMM rainfall amounts seen at Cox's Bazar, Teknaf and Bhola are 35, 32 and 19 mm respectively. It is seen that the distribution pattern of TRMM and observed rainfall are similar but TRMM derived rainfall is much lower than that of observed rainfall.

The rainfall amounts simulated using different MPs on 26 June 2015 are presented in Fig. 6(a-l). The Kessler, Lin *et al.* and WSM3 schemes have simulated heavy rainfall (Fig. 6(a, b & c)) in the SE and NW regions and light rainfall in the other regions of Bangladesh. Maximum rainfall amounts simulated are 192, 187, 175, 139, 88 and 57 mm by using Kessler, and 231, 200, 135, 145, 183 and 116 mm by using Lin et al respectively and 193, 205, 164, 141, 147 and 106 mm by using WSM3 scheme respectively at Cox's Bazar, Teknaf, Chittagong, Sitakunda, Feni and Sandwip. The model simulated maximum rainfall in the SE region is matched with the observed rainfall and minimum rainfall is also matched all through the country. The FE, WSM6 and TH schemes have simulated heavy rainfall in the SE regions and light rainfall in the other regions of Bangladesh as shown in Fig. 6(d, e & f).Maximum rainfall amounts simulated are 214, 212, 169, 154 and 131 mm by FE and 203, 187, 147, 150 and 157 mm by WSM6 and 217, 230, 202, 126 and 164 mm by Thompson scheme at Teknaf, Cox's Bazar, Feni Chittagong and Sitakunda respectively. The model simulated maximum rainfall in the SE region is matched with the observed rainfall and minimum rainfall is also matched all through the country. The MYDM scheme has simulated heavy rainfall (Fig. 6g) in the centre to NW and SE regions. Maximum rainfall is simulated at Teknaf, Cox's Bazar, Chittagong, Feni and Kutubdia regions and the amounts are 200, 195, 177, 174 and 156 mm respectively. MDM, CAM, SUB, WDM6 and NSSL-2 have simulated heavy rainfall (Fig. 6h, i, j, k & l)) in the SE regions of the country. Maximum rainfall amounts simulated are 228, 223, 222, 130 and 126 mm by MDM scheme, 167, 204, 132, 127 and 80 mm by CAM scheme, 173, 187, 204, 148 and 140 mm by SBU scheme 110, 222, 215, 180 and 200 mm by WDM6 and 127, 200, 204, 165 and 158 mm by NSSL-2 at Kutubdia, Teknaf, Cox's Bazar, Chittagong and Feni respectively.

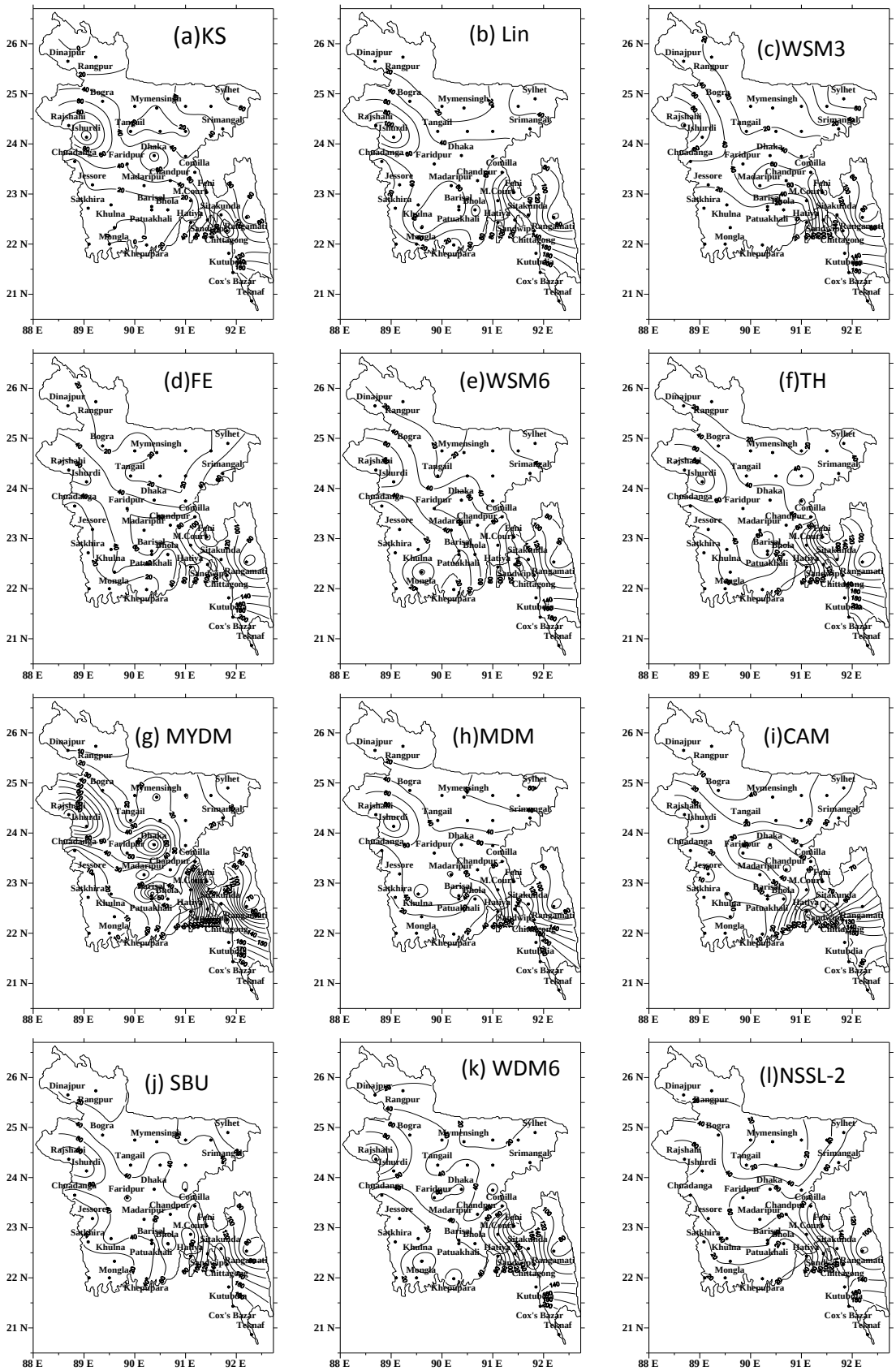

Fig.6: Distribution of 24 hour model simulated station average rainfall using different MPs of 26 June 2015 all over Bangladesh.

The model simulated maximum rainfall in the SE region and minimum rainfall all through the country is found to match with the observed rainfall on 26 June.

4.1.5 Area average rainfall during 23 -26 June 2016

Average observed rainfall of 35 BMD stations all over Bangladesh, model simulated by different MPs and TRMM rainfall during 23-26 June 2015 are presented as in Fig. 7(a-d). Model simulated rainfall by different MPs, TRMM rainfall and heavy rainfall observed in the 5 SE stations during 23-26 June 2015 are presented as in Fig. 7(e-h).On 23 June, all MPs schemes have simulated (Fig. 7(a-b) almost similar average rainfall as observed from 35 Meteorological stations over Bangladesh and SE regions. Lin et al. and MDM schemes have simulated maximum rainfall by the MP schemes over whole Bangladesh and SE regions. TRMM derived rainfall is much lower than that of observed rainfall all over Bangladesh and also 5 heavy rainfall stations in the SE region of the country during 23-26 June 2015. On 24 June, WSM6, MYDM and NSSL2 schemes have simulated (Fig. 7c) almost similar average rainfall as observed from 35 Meteorological stations over Bangladesh and Lin et al., MDM and SBU schemes simulated maximum rainfall among the MP schemes and other MP schemes has simulated less rainfall than that of observed. KS and CAM schemes have simulated lowest all Bangladesh averaged rainfall among all the MPs on this day. All MP schemes (Fig. 7d) have simulated less rainfall than that of observed in the SE region (i.e. heavy rainfall stations) on this day. On 25 June (Fig. 7e), WSM6, Thompson and MDM have simulated almost equal amount of rainfall as that of observed from all Bangladesh averaged rainfall and other MPs have simulated less rainfall. All MPs have simulated almost similar amount of rainfall (Fig. 7f) except KS, MDM and CAM schemes. MDM scheme has simulated much higher rainfall, and KS and CAM have simulated less rainfall in the SE region (i.e. heavy rainfall stations) of the country. Lin *et al*., Thompson, MDM, SBU and WDM6 schemes have simulated higher rainfall than that of observed and other MPs have simulated almost equal amount of rainfall from all Bangladesh averaged rainfall on 26 June (Fig. 7g). All MPs have simulated almost similar average rainfall (Fig. 7h) as observed in the SE regions of the country on this day.

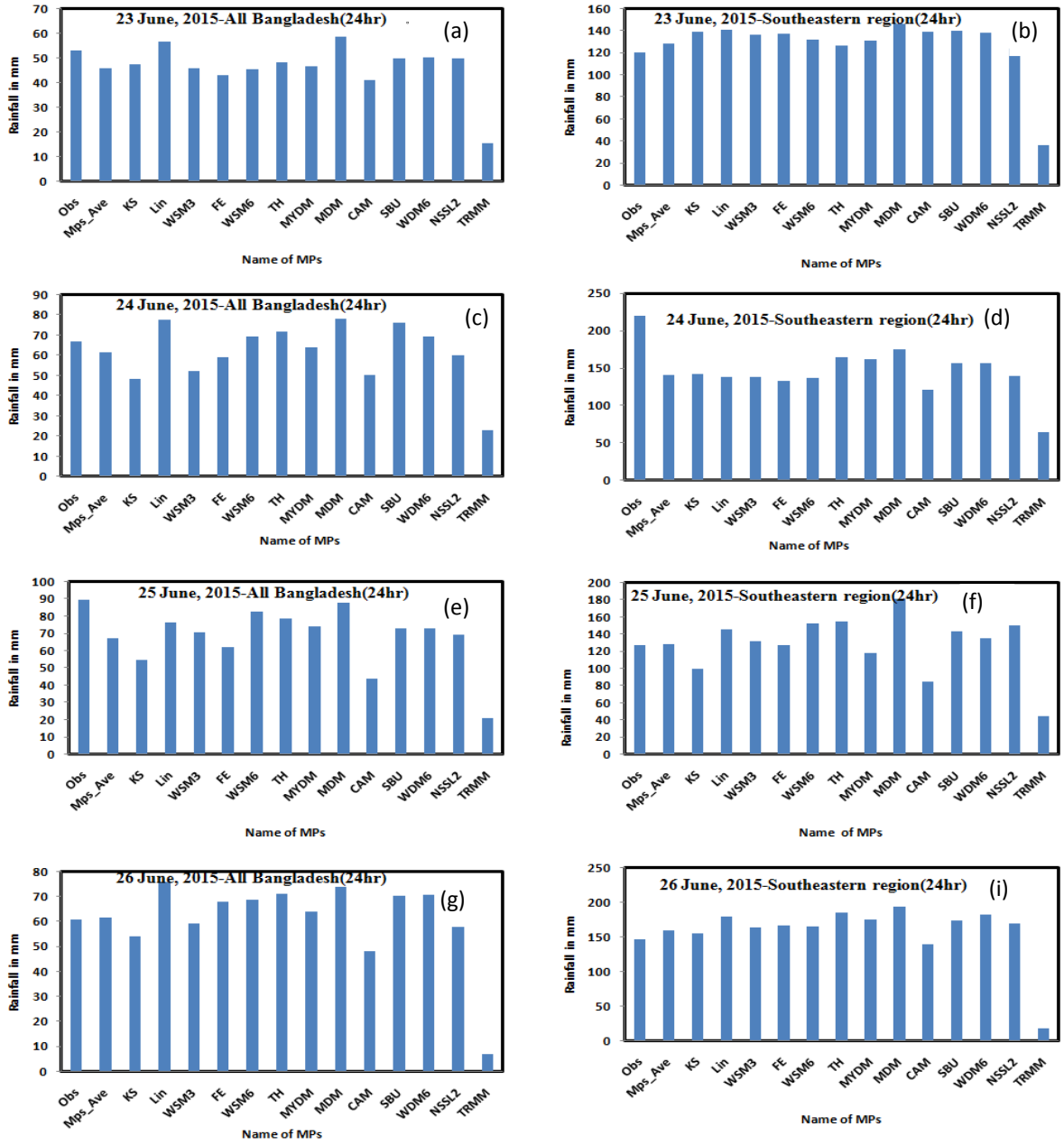

Fig. 7: Model simulated, TRMM derived and observed all Bangladesh stations average rainfall and also heavy rainfall stations (5 stations) in the SE region of the country during 23 -26 June 2015 using different MPs

4.1.6 Space and Time dependent Rain during 23-26 June 2015

Model simulated rainfall using different MPs and 3-hourly observed rainfall at Chittagong, Cox's Bazar, Kutubdia, Sitakunda and Teknaf are presented in Fig. 8(a-f)) during 23-26 June 2015. At Chittagong (Fig. 8a), the time of 3-hourly simulated maximum rainfall is almost matched with the observed maximum rainfall except some anomalies. On 24 June, the observed peak is found at 0000 UTC but some of MPs have simulated significantly higher amount of rainfall by CAM scheme on 25 June at 0000 UTC. The time of observed

maximum rainfall is almost matched with the model simulated time with little anomalies at Cox's Bazar, Kutubdia, Sitakunda and Teknaf stations as shown in Fig. 8 (b-e).

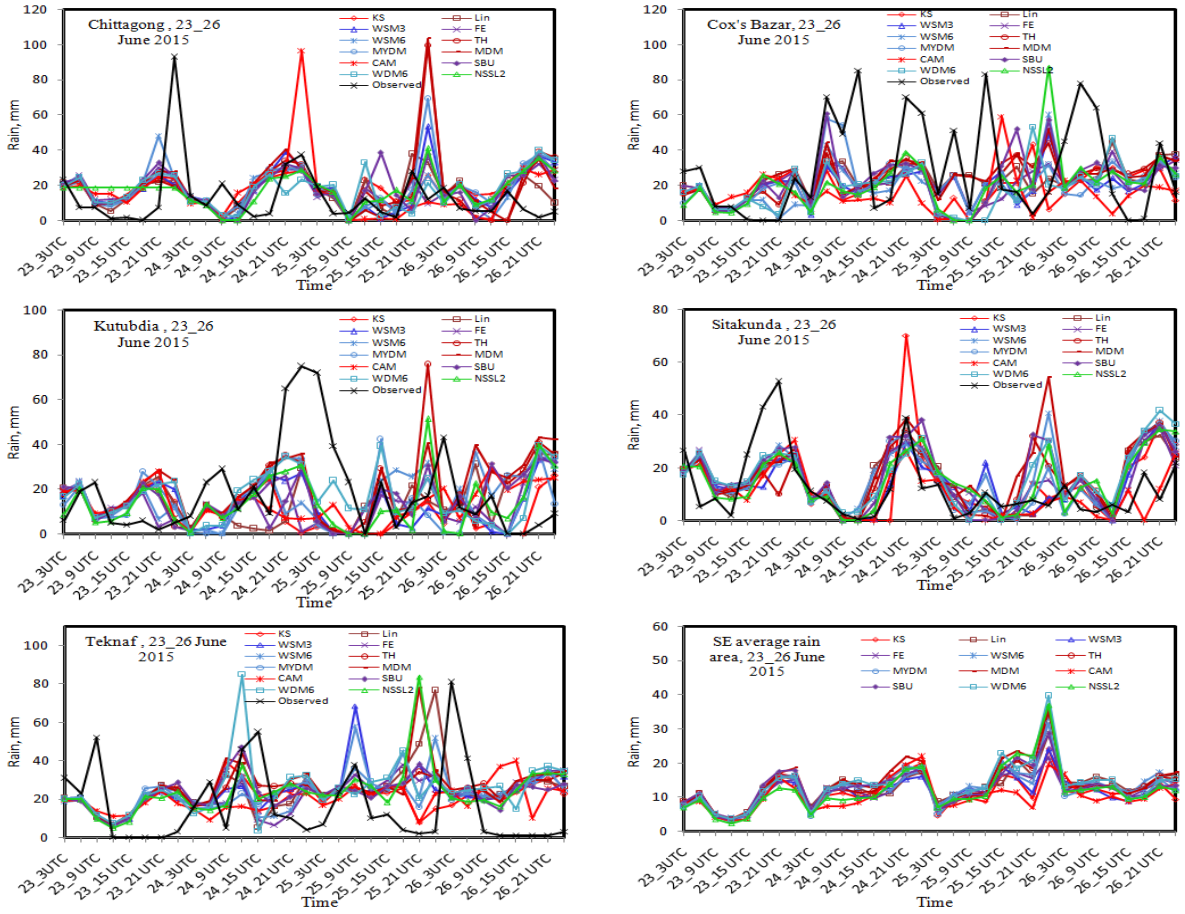

Fig.8: 3-hourly observed and model simulated rain at (a) Chittagong (b) Cox's Bazar, (c) Kutubdia,(d) Sitakunda, (e) Teknaf and (f) All 5 stations in the SE region using different MPs coupling with KF scheme during 23-26 June 2015.

4.1.7 Vertical velocity during 23-26 June 2015

The simulated position of maximum updraft has been identified for different MP schemes every day during 23-26 June 2015 when heavy rainfall is observed in the SE region of Bangladesh. Along the line of maximum updraft, vertical velocities (shaded) have been analyzed during 23-26 June but the figure has given for 25 June for different MP schemes and is presented in Fig. 9(a-l). The times and position of maximum updrafts simulated are different for different MP schemes. The maximum updrafts simulated are 9, 17, 10, 9, 12, 14, 21, 17, 5, 13, 12 and 18 ms^{-1} by KS, Lin et al., WSM3, FE, WSM6, TH, MYDM, MDM, CAM, SBU, WDM6 and NSSL-2 schemes (Figure not shown) at the times of 0900, 2100, 0900,1200, 1200, 1800, 1200, 0900, 1800, 2100, 1200 and 0900 UTC respectively on 23 June. The updraft is found maximum at around 500-200 hPa by KS, Lin, WSM6, TH

schemes and 600-200 hPa by WSM3, MYDM, MDM, SBU and WDM6 schemes on 23 June. The updraft simulated by CAM is much less on this day.

The maximum updrafts are9, 15, 11, 8, 17, 16, 26, 17, 7, 15, 16 and 16 m s^{-1}simulated by KS, Lin et al., WSM3, FE, WSM6, TH, MYDM, MDM, CAM, SBU, WDM6 and NSSL-2 schemes (Figure not shown) at 1200, 1500, 2100, 2100, 0900, 2100, 1200, 1200, 2400, 1200, 1500 and 1200 UTC respectively on 24 June 2015. The simulated updraft is maximum at around 600-200 hPa by Lin et al., WSM3, WSM6, MYDM, MDM and WDM6 schemes. The updraft simulated by KS, FE, MDM and NSSL-2 is much less on this day.

The maximum updrafts are10, 15, 13, 10, 17, 18, 17, 5, 14, 16, 14 and 16 m s^{-1} simulated by KS, Lin et al., WSM3, FE, WSM6, TH, MYDM, MDM, CAM, SBU, WDM6 and NSSL-2 schemes at 1200, 1800, 1500, 1800, 2100, 1800, 1500, 1500, 2100, 1500, 1500 and 2100 UTC respectively on 25 June and are presented in Fig. 9(a-l). The updraft is maximum at around 800-200 hPa simulated by Lin et al., MYDM and MDM schemes on this day. WSM6 and WDM6 have simulated maximum updraft at around 600-200 hPa, Thompson and NSSL-2 at 400-100 hPa. The updraft simulated by KS, CAM and FE is much less on this day. The maximum updrafts are 9, 20, 17, 5, 19, 13, 20, 10, 3, 16, 18 and 11 m s^{-1}simulated by KS, Lin et al., WSM3, FE, WSM6, TH, MYDM, MDM, CAM, SBU, WDM6 and NSSL-2 schemes at the times of 0900 UTC for all MP schemes except FE and MDM on 26 June (Figure not shown). FE scheme has simulated maximum updraft at 1200 UTC and MDM at 1500 UTC on this day. The maximum updraft is simulated at around 500-100 hPa by Lin *et al*., TH, SBU, WDM6 and NSSL-2, and at 700-100 hPa by WSM6 and MYDM on 26 June 2015. The updraft simulated by other MPs is less on this day. Maximum convection has been found by MYDM, NSSL-2, Lin *et al*., MDM schemes on 23 June, MYDM, WSM6, MDM schemes on 24 June, TH, WSM6, MYDM schemes on 25 June and Lin *et al.*, MYDM, WSM6 and WDM6 schemes on 26 June respectively. The updraft in the upper troposphere could be due to the latent heat release during glaciations and vapor deposition in all combination of MPs and KF scheme.

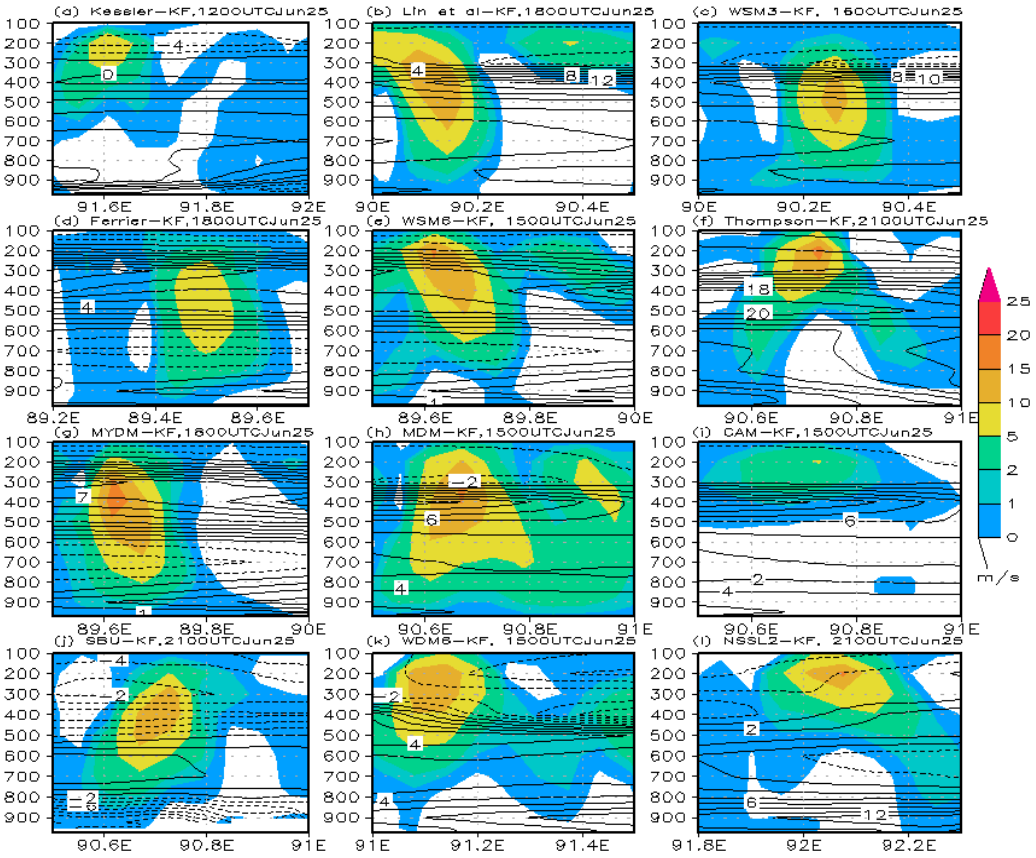

Fig. 9: WRF model simulated maximum vertical velocity (shaded) and vorticity (contour) along the line of maximum updraft using different MP schemes for 25 June 2015.

4.1.8 Vorticity

Along the line of maximum updraft, the vorticity (contour) has been studied for different MP schemes during 23-26 June and plotted for 25 June and is presented in Fig. 9(a-l). The positive vorticity has been simulated from 800 to 200 hPa levels for Lin et al., TH and SBU (Figure not shown) and negative vorticity below and above these levels on 23 June. KS, WSM3, FE, WSM6, MYDM, CAM, WDM6 and NSSL-2 schemes have simulated positive vorticity in the lower to middle troposphere from 900 to 400 hPa levels and negative vorticity in the upper troposphere on this day. On 24 June, positive vorticity has been simulated in the middle troposphere (Figure not shown) and negative vorticity in the lower troposphere and upper troposphere for all MPs except Lin *et al.*, MDM, WDM6 and NSSL-2 schemes. On 25 June, the positive vorticity is found in the lower to upper troposphere (Fig. 9(a-l)) at 900-300 hPa for KS, Lin et al., WSM3, MDM, CAM and WDM6 schemes. Ferrier, WSM6, MYDM and NSSL-2 schemes have simulated negative vorticity in the middle and upper troposphere and positive vorticity in the lower and middle to upper troposphere on this day. TH scheme has simulated positive vorticity in the lower to upper troposphere.

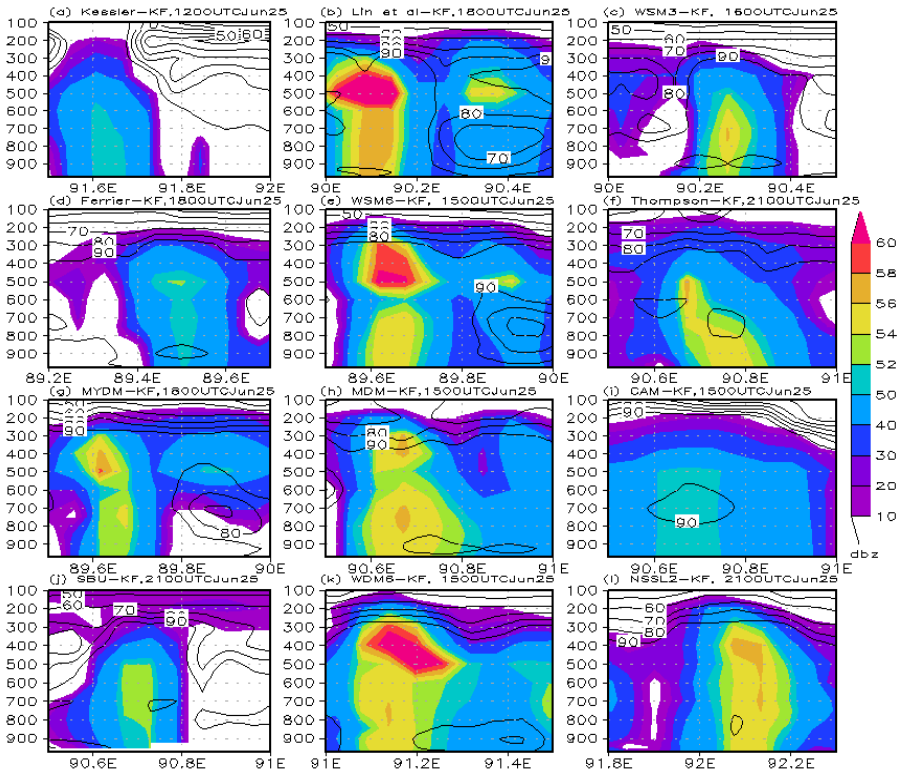

Fig. 10: WRF Model simulated reflectivity (shaded) and relative humidity (contour) using different MPs along the line of maximum vertical velocity on 25 June 2015.

4.1.9 Relative Humidity (RH)

The RH (contour) has been simulated along the line of maximum vertical velocity using different MPs on 23-26 June 2015 and is presented in Fig. 10(a-l) for 25 June. All MPs have simulated RH up to 100 hPa on 23-26 June 2015. On 23 June, all MPs schemes have simulated (Figure not shown) maximum RH >95% up to 400 hPa level except Kessler, CAM and WDM6 schemes where the vertical velocity is found maximum. Kessler scheme has simulated up to 200 hPa, and CAM and WDM6 schemes up to 300 hPa. On 24 June, RH >95% is simulated for all MPs up to 300 hPa level (Figure not shown) where the vertical velocity and reflectivity are found maximum. On 25 June, all MPs have simulated RH up to 100 hPa (Fig. 10(a-l)) and maximum RH >95% is simulated for all MPs up to 400 hPa level along the line where the vertical velocity and reflectivity is found maximum. All MPs have simulated RH >95% (Figure not shown) up to 100 hPa on 26 June except Lin *et al.*, WSM6 and WDM6 schemes along the line of maximum vertical velocity.

4.1.10 Reflectivity

The reflectivity (shaded) has been analyzed for the heavy rainfall events during 23-26 June but plotted for 25 June along the line of maximum vertical velocity using different MPs and is shown in Fig. 10(a-l). Reflectivity has been simulated up to 100 hPa by Lin *et al*., MDM and NSSL-2 on 23 June (Fig. not shown), Lin et, al., FE, TH, MYDM and MDM on 24 June (Fig. not shown), SBU and WDM6 on 25 June (Fig. 10(a-l)) and Lin *et al*., WSM6, MYDM, MDM, WDM6 and NSSL-2 on 26 June (Fig. not shown). The other MP schemes have simulated reflectivity up to 200 hPa during the period. Significant amount of reflectivity has been simulated from 500-300 hPa and from 600-300 hPa by Lin et al. and WDM6 scheme on 23 June and from 600-300 hPa by Lin *et al*., WSM6 and WDM6 scheme on 24 and 26 June. Significant amount of reflectivity has also been simulated from 600-300 hPa by Lin *et al*., WSM6 and WDM6 scheme on 25 June.

4.1.11 Cloud Water Mixing Ratio (CWMR)

The CWMR has been simulated using different MPs along the line of maximum vertical velocity during 23-26 June and is presented in Fig. 11(a-l) for 25 June. KS, WSM3, FE, MYDM and SBU schemes have simulated CWMR up to 150 hPa and Lin et al., WSM6, WDM6 and NSSL-2 schemes up to 250 hPa, and Thomson and MDM schemes have simulated CWMR up to 300 hPa on 23 and 24 June (Figure not shown). CAM scheme has simulated less CWMR and also minimum vertical velocity during 23-24 June. MYDM and SBU schemes have simulated CWMR maximum at 500-250 hPa, Lin et al., WSM3, FE and WSM6 at 700-300 hPa during 23-24 June. FE scheme has simulated maximum CWMR at 800-300 hPa, MYDM and SBU schemes have been simulated maximum CWMR at 500-300 hPa level on 25 June (Fig.11(a-l)). Significant amount of CWMR has been simulated by Thompson, MYDM and SBU schemes at 500-250 hPa level (Figure not shown) on 26 June.

The area averaged CWMR have been analyzed in the SE region of the country and plotted for different MPs during 23-26 June 2015. The results are presented as in Fig. 12(a-d). On 23 and 24 June, all MP schemes have simulated two maxima of CWMR from surface to 100 hPa. The first maximum is found at 800 hPa (Fig. 12(a-b)) and second maxima at 500 hPa level by all MPs schemes except Kessler scheme. Kessler scheme has simulated first maxima of CWMR at 800 hPa and second maxima at 200 hPa on 23 and 24 June 2015. The significant amount of CWMR is simulated up to 400 hPa by CAM and FE schemes and at 300 to 150 hPa by KS scheme during 23-26 June 2015. The maximum CWMR of 98 mg/kg is simulated

at 200 hPa by KS scheme on 23 June. The maximum values of CWMR simulated at 500 hPa are122 and 68 mg/kg by CAM and Ferrier schemes respectively. The CAM scheme has simulated significantly higher CWMR than that of all other MPs from surface to 500 hPa level on 24 June. The maximum values of CWMR simulated at 500 and 550 hPa are346 and 161 mg/kg by FE scheme on 25 and 26 June respectively. The NSSL-2 scheme has simulated lower area averaged CWMR and Ferrier scheme has simulated higher CWMR on 23, 25 and 26 June 2015.

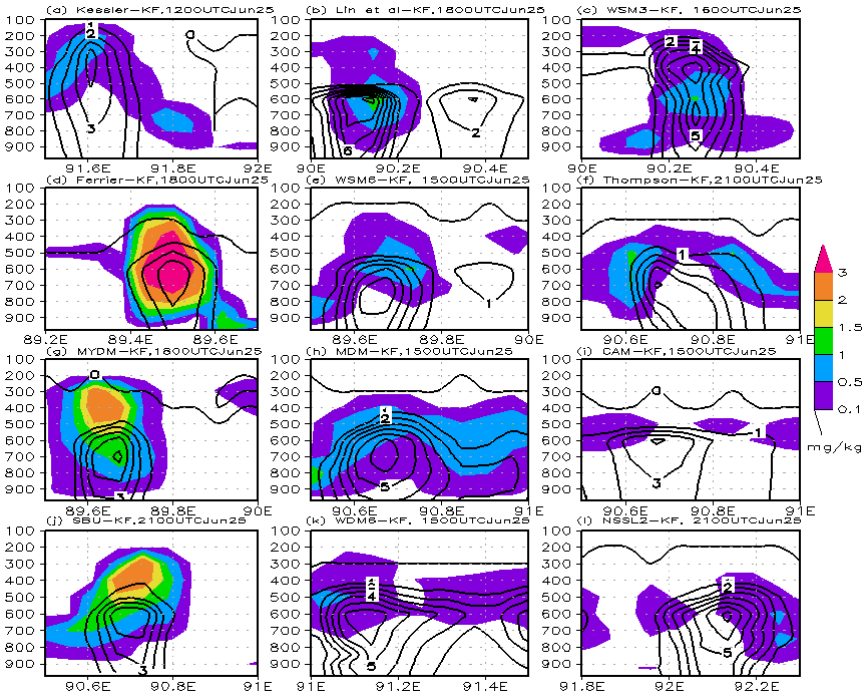

Fig.11: WRF Model simulated CWMR (shaded, g/kg) and RWMR (contour, g/kg) using different MPs along the line of maximum vertical velocity on 25 June 2015.

4.1.12 Rain Water Mixing Ratio (RWMR)

The RWMR (contour) has been simulated using different MPs along the line of maximum vertical velocity during 23-26 June and is presented in Fig. 11(a-l) for 25 June. WSM3 and KS schemes have simulated RWMR up to 100 and 200 hPa respectively and all other schemes simulated up to 500 hPa on 23 (Fig. not shown), 24 (Fig. not shown), 25 and 26 (Fig. not shown) June. The CWMR is found to have maximum along the vertical line where the vertical velocity and reflectivity are also maximum during the period. Kessler and WSM3 schemes have simulated maximum RWMR at 700-300 hPa and 400-200 hPa level respectively. The maximum RWMR has been simulated along the line of maximum vertical velocity by KS, Lin *et al.*, WSM3, Ferrier, WSM6, Thompson, MYDM, MDM, CAM, SBU,

WDM6 and NSSL-2 are 9, 4, 7, 1, 4, 2, 4, 3, 2, 4, 6 and 4 mg/kg respectively on 23 June. The maximum RWMR has been simulated by KS, Lin et al., WSM3, Ferrier, WSM6, Thompson, MYDM, MDM, CAM, SBU, WDM6 and NSSL-2 are 7, 6, 9, 1, 3, 6, 5, 4, 6, 2, 6 and 4 mg/kg respectively on 24 June 4; 8, 6, 3, 5, 5, 5, 6, 4, 4, 6 and 7 mg/kg on 25 June; 3, 4, 9, 0, 3, 3, 4, 2, 3, 4, 4 and 3 mg/kg on 26 June respectively.

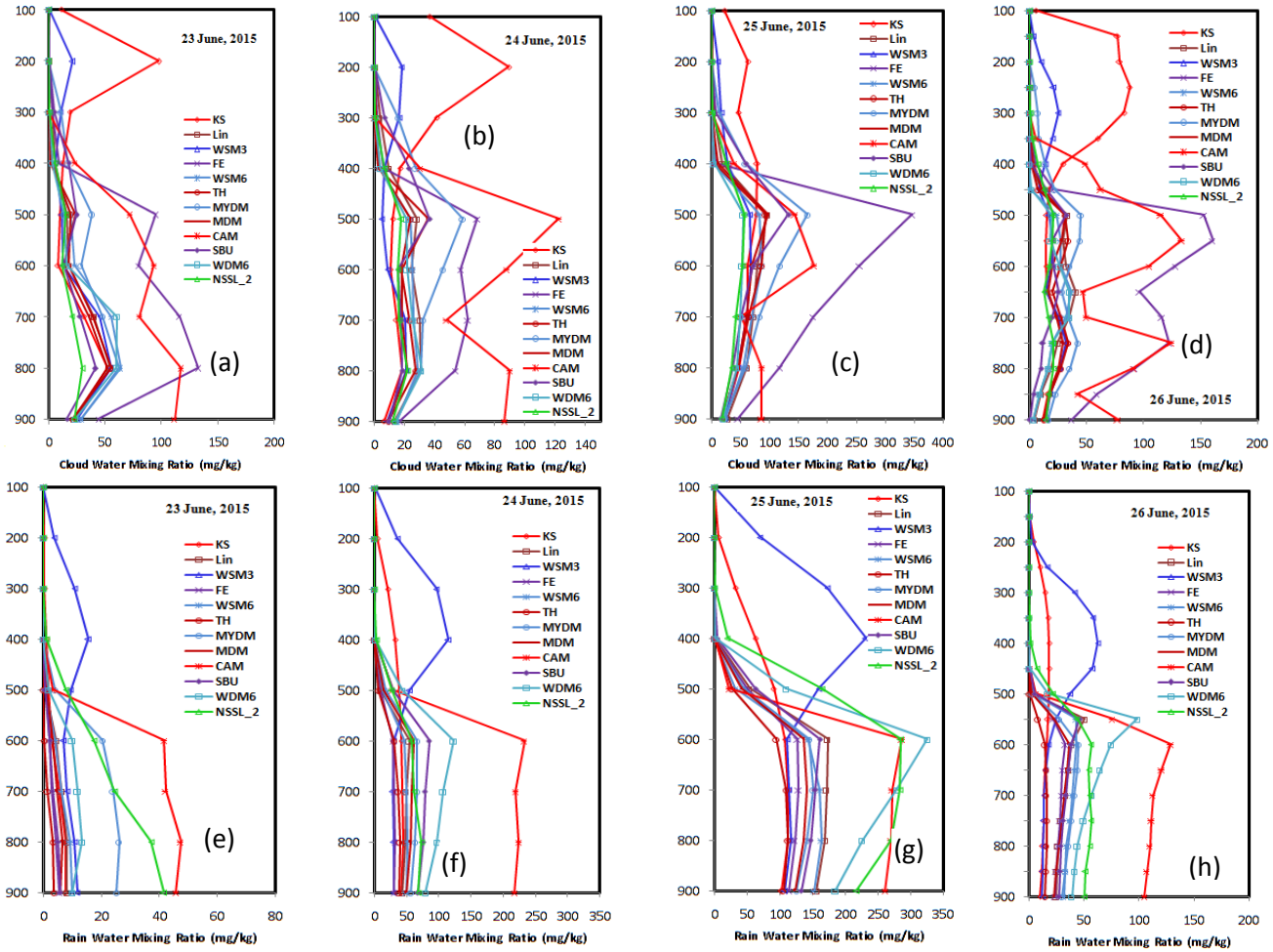

Fig. 12: Vertical profiles of time and space averaged (a-d) CWMR and (e-h) RWMR simulated by different MPs coupling with KF scheme during 23-26June 2015.

The area averaged RWMR has been plotted and analyzed using different MPs during 23-26 June 2015 in the SE region of the country and the results are presented as in Fig. 12(e-h). The RWMR has been simulated by all MP schemes except KS and WSM3 schemes up to 500 hPa level, where KS and WSM3 simulated up to 100 hPa level during the heavy rainfall period 23-26 June. Significant amount of RWMR has been simulated by CAM, NSSL-2 and WDM6 schemes up to 600 hPa. The other schemes have simulated lower RWMR but have increased continuously during 23-25 June throughout the troposphere. The highest amount of RWMR has been simulated by CAM scheme after that NSSL-2, MYDM and WDM6 schemes

respectively on 23 June (Fig. 12e). On 24 June (Fig. 12f), the highest amount of RWMR has been simulated by CAM scheme and lowest amount by FE scheme. The maximum values of RWMR have been simulated at 600 hPa and are 233 and 123 mg/kg by CAM and WDM6 schemes respectively. The simulated RWMR are as follows: CAM>WDM6>SBU>MYDM> NSSL-2 schemes. On 25 June, WDM6 scheme has simulated maximum RWMR and Thompson scheme simulated minimum RWMR throughout the troposphere (Fig. 12g). On 26 June, CAM and TH schemes have simulated maximum and minimum amount of area averaged RWMR throughout the troposphere (Fig. 12h). The maximum RWMR has been simulated by CAM and WDM6 schemes at 600 and 550 hPa, having 129 and 99 mg/kg on 26 June 2015 respectively. This suggests that the amount of rain simulated depends on RWMR in the lower to middle troposphere.

4.1.13 Cloud Ice Mixing Ratio (CIMR)

Area and time averaged vertical profiles of CIMR (mg/kg) using different MPs during 23-26 June are presented in Fig. 13(a-d). The area averaged CIMR has been simulated at 500-100 hPa level and found maximum at 300-150 hPa during 23-26 June 2015. MYDM scheme has simulated significantly higher amount of CIMR than that of other MP schemes during 23-26 June. It is evident that substantial difference exists between the various cloud ices. The MYDM profile has exhibited a prominent spike containing much larger CIMR values between 300-150 hPa and TH scheme has simulated less CIMR during 23-26 June. On 23 June, the order of the MPs schemes of simulated area averaged CIMR is MYDM> MDM> WSM6> WDM6> NSSL-2> Lin> SBU> CAM> Thompson schemes respectively. During 24-26 June, the order of the MPs schemes of simulated area averaged CIMR is MYDM> MDM> WDM6>WSM6>NSSL-2>Lin> CAM>SBU>TH schemes respectively.

4.1.14 Cloud Graupel Mixing Ratio

Area and time averaged vertical profiles of CGMR (mg/kg) using different MPs during 23-26 June are shown in Fig. 13(e-h). The CGMR has been simulated by Lin, WSM6, Thompson, MYDM, CAM, WDM6 and NSSL-2 and the other MPs have not simulated. The area averaged CGMR has been simulated at 700-100 hPa level and found maximum at 600-300 hPa during 23-26 June 2015. WDM6 and Thompson schemes have simulated maximum and minimum CGMR during 23-26 June except 23 June. It is evident that substantial difference exists between the various MPs for the simulation of cloud graupel. All MP schemes have

exhibited a prominent spike containing much larger CGMR values between 500-400 hPa, and Thompson and NSSL-2 schemes have simulated less CGMR.

On 23 June, the order of MPs schemes for simulated area averaged CGMR (Fig. 14a) is MYDM>WDM6>WSM6> Lin> CAM> NSSL-2>TH schemes respectively. On 24 June (Fig. 14b), the order of MPs schemes for simulated area averaged CGMR is WDM6> MYDM> WSM6> Lin> CAM> NSSL-2> Thompson schemes respectively. On 25 June (Fig.14c), the order of MPs schemes for simulated area averaged CGMR is WDM6> WSM6> MYDM> Lin> NSSL-2> CAM> Thompson schemes respectively. On 26 June (Fig. 14d), the order of MPs schemes for simulated area averaged CGMR is WDM6> WSM6> Lin> MYDM> CAM> NSSL-2> Thompson schemes respectively. Sharp spikes of graupel are found to be76, 209 and 78 mg/kg at 500 hPa level on 24, 25 and 26 June respectively for WDM6 scheme.

4.1.15 Cloud Snow Mixing Ratio

Area and time averaged vertical profiles of CSMR (mg/kg) using different MPs in combination with KF scheme during 23-26 June are shown in Fig. 13(i-l). The CSMR has been simulated by Lin, FE, WSM6, TH, MYDM, MDM, CAM, SBU, WDM6 and NSSL-2 schemes and the other MPs have not simulated CSMR. The area averaged CSMR has been simulated at 600-100 hPa level and found maximum at 500-200 hPa during 23-25 June 2015. SBU and Lin et al. schemes have simulated maximum and minimum CSMR during 23-26 June. Significant amount of CSMR has been simulated by SBU, CAM, MDM, MYDM and Thompson MPs during 23-26 June. It is evident that substantial difference exists between the various MPs for the simulation of cloud snow. All MP schemes have exhibited a prominent spike containing much larger CSMR values between 400-100 hPa, and Thompson and MYDM schemes has simulated less CSMR. CAM has simulated maximum CSMR at 500 hPa, SBU at 300 hPa and all other MPs have simulated maximum at 400 hPa level.

Significantly higher amount of CSMR has been simulated for all MP schemes during 24-25 June than that of 23 and 26 June. On 23 June, the SBU scheme has generated the greatest amount of snow between 400 to 100 hPa. The MYDM has simulated approximately half of the snow than that of SBU scheme, CAM and another all MPs schemes have simulated approximately half of the snow than that of MYDM scheme. The orders of MPs Schemes for simulation of CSMR are SBU>TH>CAM>MDM>MYDM> WDM6>WSM6>NSSL-2>FE and Lin schemes on 24 June (Fig. 13j), SBU> MDM> TH> CAM> MYDM> FE> WDM6>

NSSL-2> WSM6> and Lin schemes on 25 June (Fig. 13k) and SBU>TH>MDM> MYDM> FE> WDM6>NSSL-2>WSM6>CAM and Lin schemes on 26 June (Fig. 13l)

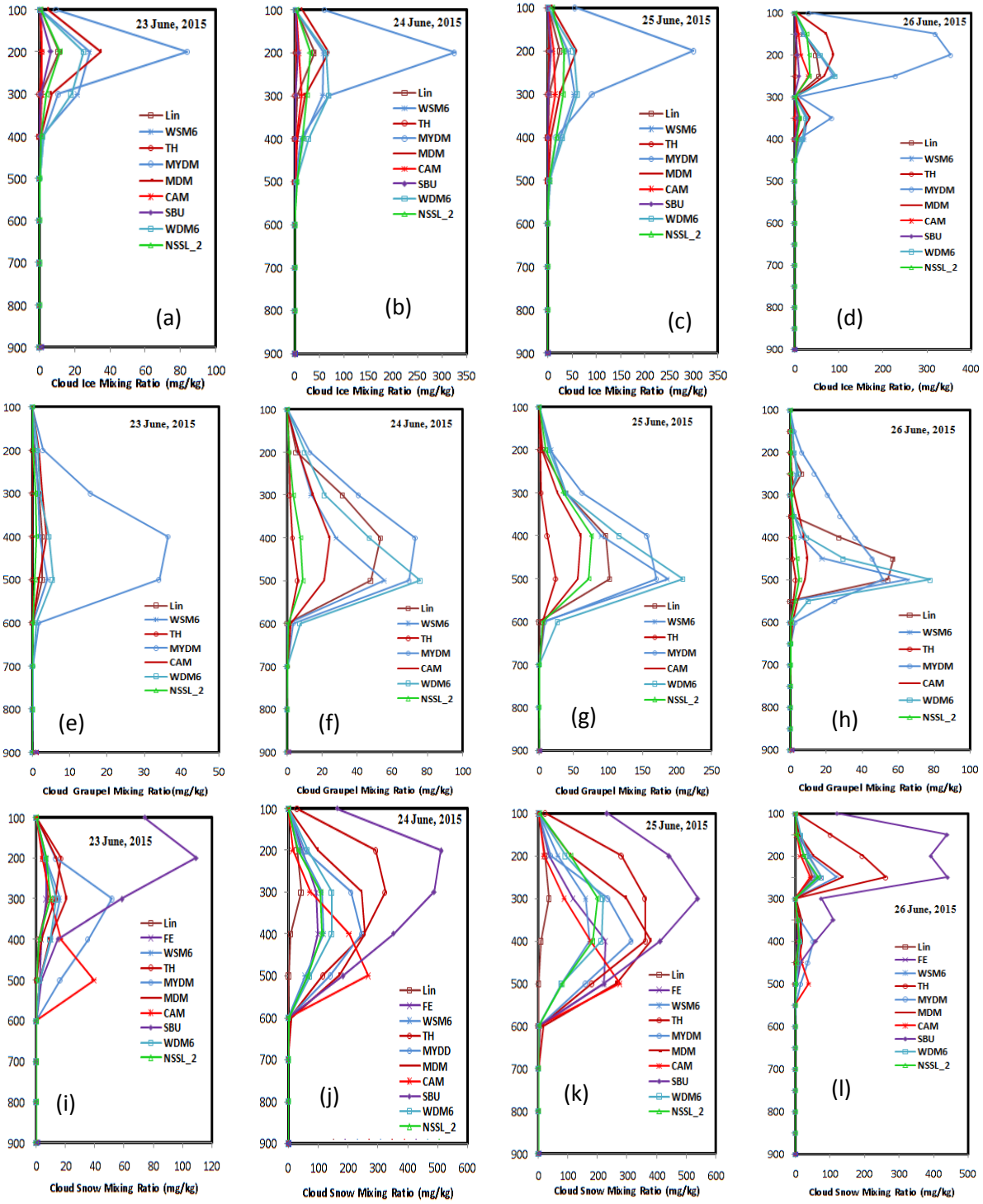

Fig. 13: Vertical profiles of time and space averaged (a-d) CIMR, (e-h) CGMR and (i-l) CSMR simulated by different MPs during 23-26 June 2015.

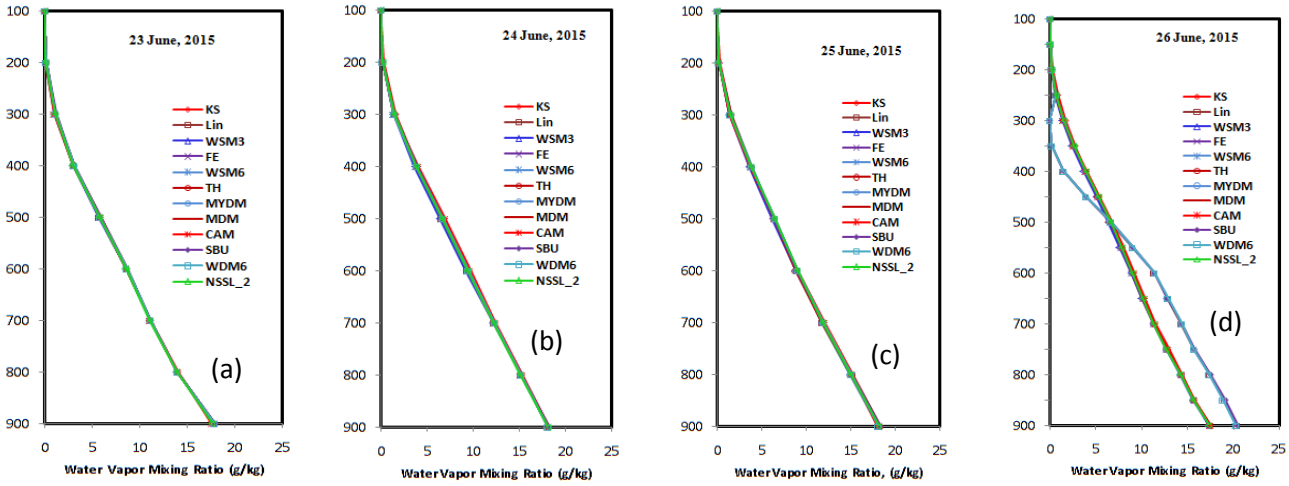

Fig. 14: Vertical profiles of time and space averaged (a-d) WVMR simulated by different MPs coupling with KF scheme during 23-26 June 2015.

4.1.16 Water Vapor Mixing Ratio (WVMR)

Space and time averaged vertical profiles of WVMR is constant during 23-26 June 2015 for different MPs schemes are shown in Fig. 14(a-d). The patterns of water vapor profiles are similar up to 100 h Pa level for all MP schemes during 23-26 June. It is found that the water vapor mixing ratio is significantly higher for WDM6 and SBU schemes on 26 June and the others are constant during the simulation time.

4.2 Heavy rainfall during 23 – 26 July 2015

4.2.1 Observed, TRMM and Model Simulated Rainfall for 23 July 2015

The observed and TRMM rainfall over Bangladesh during 23-26 July 2015are presented in Fig. 15(a-h). The heavy rainfall is observed on 23 July in the SE and NE region and light rainfall is found in the central to W-NW and SW regions of Bangladesh. Maximum rainfall amounts observed (Fig. 15a) at Chittagong, Sandwip and Sylhet are 102, 90 and 80 mm respectively. TRMM derived light rainfall (Fig. 15e) all over the country on 23July. Maximum rainfall observed at Sandwip, Hatiya and Cox's Bazar are 36, 30 and 24 mm respectively. It is seen that the distribution patterns of TRMM and observed rainfall are similar but TRMM derived rainfall is much lower than that of observed rainfall.

The rainfall simulated using different microphysics schemes on 23 July 2015 are presented in Fig. 16(a-l). The Kessler scheme has simulated heavy rainfall (Fig. 16a) in the S-SE, NE and SW regions, light rainfall in the central region and very light rainfall in the west northwestern regions of Bangladesh. Maximum rainfall is simulated at Sylhet, Chandpur and M. Court regions and the amounts are 136, 131 and 122 mm respectively. The Lin *et al.* scheme has simulated heavy rainfall (Fig. 16b) in the SW, S-SE and NE regions of the country on that day and light rainfall is simulated at the W-NW regions. Maximum rainfall is simulated at Khepupara, Hatiya and Feni regions and the amounts are 122, 114 and 92 mm respectively and observed maximum is seen at Chittagong, which indicates that the model simulated maximum rainfall is shifted from Chittagong towards west. WSM3 has simulated heavy rainfall in the SE and NE regions and light rainfall is simulated from central to W-NW region (Fig. 16c). Maximum rainfall amounts simulated at M. Court, Hatiya and Feni are 136, 131 and 122mm respectively, which is shifted from the observed maximum rainfall position towards W-NW. Ferrier scheme has simulated heavy rainfall in the S-SE and NE regions and light rainfall in the center to W-NW regions (Fig. 16d). Maximum rainfall amounts simulated at Sylhet, Khepupara and Feni are 102, 82 and 75 mm respectively. The model simulated maximum rainfall is matched with the observed rainfall at Sylhet but maximum rainfall in the SE region is shifted towards west. WSM6 has simulated heavy rainfall in the S-SE and NE regions and light rainfall occurred in the center to W-NW regions (Fig. 16e). Maximum rainfall simulated at Sylhet, Hatiya and Teknaf and the amounts are 138, 113 and 75 mm respectively. The model simulated maximum rainfall in the NE region is matched with the observed rainfall and minimum rainfall is also matched all through the country. The observed maximum rainfall position at Chittagong is shifted towards west (Hatiya).

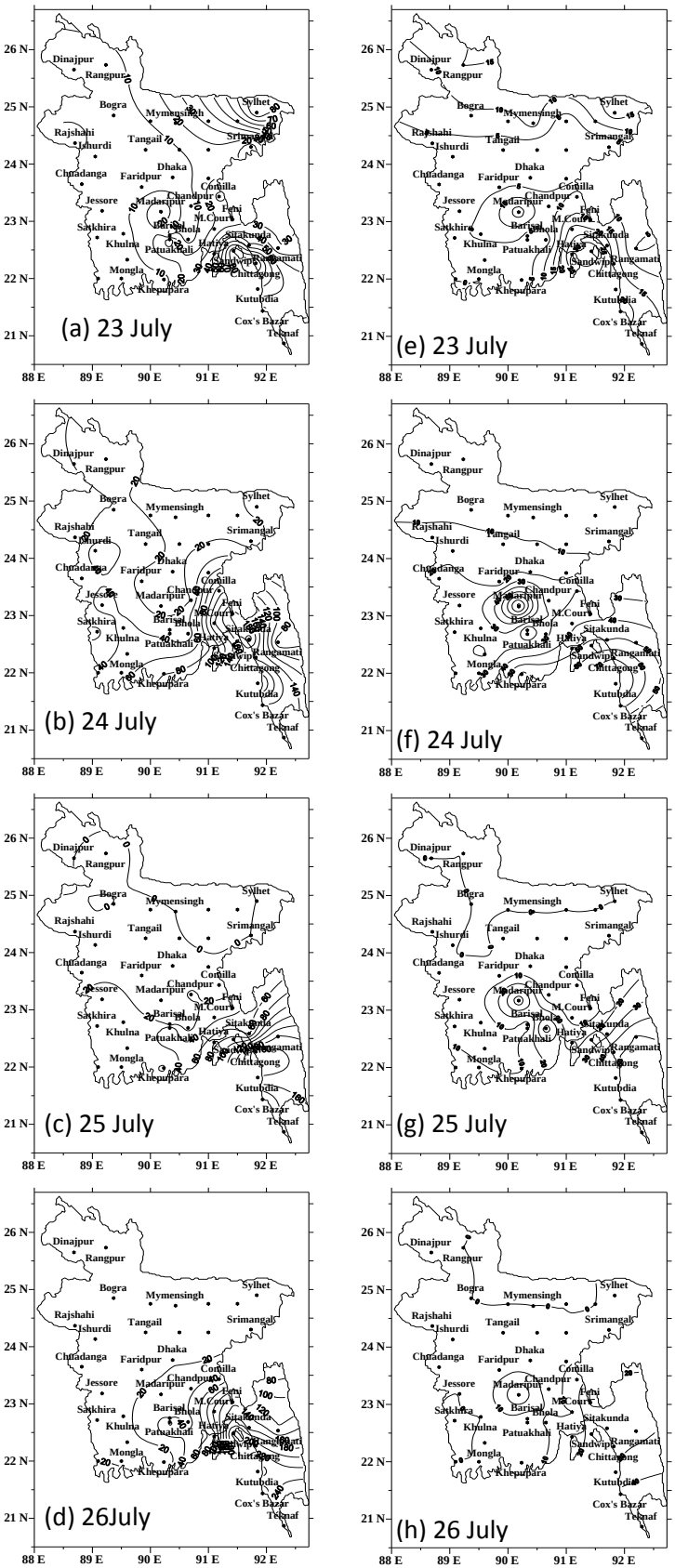

Fig. 15: Distribution of (a-d) Observed and (e-h) TRMM rainfall of 23-26 July 2015 all over Bangladesh.

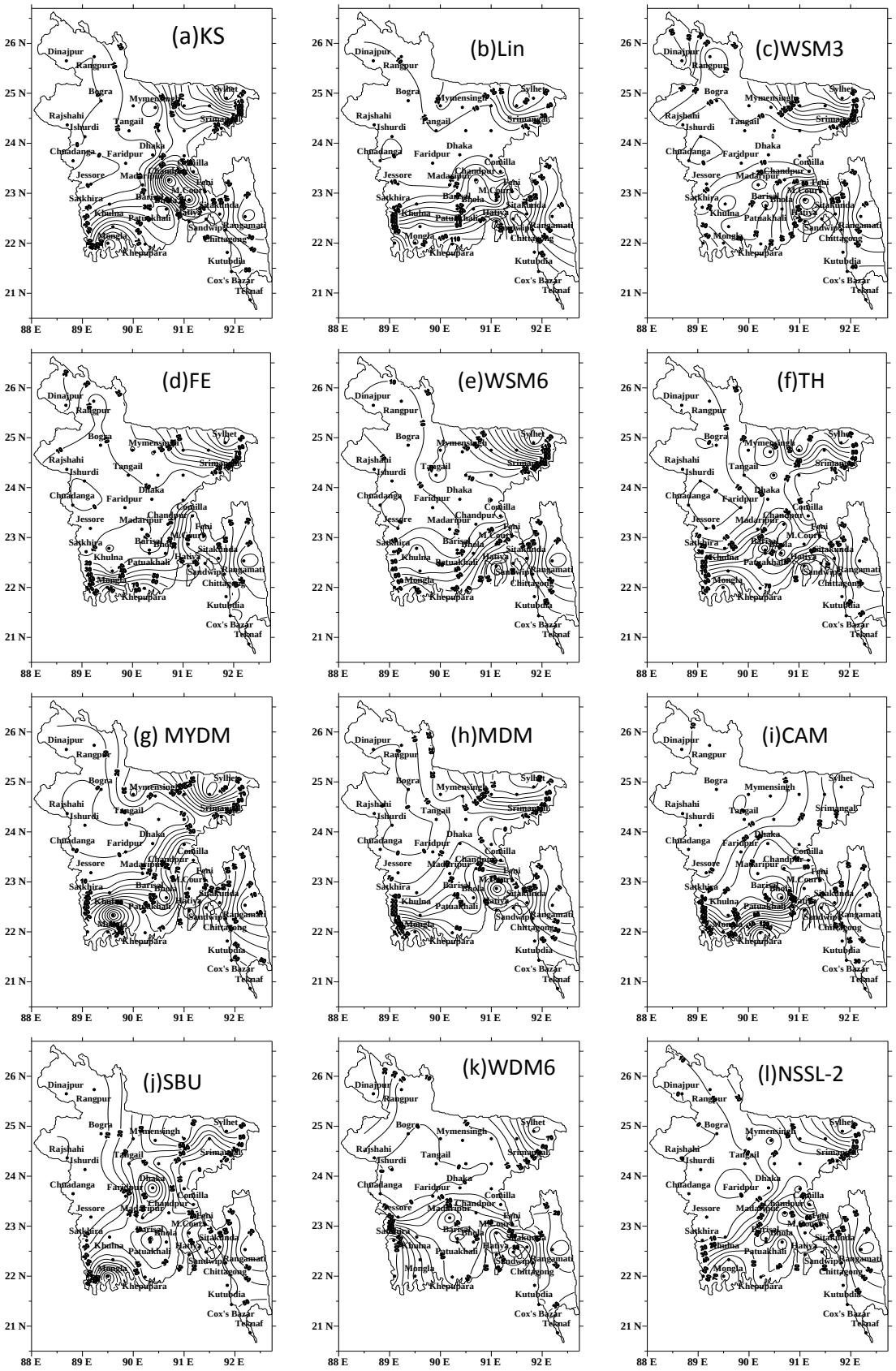

Fig. 16: Distribution of 24 hour model simulated station averaged rainfall using different MPs of 23 July 2015 all over Bangladesh.

Thomson scheme has simulated heavy rainfall in the S-SE, SW and NE regions and light rainfall occurred in the center to W-NW regions (Fig. 16f). Maximum rainfall amounts simulated at Hatiya, Barisal and Mongla are 98, 96 and 82 mm respectively, whereas the observed maximum rainfall is found at Chittagong, Sandwip and Sylhet regions which indicates that the maximum rainfall position is shifted from the observed maximum rainfall position.

MYDM has simulated heavy rainfall in the SW to SE and NE regions and light rainfall in the central to western and NW regions (Fig. 16g). Maximum rainfall has been simulated at Mongla, Hatiya and Sylhet and the amounts are 152, 105 and 101 mm respectively on 23 July 2015. The model simulated maximum rainfall is almost in line with the observed rainfall at Sylhet but maximum rainfall in the SE region is shifted from Chittagong towards Hatiya-Sandwip regions. MDM scheme has simulated heavy rainfall in the SE to SW and NE regions and light rainfall in the West to NW regions (Fig. 16h) on 23 July. Maximum rainfall is found at M. Court, Sylhet and Teknaf are 112, 82 and 78mm respectively, which indicate that the model simulated maximum rainfall is matched with the observed rainfall at Sylhet region and maximum rainfall in the SE region shifted from Chittagong towards M. Court region. The observed heavy rainfall in the NE and SE region is matched with the simulated rainfall but time and space deviation is found.

CAM scheme has been simulated heavy rainfall in the S-SW and SE regions and light rainfall in the NE regions (Fig. 16i). Maximum rainfall has been simulated at Khepupara, Hatiya and M. Court are 168, 108 and 78 mm respectively, where the model simulated maximum rainfall is shifted from Chittagong towards W-NW regions.SBU scheme has been simulated heavy rainfall at Dhaka, SW and NE regions and light rainfall occurred in the W-NW regions (Fig. 16j). Maximum rainfall occurred at Dhaka, Teknaf and Feni are 95, 80 and 73 mm respectively. The model simulated maximum rainfall position is shifted from Chittagong towards NW (i.e. Feni) region.

WDM6 scheme has been simulated heavy rainfall in the SW, SE and NE regions and light rainfall in the center to W-NW regions (Fig. 16k). Maximum rainfall simulated at Satkhira, Sylhet and Mongla are 108, 82 and 75 mm respectively. The model simulated maximum rainfall is matched with the observed rainfall at Sylhet, but the other observed maximum rainfall position in the SE region is not matched.NSSL-2scheme has simulated heavy rainfall in the S-SW and NE regions and light rainfall in the center to W-NW regions. Maximum rainfall amounts occurred at Sylhet, Sitakunda and Feni are 98, 79 and 77mm respectively.

The model simulated maximum rainfall is almost matched with the observed rainfall at Sylhet and Chittagong. The simulated maximum rainfall is found to match with the observed rainfall at Sylhet i.e. NE region for different microphysics schemes and observed heavy rainfall position at Chittagong is shifted towards Sitakunda-Feni regions.

4.2.2 Observed, TRMM and Model Simulated Rainfall for 24 July 2015

The heavy rainfall is observed on 24 July in the SE region and light rainfall is found in all other regions of Bangladesh. Significant amount of rainfall observed at Kutubdia, Sitakunda, Feni, Cox's Bazar and Chittagong are 240, 211, 185, 154 and 156 mm respectively on 24 July 2015(Fig. 15b). Maximum TRMM rainfalls (Fig. 15f) is seen at Kutubdia, Chittagong, Cox's Bazar, Khepupara and Sandwip are 87, 70, 63, 62 and 54 mm respectively. It is seen that the distribution patterns of TRMM and observed rainfall are similar but TRMM derived rainfall is much lower than that of observed rainfall.

The rainfall amounts simulated by using 12 different microphysics schemes on 24 July 2015 are presented in Fig. 17(a-l). The Kessler scheme has simulated heavy rainfall (Fig. 17a) in the SE regions and light rainfall in the central region to W-NW and NE regions of Bangladesh. Maximum rainfall is simulated at Kutubdia, Cox's Bazar, Sitakunda, Teknaf and Chittagong regions and the amounts are 259, 243, 178, 177 and 198 mm respectively. The simulated position of maximum rainfall in the SE region is matched with the observed rainfall. The Lin *et al.* scheme has simulated heavy rainfall (Fig. 17b) in the SE and center to NW regions of the country on that day. Maximum rainfall is simulated at Kutubdia, Cox's Bazar, Teknaf, Sandwip, Chittagong and Sitakunda regions and the amounts are 296, 233, 198, 147, 143 and 129 mm respectively. The simulated heavy rainfall distribution pattern is matched with the observed maximum rainfall. WSM3 has simulated heavy rainfall in the SE and SW regions and light rainfall is simulated from central region to W-NW and NE regions (Fig. 17c). Maximum rainfall is simulated at Cox's Bazar, Teknaf, Kutubdia, Sitakunda, Chittagong and Sandwip and the amounts are 184, 184, 178, 176, 150 and 100 mm respectively which is matched with the position of observed maximum rainfall. Ferrier scheme has simulated heavy rainfall in the SE and northern regions and light rainfall in the central region to W-NW and SW regions (Fig. 17d).

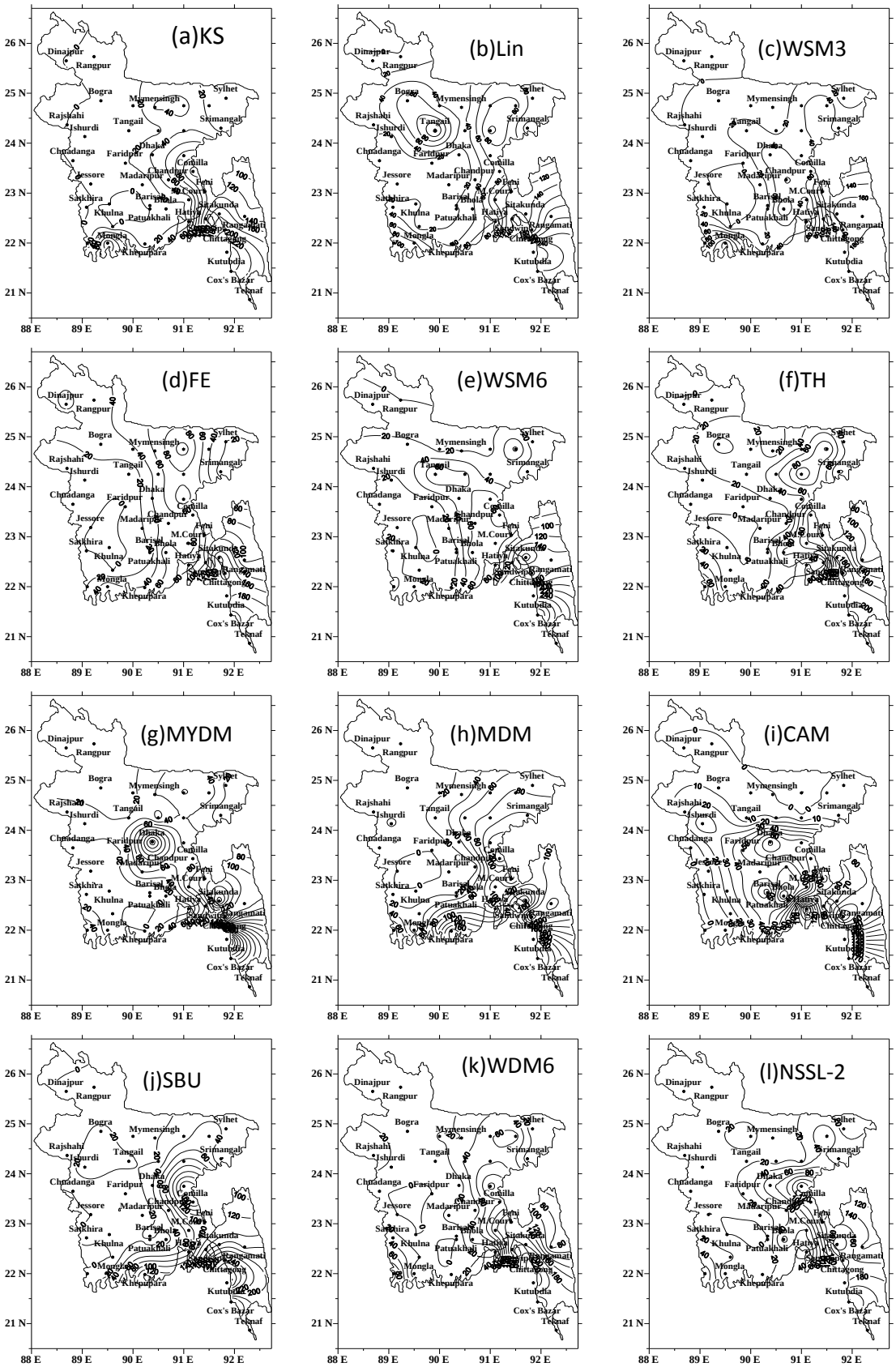

Fig. 17: Distribution of 24 hour model simulated station averaged rainfall using different MPs of 24 July 2015 all over Bangladesh.

Maximum rainfall amounts simulated at Cox's Bazar, Teknaf, Chittagong, Sitakunda and Kutubdia are 232, 206, 190, 188, 171 and 98 mm respectively. The model simulated maximum rainfall position is matched with the observed rainfall position. WSM6 has simulated heavy rainfall in the SE region and light rainfall in the central region to W-NW, SW and NE regions (Fig. 17e) of the country. Maximum rainfall amounts simulated at Cox's Bazar, Kutubdia, Sitakunda, Teknaf, Sandwip and Chittagong are 354, 245, 200, 200, 145 and 105 mm respectively. The model simulated maximum rainfall in the SE region is matched with the observed rainfall and minimum rainfall is also matched all through the country. Thomson scheme has simulated heavy rainfall in the SE and NE regions and light rainfall in the central region to W-NW and SW regions (Fig. 17f). Maximum rainfall amounts simulated at Cox's Bazar, Chittagong, Teknaf, Sitakunda and Kutubdia are 230, 210, 202, 188 and 173 mm respectively, whereas another observed maximum rainfall is found at Sandwip region which indicates that the maximum rainfall position is shifted toward north from the observed maximum rainfall position. MYDM has simulated heavy rainfall in the central and SE regions and light rainfall in the west, NW and SW regions (Fig. 16g). Maximum rainfall has been simulated at Kutubdia, Cox's Bazar, Sitakunda, Teknaf and Feni and the amounts are 486, 335, 222, 182 and 132 mm respectively on 24 July 2015. The model simulated maximum rainfall is almost in line with the observed rainfall but maximum rainfall in the SE region is shifted from Sandwip towards Feni region. MDM has been simulated heavy rainfall in the S-SE regions and light rainfall in the central to W-NW regions (Fig. 16h) on 24 July. Maximum rainfall is simulated at Cox's Bazar, Kutubdia, Sitakunda, Teknaf and Sandwip and the amounts are 298, 271, 214, 198 and 178mm respectively, which indicate that the model simulated maximum rainfall is matched with the observed rainfall at Sylhet region and maximum rainfall in the SE region shifted from Chittagong towards M. Court region. CAM has been simulated heavy rainfall in the SE region and light rainfall in the central to W-NW, SW and NE regions (Fig. 16i). Maximum rainfall amounts at Teknaf, Cox's Bazar, Hatiya, Kutubdia and Feni are 184, 184, 159, 114 and 107 mm respectively, where the model simulated maximum rainfall is shifted from Chittagong towards Teknaf and Sitakunda towards Hatiya. SBU scheme has simulated heavy rainfall in the S-SE and eastern regions and light rainfall in the central towards western regions (Fig. 16j). Maximum rainfall amounts at Kutubdia, Chittagong, Teknaf, Comilla, Sitakunda and Cox's Bazar are 333, 253, 197, 182, 159 and 115 mm respectively, where the model simulated maximum rainfall pattern is matched with the observed rainfall pattern and light rainfall position is also matched with the observed rainfall position. WDM6 scheme has simulated heavy rainfall in the SE region

and light rainfall in the central region to other regions (Fig. 16k). Maximum rainfall amounts found at Kutubdia, Teknaf, Chittagong, Sitakunda and Cox's Bazar are242, 233, 229, 178 and 158 mm respectively. The model simulated maximum rainfall is matched with the observed rainfall and the light rainfall is also matched.NSSL-2 scheme has simulated heavy rainfall in the E-SE regions and light rainfall in the central region to W–NW and S-SW regions. Maximum rainfall simulated at Cox's Bazar, Sitakunda, Teknaf, Kutubdia and Comilla are 250, 204, 177, 176, 155 and 115 mm respectively, The model simulated heavy rainfall on 24 July 2015 in the SE region of Bangladesh is almost matched with the observed rainfall for all MP schemes. The simulated rainfall is much higher than that of observed rainfall.

4.2.3 Observed, TRMM and Model Simulated Rainfall for 25 July 2015

The heavy rainfall is observed on 25 July (Fig. 15c) in the SE region and light rainfall in all other regions of the country. The amounts of rainfall observed are198, 178, 161 and 148 mm at Chittagong, Kutubdia, Rangamati and Teknaf respectively. On that day, TRMM (Fig. 15g) derived light rainfall all over the country. Maximum rainfall is seen at Cox's Bazar, Rangamati, Kutubdia, Chittagong and Teknaf and the amounts are 56, 50, 48, 47 and 42 mm respectively. It is seen that the distribution pattern of TRMM and observed rainfall are similar but TRMM derived rainfall is much lower than that of observed rainfall.

The rainfall simulated using different MP schemes coupling with KF scheme on 25 July 2015 are presented in Fig. 18(a-l). The Kessler scheme has simulated heavy rainfall (Fig. 18a) in the S-SE and SW regions and light rainfall in the central to W-NW and NE regions of Bangladesh. Significant amounts of rainfall simulated at Rangamati, Sitakunda, Chittagong, Sandwip and Cox's Bazar regions are 394, 378, 308, 294 and 242mm respectively. The model simulated heavy rainfall in the region where the heavy rainfall was observed but the model simulated rainfall is much higher than that of BMD observed rain. The Lin *et al.* scheme has simulated heavy rainfall (Fig. 18b) in the SE and SW regions and light rainfall in the W-NW and NE regions of the country. The simulated maximum rainfall is found at Rangamati Chittagong, Teknaf, Sitakunda and Cox's Bazar regions are 325, 310, 242, 215 and 206 mm respectively and the distribution pattern of heavy rainfall is matched with the observed maximum rainfall. WSM3 and Ferrier scheme have simulated heavy rainfall in the SE and SW regions and light rainfall in other regions of the country (Fig. 18c& d). Maximum rainfall amounts of 289, 221, 181, 160 and 100 mm are simulated by WSM3 and 251, 227,

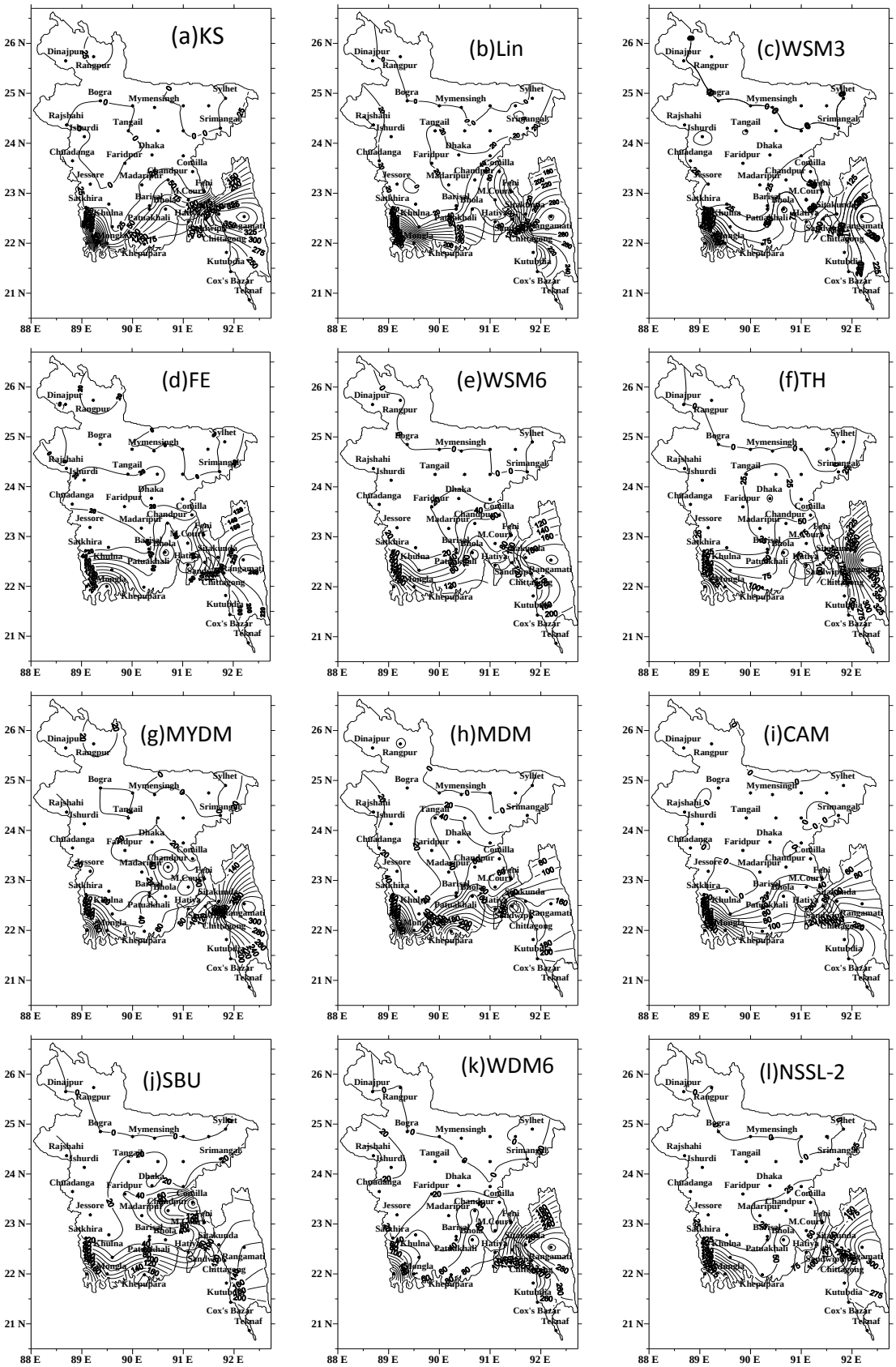

Fig. 18: Distribution of model simulated rainfall for 24 hour prediction using different MPs coupling with KF scheme on 25 July 2015 all over Bangladesh.

151, 210 and 148 mm are simulated by Ferrier scheme at Rangamati, Teknaf, Cox's Bazar, Chittagong and Sitakunda respectively, which is matched with the observed maximum rainfall position. The model simulated maximum rainfall position is matched with the observed rainfall position in the SE region but the simulated heavy rainfall in the SW region could not match with the observed rainfall. WSM6 and Thomson schemes have simulated heavy rainfall in the S-SE and SW regions and light rainfall in the central region to W-NW and NE regions (Fig. 18e& f). Maximum rainfall amounts simulated are 222, 206, 206, 199 and 141 mm by WSM6 and 256, 253, 497, 129 and 158 mm by Thompson scheme at Teknaf, Cox's Bazar, Rangamati, Sitakunda and Chittagong respectively. The model simulated maximum rainfall in the SE region is matched with the observed rainfall and minimum rainfall is also matched all through the country. MYDM, MDM and CAM schemes have simulated heavy rainfall in the SE and SW regions and light rainfall in the central to W, NW and NE regions (Fig. 18(g-i)). Maximum rainfall has been simulated at Rangamati, Chittagong, Teknaf, Cox's Bazar and Sitakunda regions and the amounts are 333, 273, 237, 161 and 103 mm by MYDM, 162, 155, 261, 222 and 169 mm by MDM and 148, 197, 192, 236 and 154 by CAM schemes respectively on 25 July 2015. Model simulated heavy rainfall and its position are matched with the BMD observed rainfall. SBU scheme has simulated heavy rainfall in the S-SE, SW and eastern regions and light rainfall in the central to W-NW regions (Fig. 18j). Maximum rainfall simulated at Teknaf, Cox's Bazar, Comilla, Khepupara, Rangamati, Chittagong and Sitakunda and the amounts are 231, 226, 218, 190, 141, 131 and 117 mm respectively. The model simulated maximum rainfall position is matched with the observed rainfall in the SE region but SW, eastern and southern region could not match with the observed rainfall. WDM6 scheme has simulated heavy rainfall in the SE and SW region and light rainfall in the central region to W-NW and NE regions (Fig. 18k). Maximum rainfall simulated at Rangamati, Cox's Bazar, Sitakunda Chittagong and Teknaf and the amounts are 242, 233, 229, 178 and 158 mm respectively. The model simulated maximum rainfall is matched with the observed rainfall. NSSL-2 scheme has simulated heavy rainfall in the SE and SW regions and light rainfall in the central region to W–NW and NE regions. Maximum rainfall simulated at Rangamati, Cox's Bazar, Teknaf, Sitakunda, and Chittagong and the amounts are 326, 240, 222, 202 and 149 mm respectively. The model simulated maximum rainfall position and amounts are matched with the observed rainfall position and amounts. All MPs have simulated maximum rainfall in the SE and SW regions but observed rainfall is found only in the SE region.

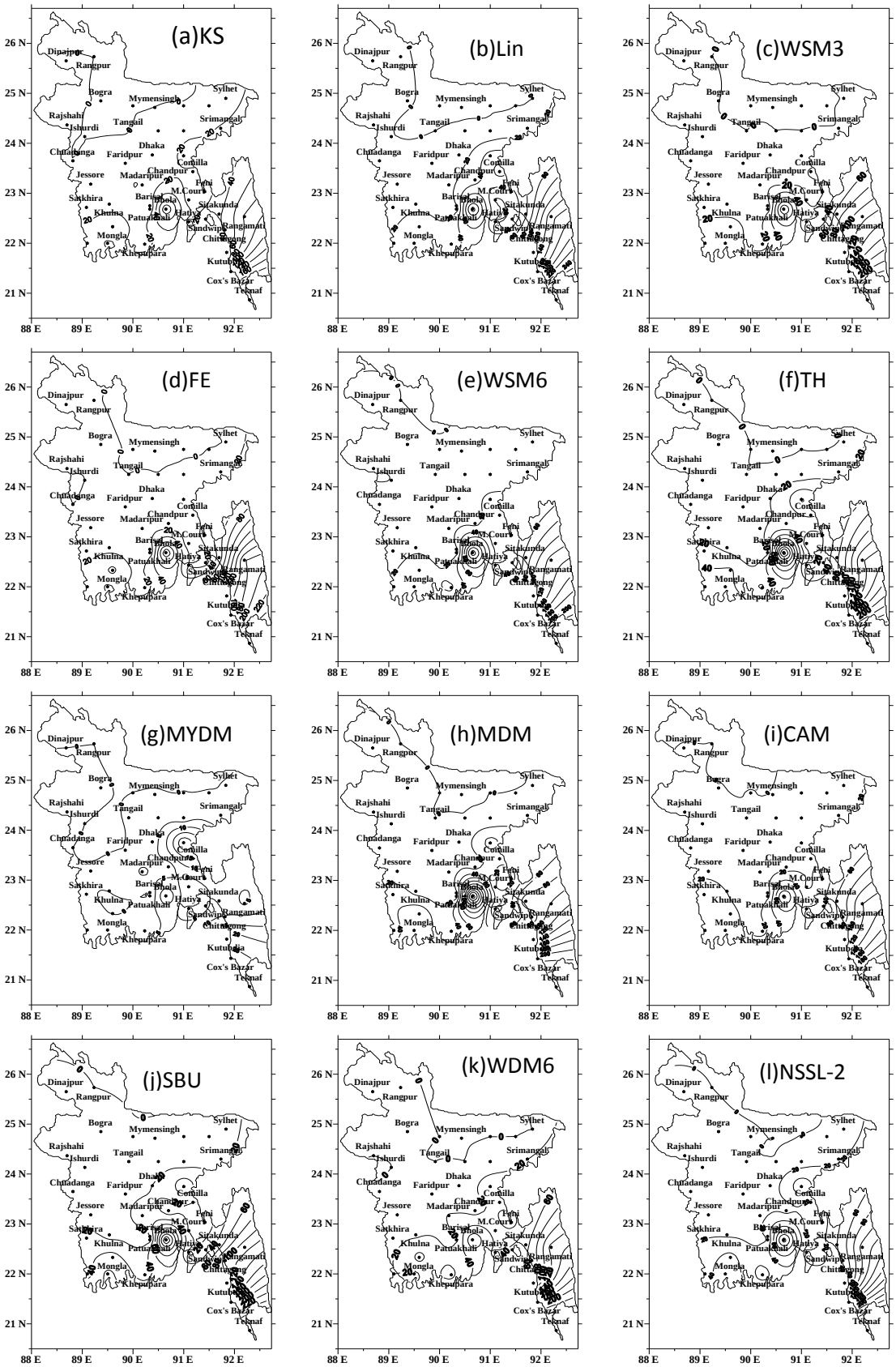

Fig. 19: Distribution of 24 hour model simulated station averaged rainfall using different MPs on 26 July 2015 all over Bangladesh.

4.2.4 Observed, TRMM and Model Simulated Rainfall for 26 July 2015

The heavy rainfall is observed by Bangladesh Meteorological Department (BMD) in the SE region (Fig. 15d) and light rainfall is found in all other regions of the country on 26 July. The amounts of rainfall observed are 331, 253, 210, 151 and 122 mm at Teknaf, Kutubdia, Sitakunda, Chittagong and Rangamati respectively. On that day TRMM (Fig. 15h) derived light rainfall in the SE region of the country. The TRMM rainfall is seen at Cox's Bazar, Rangamati, Kutubdia, Chittagong and Teknaf stations and the amounts are 56, 50, 48, 47 and 42 mm respectively. It is seen that the distribution pattern of TRMM and observed rainfall are similar but TRMM derived rainfall is much lower than that of observed rainfall.

The rainfall amounts simulated using different microphysics schemes on 26 July 2015 are presented in Fig. 19(a-l). The Kessler, Lin *et al*., and WSM3 schemes have simulated heavy rainfall (Fig. 19(a-c)) in the SE regions and light rainfall in all other regions of Bangladesh. Maximum rainfall is simulated at Teknaf, Cox's Bazar, Bhola and Rangamati regions and the amounts are 264, 135, 101 and 82mm respectively. The model simulated maximum rainfall in the SE region is matched with the observed rainfall and minimum rainfall is also matched all through the country. The maximum rainfall is simulated at Teknaf, Cox's Bazar, Rangamati Bhola and Kutubdia regions and the amounts are 358, 158, 158, 135 and 122 mm respectively for Lin et al (Fig. 19b) and at Teknaf, Cox's Bazar, Rangamati, Bhola, Kutubdia and Chittagong and the amounts are 285, 169, 126, 113, 105 and 101 mm respectively for WSM3 (Fig. 19c) which are found to match with the observed maximum rainfall pattern. FE, WSM6 and Thompson schemes have simulated heavy rainfall in the SE regions and light rainfall in other regions (Fig. 19(d-f)). Maximum rainfall simulated at Teknaf, Rangamati, Cox's Bazar, Kutubdia and Bhola and the amounts are 290, 178, 149, 146 and 124 mm for FE and 284, 128, 153, 100 and 160 mm for WSM6 scheme and 315, 138, 172, 82 and 199 mm for Thompson scheme respectively. The model simulated maximum rainfall is almost matched with the observed rainfall but maximum observed rainfall position at Sandwip is shifted towards Bhola. MYDM scheme has simulated light rainfall all over country on this day (Fig. 19g). MDM, CAM and SBU schemes have simulated heavy rainfall in the SE regions and light rainfall in the other regions (Fig. 19(h-j)). Maximum rainfall has been simulated at Teknaf, Cox's Bazar, Bhola, Kutubdia and Rangamati and the amounts are 265, 214, 228, 121 and 101 mm for MDM and 278, 138, 110, 102 and 120 mm for CAM and 324, 181, 169, 96 and 112 mm for SBU scheme respectively. The model simulated maximum rainfall is almost matched with the observed rainfall. WDM6 and NSSL-2 schemes have simulated

heavy rainfall in the SE regions and light rainfall in the other regions (Fig. 19(h-j)). Maximum rainfall simulated at Teknaf, Cox's Bazar, and Rangamati and the amounts are 295, 192 and 127 mm for WDM6 and 358, 155 and 108 mm for NSSL-2 scheme respectively. The model simulated maximum rainfall is almost matched with the observed rainfall. The model simulated maximum rainfall position and amounts for different MP schemes except MYDM have almost matched with the observed rainfall position and amount. All MPs have simulated maximum rainfall in the SE region and observed rainfall is also found in the SE region on this day.

4.2.5 Area averaged rainfall during 23 -26 July 2016

Observed, TRMM and model simulated rainfall averaged over 35 Meteorological stations of all over Bangladesh and in the southeastern 5 stations for all MPs during 23-26 July 2015 and are presented in Fig. 20(a-h). On 23 July, Ferrier scheme has simulated (Fig. 20a) almost similar average rainfall as observed from 35 Meteorological stations of all over Bangladesh and all other MP schemes have simulated higher rainfall and MYDM simulated maximum rainfall among the MP schemes. WSM6, SBU and NSSL2 schemes have simulated almost same amount of rainfall (Fig. 20b) and all other MPs have simulated less rainfall in the SE region (i.e. heavy rainfall stations) of the country. TRMM derived rainfall is much lower than that of observed rainfall all over Bangladesh and also heavy rainfall stations (5 stations) in the SE region of the country. On 24 July, Lin et al., WSM6, MYDM, MDM and SBU schemes have simulated (Fig. 20c) almost similar average rainfall as observed from 35 Meteorological stations of all over Bangladesh and all other MP schemes have simulated less rainfall than that of observed. CAM scheme has simulated lowest all Bangladesh station average rainfall among all the MPs on this day. Kessler, Lin et al., Ferrier, WSM6, MDM, SBU and WDM6 (Fig. 20d) schemes have simulated almost similar amount of rainfall (Fig. 20b), MYDM scheme simulated higher rainfall and all other MPs have simulated less rainfall in the SE region (i.e. heavy rainfall stations) of the country. TRMM also derived much lower average rainfall than that of observed for all Bangladesh stations averaged rainfall and also heavy rainfall stations (5 stations) in the SE region of the country on 24 July.

On 25 July (Fig. 20e), Kessler, Lin *et al*., Thompson, MDM and WDM6 have simulated much higher rainfall and CAM has simulated almost equal amount of rainfall than that of observed from all Bangladesh station averaged rainfall. WSM3, Ferrier, WSM6 and SBU (Fig. 20f) schemes have simulated almost similar amount of rainfall (Fig. 20b), Kessler scheme has simulated much higher rainfall and all other MPs have simulated higher rainfall

in the SE region (i.e. heavy rainfall stations) of the country. TRMM derived much lower average rainfall than that of observed for all Bangladesh station average rainfall and also heavy rainfall stations (5 stations) in the SE region of the country on 25 July. On 26 July, all MPs failed to simulate all Bangladesh station averaged rainfall and also heavy rainfall stations (5 stations) in the SE region of the country.

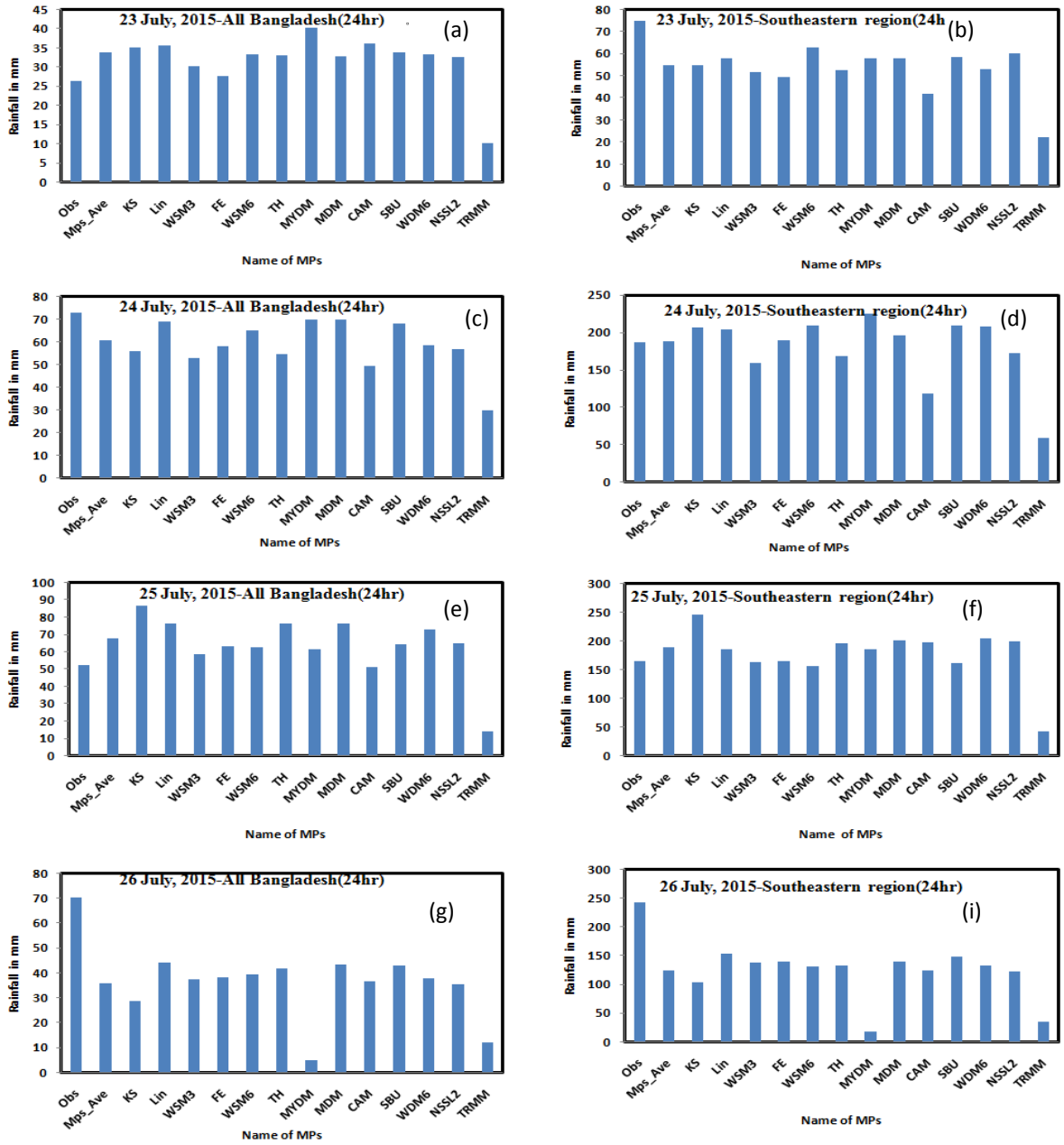

Fig. 20: Model simulated, TRMM derived and observed all Bangladesh stations averaged rainfall and also heavy rainfall stations (5 stations) in the SE region of the country during 23 - 26 July 2015 using different MPs coupling with KF.

All MPs have simulated almost 50% rain on 26 July except that MYDM. MYDM has simulated little average rainfall on this day. TRMM derived much lower average rainfall than

that of observed for all Bangladesh station averaged rainfall and also heavy rainfall stations (5 stations) in the SE region of the country on 26 July.

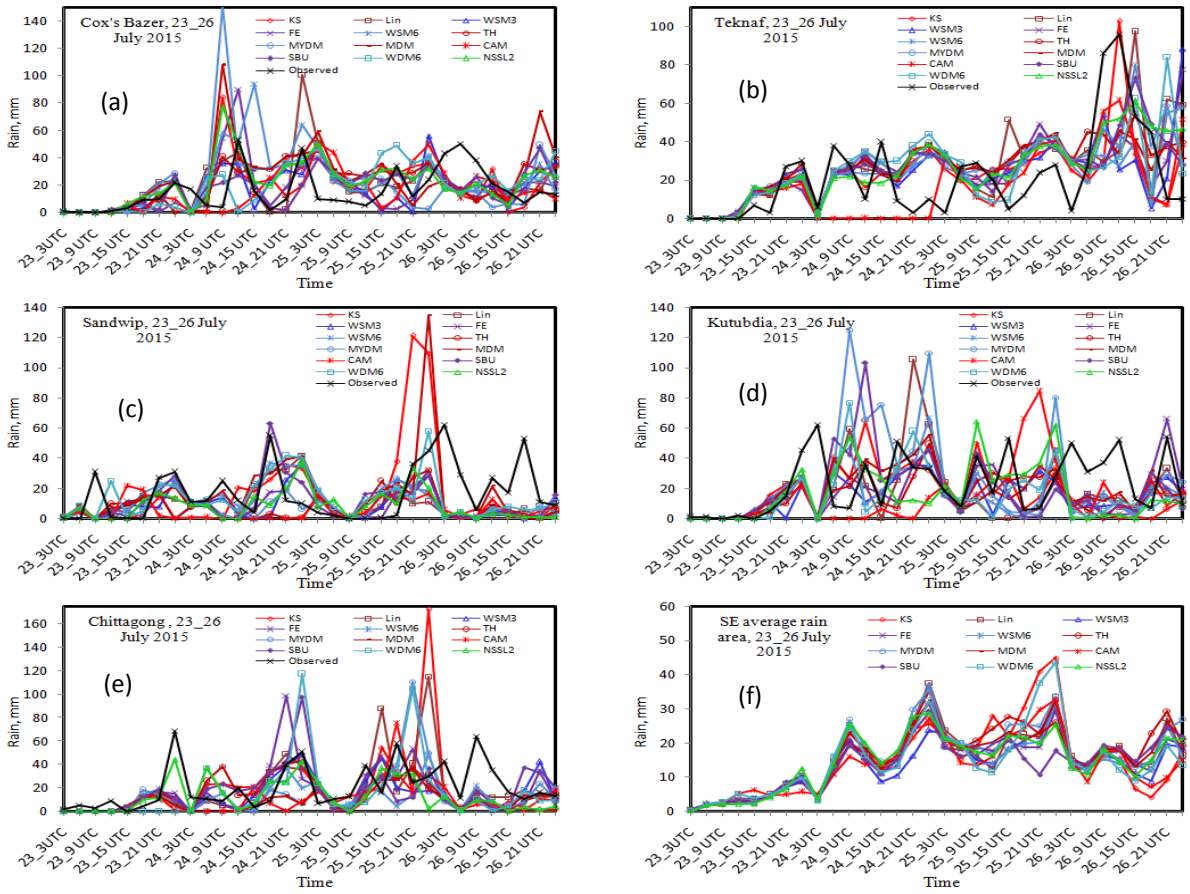

Fig. 21: 3-hourly observed and model simulated rain at (a) Cox's Bazar, (b) Teknaf, (c) Sandwip, (d) Kutubdia, (e) Chittagong and (f) All 5 stations in the SE region using different MPs coupling with KF scheme during 23 -26 July 2015.

4.2.6 Space and Time dependent Rain during 23-26 July 2015

3-hourly observed and model simulated rainfall at Cox's Bazar, Teknaf, Sandwip, Kutubdia, Chittagong and all 5 stations in the SE region averaged rainfall using different MPs coupling with KF scheme during 23-26 July 2015 are presented in Fig. 21(a-f). At Cox's Bazar (Fig. 21a) the time of 3-hourly simulated maximum rainfall is almost found to match with the observed maximum rainfall except some anomalies. On 24 July, the observed peak is found at 1200 UTC but some of MPs have simulated significantly higher peak at 0900 UTC. The time of observed maximum rainfall is almost matched with the model simulated time with little anomalies at Teknaf, Sandwip, and Kutubdia and Chittagong as shown in Fig. 21 (b-e).

4.2.7 Vertical velocity during 23-26 July 2015

At first the simulated position of maximum updraft is identified for different MP schemes every day during 23-26 July 2015. Along the line of maximum updraft, vertical velocities (shaded) have been plotted on23 July for different MP schemes and are presented in Fig. 22(a-l). The times and position of maximum updrafts simulated are different for different MP schemes. The maximum updrafts of 14, 25, 15, 10, 24, 16, 21, 25, 8, 18, 16 and 13 ms^{-1} are simulated by KS, Lin *et al*., WSM3, FE, WSM6, TH, MYDM, MDM, CAM, SBU, WDM6 and NSSL-2 schemes respectively at the times of 0600 UTC for all MP schemes except WDM6 and NSSL-2. WDM6 scheme has simulated maximum updraft at 0300 UTC and NSSL-2 at 1800 UTC. The maximum updraft is simulated at around 400-200 hPa by Lin, WSM6, MYDM and MDM schemes on 23 July.

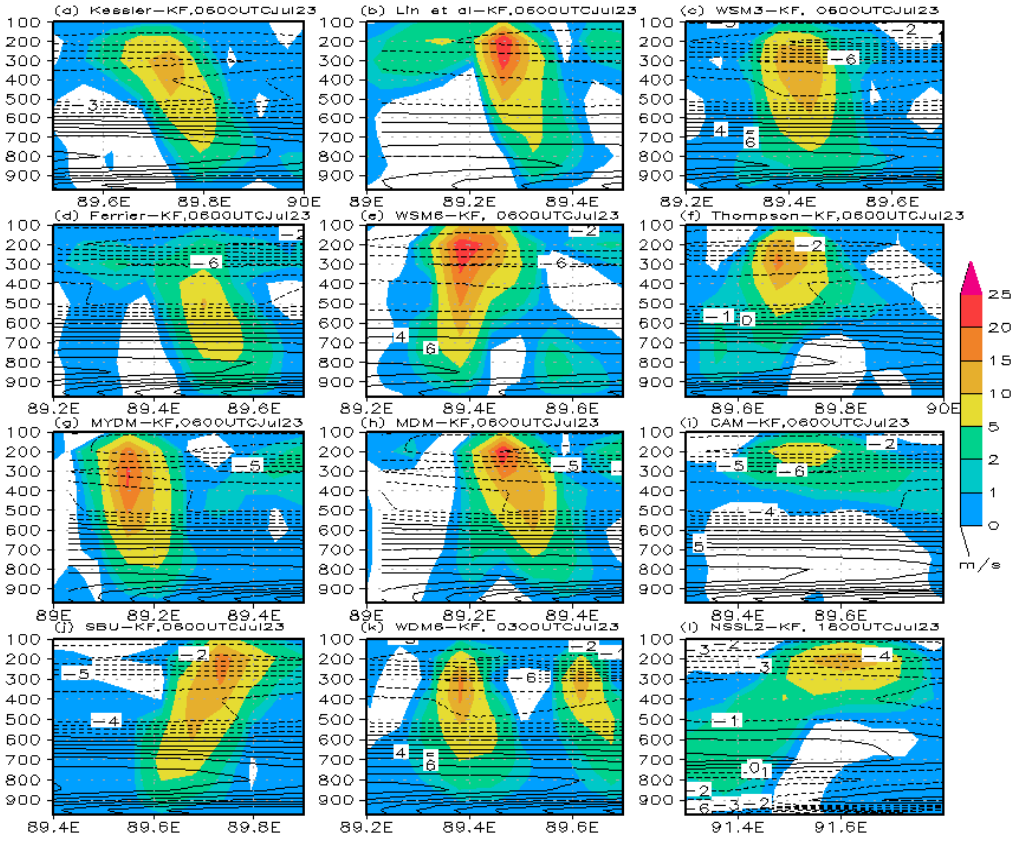

Fig. 22: WRF model simulated maximum vertical velocity (shaded) and vorticity (contour) along the line of maximum updraft using different MP schemes for 23 July 2015.

The updraft simulated is much less by CAM, FE and NSSL-2 on this day. The updraft in the middle and upper troposphere is surrounded by downdraft for all MPs coupling with KF scheme. The updraft in the upper troposphere could be due to the latent heat release during

glaciations and vapor deposition in all combination of MPs and KF scheme. The maximum updrafts of 9, 14, 18, 9, 15, 15, 17, 15, 5, 18, 15 and 15 ms^{-1} (Figure not shown) are simulated by KS, Lin *et al*., WSM3, FE, WSM6, TH, MYDM, MDM, CAM, SBU, WDM6 and NSSL-2 schemes at times of 2100, 2400, 1800, 2400, 2100, 2400, 2400, 0600, 0900, 1200, 1200 and 2100 UTC respectively. The maximum updraft is simulated at around 400-100 hPa by WSM3, WSM6, MYDM, MDM, SBU and NSSL-2 schemes on 24 July 2015. The updraft simulated by KS, CAM and FE is much less on this day.

The maximum updrafts of 11, 18,16, 11, 16, 18, 20, 20, 7, 19, 13 and 16 ms^{-1} (Figure not shown) are simulated by KS, Lin et al., WSM3, FE, WSM6, TH, MYDM, MDM, CAM, SBU, WDM6 and NSSL-2 schemes at times of 2100, 0900, 1200, 2100, 2400, 1800, 1800, 0900, 1200, 1800, 2100 and 1500 UTC respectively on 25 July. The updraft simulated by KS, CAM and FE is much less on this day. The maximum updrafts of 15, 12, 19, 9, 23, 14, 18, 19, 7, 18, 12 and 13 ms^{-1} are simulated by KS, Lin *et al.*, WSM3, FE, WSM6, TH, MYDM, MDM, CAM, SBU, WDM6 and NSSL-2 schemes at the times of 0900, 1500, 0900, 1500, 0900, 0900, 2100, 2100, 1800, 0900, 1500 and 2100 UTC respectively on 26 July 2015. The updraft simulated by CAM, FE and WDM6 is less on this day.

4.2.8 Vorticity

Along the line of maximum updraft, the vorticity (contour) have been plotted for different MP schemes at 23 July and are presented in Fig. 22(a-l). The positive vorticity has been simulated in the lower to middle troposphere from 900 to 600 hPa levels and negative vorticity in the middle to upper troposphere from 600 to 100 hPa levels for all MPs except NSSL-2 on 23 July. NSSL-2 has simulated negative vorticity in the lower troposphere and also in the upper troposphere and positive vorticity in the middle troposphere on this day. On 24 July, positive vorticity has been simulated in the lower to middle troposphere (Figure not shown) and negative vorticity has been simulated in the middle to upper troposphere by WSM3, WSM6, MYDM, WDM6 and NSSL-2 schemes. The other MP schemes have simulated negative vorticity in the lower and upper troposphere and positive vorticity in the middle troposphere. On 25 July, the positive vorticity has been simulated in the lower to upper troposphere (Figure not shown) in the layer 900-200 hPa for all MP schemes except Kessler and WDM6 schemes. The Kessler and WDM6 schemes have simulated negative vorticity in the middle to upper troposphere and positive vorticity in the lower troposphere. On 26 July, the positive vorticity has been simulated in the lower to upper troposphere (Figure not shown) in the layer 900-200 hPa for all MP schemes.

4.2.9 Relative Humidity (RH)

The RH (contour) is simulated along the line of maximum vertical velocity using different MPs on 23, 24, 25 and 26 July 2015 and is presented in Fig. 23(a-l) for 25 July. All MPs coupling with KF scheme have simulated RH up to 100 hPa on 23 and 24 July. On 23 July, all MPs coupling with KF scheme have simulated (Figure not shown) maximum RH >95% up to 300 hPa level is simulated by all MPs except Kessler, MYDM and CAM schemes where the vertical velocity and reflectivity is found maximum. Kessler and MYDM scheme have simulated maximum RH up to 200 hPa and CAM has simulated in the middle troposphere. The maximum RH >95% is simulated by all MPs up to 400 hPa level where the vertical velocity and reflectivity is found maximum.

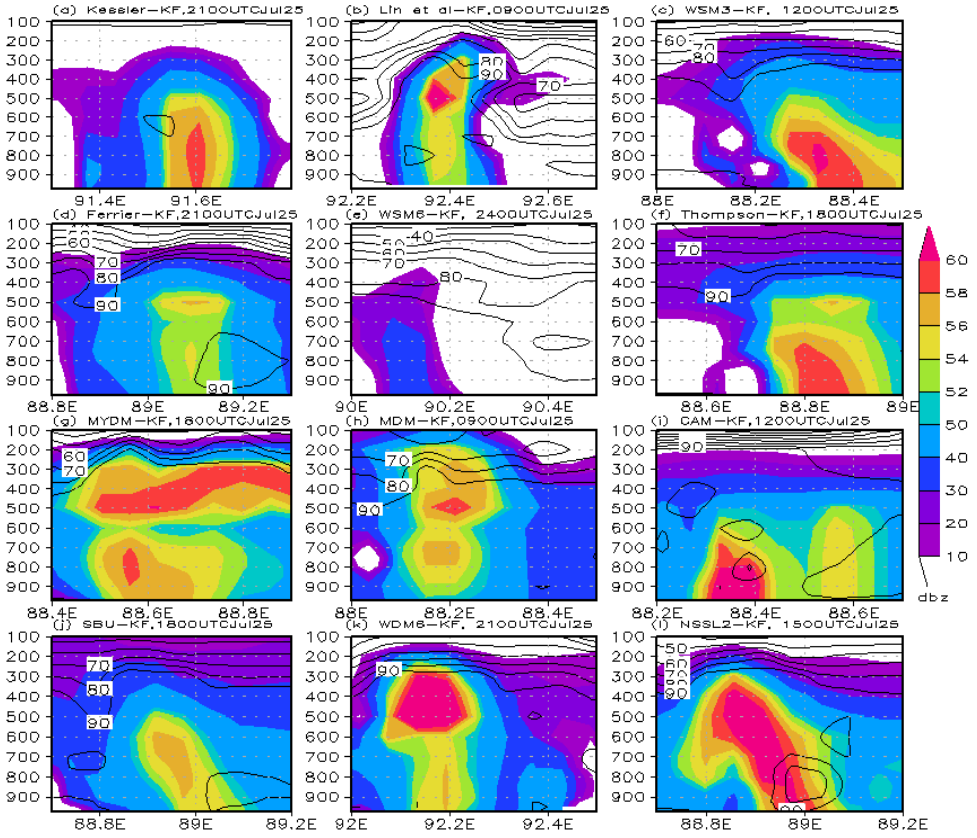

Fig. 23: WRF Model simulated reflectivity (shaded) and relative humidity (contour) using different MPs along the line of maximum vertical velocity on 25 July 2015.

On 25 July, all MPs coupling with KF scheme have simulated RH up to 100 hPa (Fig. 23(a-l)) and maximum RH >95% is simulated by all MPs up to 300 hPa level where the vertical velocity and reflectivity is found maximum. On 26 July, all MPs coupling with KF scheme have simulated RH up to 100 hPa (Figure not shown) and maximum RH >95% is simulated

by all MPs except Kessler, MYDM and CAM schemes up to 300 hPa level where the vertical velocity and reflectivity is found maximum. Kessler, MYDM and CAM schemes have simulated maximum RH up to 200 hPa level where the vertical velocity is found maximum.

4.2.10 Reflectivity

The reflectivity (shaded) has been plotted for the heavy rainfall on 23, 24, 25 and 26 July along the line of maximum vertical velocities using different MPs schemes coupling with KF scheme and is shown in Fig. 23(a-l) for 25 July. Lin, WSM6, TH, MYDM, MDM, SBU and NSSL-2 schemes coupling with KF has simulated reflectivity up to 100 hPa, Kessler, WSM3, Ferrier and CAM has simulated reflectivity up to 200 hPa and WDM6 scheme has simulated reflectivity up to 300 hPa. The reflectivity has been simulated around 60 dBz from 600-300 hPa by Lin et al., WSM6 and WDM6 schemes on that day. On 24 July 2015, WSM3, TH, SBU, WDM6 and NSSL-2 schemes coupling with KF has simulated reflectivity up to 100 hPa, and other schemes have simulated reflectivity up to 200 hPa. The reflectivity has been simulated around 60 dBz from 600 to 300 hPa by Lin et al., WSM6, TH, WDM6 and from 800 to 500 hPa by NSSL-2 schemes on that day. The simulated reflectivity is much higher on 25 July than that of 23 and 24 July. All MPs have simulated around 60 dBz reflectivity at different levels. Kessler, WSM3, TH and CAM has simulated maximum reflectivity from surface to 700 hPa level, NSSL-2 has simulated maximum reflectivity from surface to 300 hPa schemes. The maximum reflectivity has been simulated by Lin, CAM and WDM6 schemes coupling with KF at different hPa level on 26 July. Other schemes have simulated less reflectivity on this day.

4.2.10 Cloud Water Mixing Ratio (CWMR)

The CWMR along the line of maximum vertical velocity on 23, 24, 25 and 26 July 2015 using different MPs is presented in Fig. 24(a-l) for 23 July. KS and WSM3 schemes have simulated CWMR up to 100 hPa and Ferrier, WSM6, MYDM and WDM6 schemes up to 200 hPa, and Thomson, MDM and NSSL-2 schemes have simulated up to 300 hPa on 23 July. The CWMR is found to have maximum along the vertical line where vertical velocity and reflectivity are also maximum. Ferrier scheme has simulated maximum CWMR at 800-400 hPa, MYDM and SBU has simulated maximum at 500-300 hPa level. KS and WSM3 schemes have simulated CWMR up to 100 hPa (Figure not shown), and MYDM and SBU schemes have simulated up to 200 hPa and other schemes have simulated up to 300 hPa on 24, 25 and 26 July. Ferrier scheme has simulated maximum CWMR at 800-500 hPa, MYDM

and SBU have simulated maximum at 500-300 hPa level. Ferrier scheme has simulated maximum CWMR at 900-500 hPa, MYDM has simulated at 600-300 hPa, SBU has simulated maximum at 800-300 hPa level and 800-400 hPa level on 25 July. Maximum CWMR has been simulated by Thompson, MYDM and SBU schemes at 500-300 hPa level on 26 July

The area averaged CWMR is plotted and analyzed using different MPs during 23-26 July 2015 in the SE region of the country and is presented as in Fig. 25(a-d). On 23 July, all MP schemes have simulated two maxima of CWMR from surface to 100 hPa.

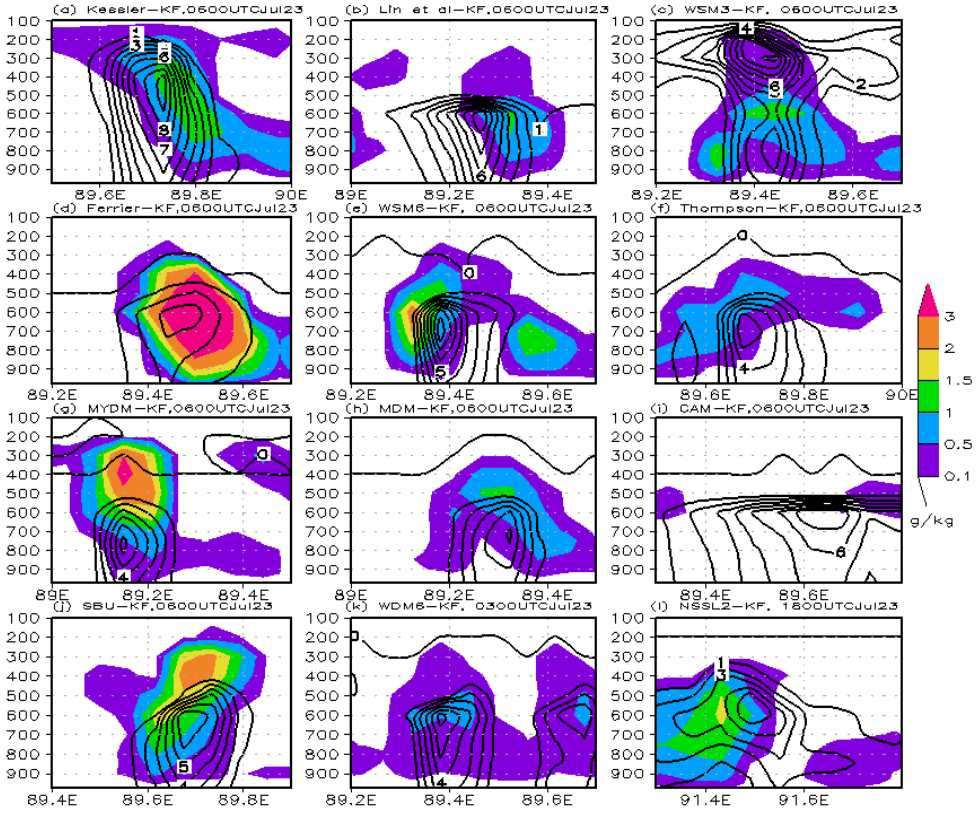

Fig. 24: WRF Model simulated CWMR (shaded, g/kg) and RWMR (contour, g/kg) using different MPs along the line of maximum vertical velocity on 23 July 2015.

The first maxima have been found at 925-900 hPa (Fig. 25a) and second maxima are found at 500 hPa except CAM, Kessler and WSM3 schemes. Kessler and WSM3 schemes have simulated first maxima of CWMR at 925-900 hPa and second maxima at 200 hPa level and for CAM scheme the first maxima is simulated at 800 hPa and second maxima at 500 hPa level on 23 July 2015. The significant amount of CWMR is simulated at 900 to 400 hPa by CAM scheme. The maximum CWMR simulated at 200 hPa is 59 mg/kg by KS scheme on 23 July. On 24 July (Fig. 25b), the area averaged CWMR has been simulated with one maximum

at 500 hPa level for all MPs except Kessler and WSM3. Although all MPs have simulated one maximum at 500 hPa level but this maximum CWMR is much higher than that of 23 July. The maximum CWMRs simulated at 600 hPa are275 and 250 mg/kg by CAM and Ferrier schemes respectively. The Ferrier scheme has simulated significantly higher CWMR than that of all other MPs from surface to 500 hPa level during 24-26 July 2015. The maximum CWMRs simulated at 600 hPa are 323 and 185 mg/kg by FE scheme on 25 and 26 July respectively. The NSSL-2 scheme has simulated lower area averaged CWMR and Ferrier scheme has simulated higher CWMR during 24-26 July 2015.

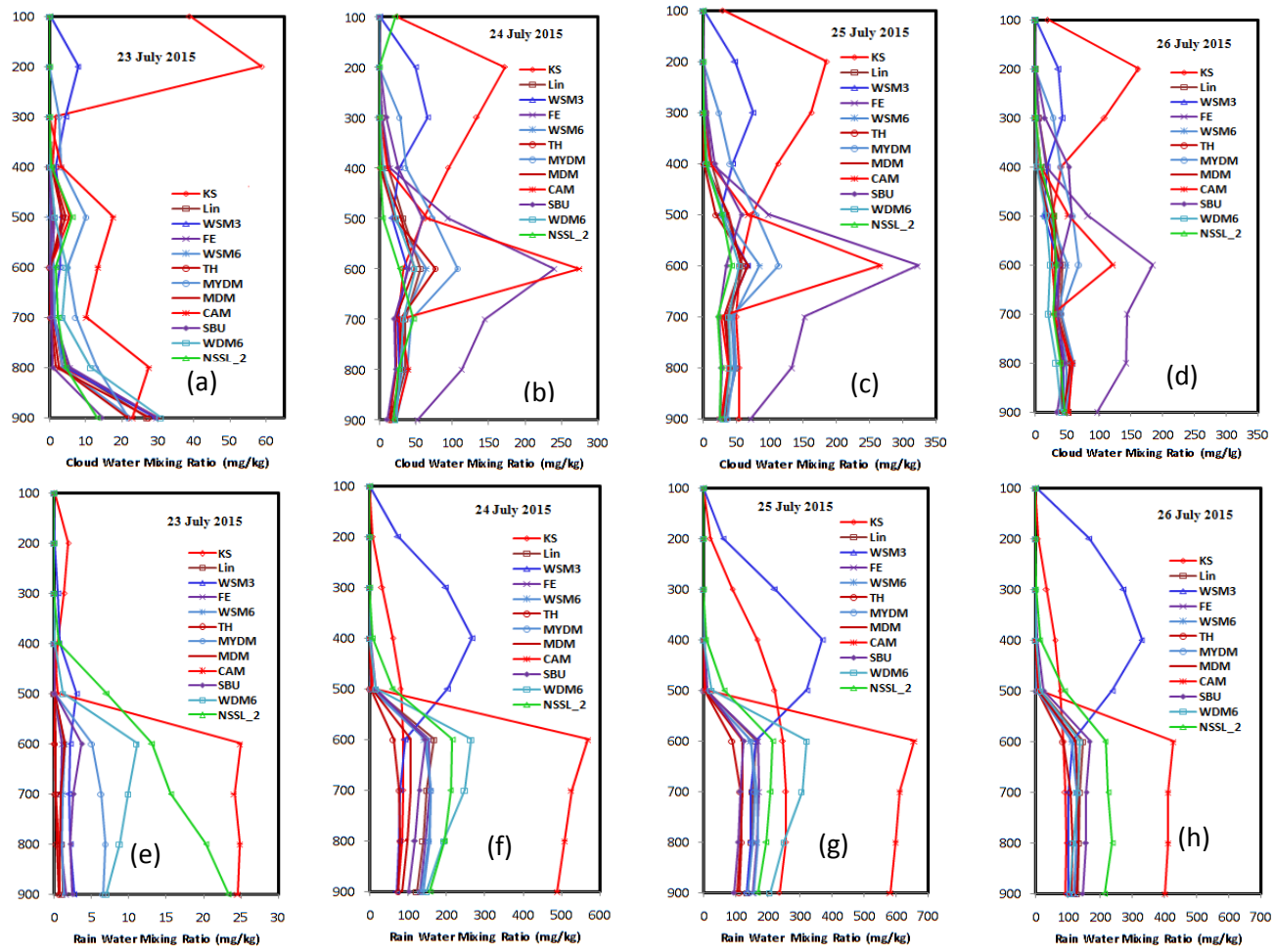

Fig. 25: Vertical profiles of time and space averaged (a-d) CWMR and (e-h) RWMR simulated by different MPs coupling with KF scheme during 23-26 July 2015.

4.2.10 Rain Water Mixing Ratio (RWMR)

The RWMR (contour) has been simulated along the line of maximum vertical velocity on 23, 24, 25 and 26 July 2015 using different MPs and is presented in Fig. 24(a-l) for 23 July. KS and WSM3 schemes have simulated RWMR up to 100 hPa and other MPs have simulated RWMR up to 500 hPa level during 23-26 July. The CWMR is found to have maximum along

the vertical line where vertical velocity and reflectivity are also maximum. Kessler scheme has simulated maximum RWMR at 600-400 hPa and WSM3 simulated maximum RWMR at 400-200 hPa level. The maximum RWMRs simulated by KS, Lin *et al*., WSM3, Ferrier, WSM6, Thompson, MYDM, MDM, CAM, SBU, WDM6 and NSSL-2 are 9, 8, 10, 3, 8, 5, 6, 5, 7, 6, 6 and 5 mg/kg respectively. Kessler scheme has simulated maximum RWMR at 800-500 hPa and WSM3 simulated maximum RWMR at 300-200 hPa level on 24 July. The maximum RWMRs simulated on 24 July by KS, Lin *et al*., WSM3, Ferrier, WSM6, Thompson, MYDM, MDM, CAM, SBU, WDM6 and NSSL-2 are 8, 7, 11, 2, 6, 7, 5, 6, 3, 6, 4 and 9 mg/kg respectively.

Kessler scheme has simulated maximum RWMR at 800-500 hPa and WSM3 has simulated double maximum of RWMR, one at 850-700 hPa and other maxima at 400-200 hPa level and NSSL-2 has simulated maximum at 700-500 hPa on 25 July. The maximum amount of RWMRs have been simulated on 25 July by KS, Lin et al., WSM3, Ferrier, WSM6, Thompson, MYDM, MDM, CAM, SBU, WDM6 and NSSL-2 and are 9, 6, 10, 4, 0, 8, 8, 7, 13, 7, 6 and 17 mg/kg respectively. The maximum RWMRs simulated on 26 July by KS, Lin *et al*., WSM3, Ferrier, WSM6, Thompson, MYDM, MDM, CAM, SBU, WDM6 and NSSL-2 are 10, 5, 7, 1, 5, 6, 4, 7, 8, 5, 4 and 6 mg/kg respectively.

The area averaged RWMR have been plotted and analyzed using different MPs during 23-26 July 2015 in the SE region of the country and are presented as in Fig. 25(e-h). On 23 July, all MP schemes have simulated RWMR from surface to 500 hPa except Kessler and NSSL-2 schemes (Fig. 25e). The NSSL-2 scheme has simulated up to 400 hPa and Kessler up to 100 hPa level. Significant amount of RWMR has been simulated by CAM, NSSL-2, WDM6, MYDM, SBU and WSM3 schemes. The other schemes have simulated little amount of RWMR throughout the troposphere. The highest amount of RWMR has been simulated by CAM scheme after that NSSL-2, WDM6, MYDM, SBU and WSM3 schemes respectively. The maximum RWMR has been simulated at 600 hPa 25 mg/kg by CAM scheme on 23 July. On 24 July all MP schemes have simulated significant amount of RWMR from surface to 500 hPa except Kessler, WSM3 and NSSL-2 schemes (Fig. 25f). The NSSL-2 scheme has simulated up to 400 hPa and Kessler and WSM3 schemes up to 100 hPa. The highest amount of RWMR has been simulated by CAM scheme and lowest amount by WSM3 scheme. The maximum RWMRs simulated at 600 hPa are570 and 250 mg/kg by CAM and WDM6 schemes respectively. The orders of the schemes which have simulated RWMR are as

follows: CAM> NSSL-2> WDM6> WSM6> FE> MYDM> Lin> SBU> MDM> Kessler> TH> WSM3 schemes.

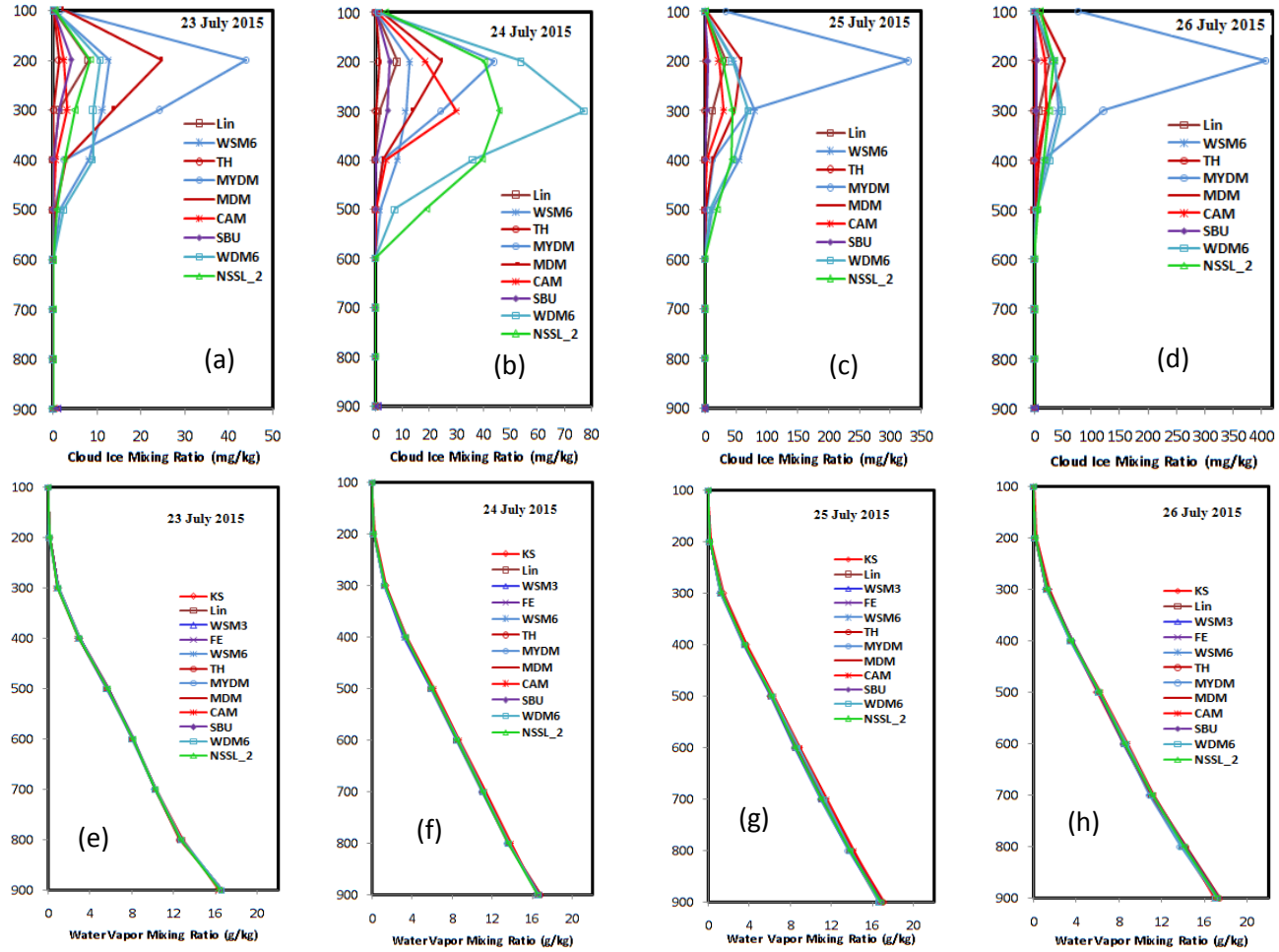

Fig. 26: Vertical profiles of time and space averaged (a-d) CIMR and (e-h) WVMR simulated by different MPs coupling with KF scheme during 23-26 July 2015.

On 25 July CAM scheme has simulated maximum RWMR and SBU simulated minimum RWMR throughout the troposphere (Fig. 25g). On 26 July, CAM scheme has simulated maximum amount of area averaged RWMR and KS scheme has simulated minimum amount of area averaged RWMR throughout the troposphere (Fig. 25h). The maximum RWMR has been simulated by CAM at 600 hPa with values of557 and 430 mg/kgon25 and 26 July 2015 respectively. It is found that the RWMR has been simulated maximum by CAM scheme on 25 July. After that the RWMR has been simulated by KS, WDM6, NSSL-2, WSM6 and FE schemes and rain is also found maximum and decreasing order by these schemes except CAM on 25 July. This suggests that the amount of rain simulated depends on RWMR in the lower to middle troposphere.

4.2.13 Cloud Ice Mixing Ratio (CIMR)

Area and time averaged vertical profiles of CIMR (mg/kg) using different MPs in combination with KF scheme during 23-26 July are shown in Fig. 26(a-d). The area averaged CIMR has been simulated at 600-100 hPa level and found maximum at 300-200 hPa during 23-26 July 2015. MYDM scheme has simulated maximum CIMR during 23-26 July except 24 July. It is evident that substantial difference exists between the various cloud ices. The MYDM profile has exhibited a prominent spike containing much larger CIMR values between 400-100 hPa and Thompson scheme has simulated less CIMR. On 23 July, the orders of simulated area averaged CIMRs are according to the order of schemes: MYDM> MDM> WSM6> WDM6> NSSL-2> Lin> SBU> CAM> Thompson schemes respectively. On 24 July, the orders of simulated area averaged CIMR are according to the order of schemes: WDM6> NSSL-2> MYDM> CAM> MDM> WSM6> Lin> SBU> Thompson schemes respectively. On 25 July, the orders of simulated area averaged CIMR are according to the order of schemes: MYDM> WSM6> WDM6> MDM> NSSL-2> CAM> Lin> SBU schemes respectively.

4.2.14 Water Vapor Mixing Ratio (WVMR)

Space and time averaged vertical profiles of WVMR are constant during 23-26 July 2015 for different MPs schemes as shown in Fig. 26(e-h). The patterns of water vapor profile are similar up to 100 h Pa level for all MP schemes during the study period. The cloud vapor mixing ratio has been decreased continuously from surface to 200 hPa level during 23-26 July.

4.2.15 Cloud Graupel Mixing Ratio

Area and time averaged vertical profiles of CGMR (mg/kg) using different MPs in combination with KF scheme during 23-26 July are shown in Fig. 27(a-d). The CGMR has been simulated by Lin, WSM6, Thompson, MYDM, MDM, WDM6 and NSSL-2 and the other MPs have not simulated CGMR in the troposphere. The area averaged CGMR has been simulated at 700-100 hPa level and is found maximum at 500-400 hPa during 23-26 July 2015. MYDM and Thompson schemes have simulated maximum and minimum CGMR during 23-26 July. Significant amount of CGMR has been simulated by the 7 mentioned MPs during 24-26 July. It is evident that substantial difference exists between the various MPs for the simulation of cloud graupel. All MP schemes have exhibited a prominent spike containing much larger CGMR values between 500-400 hPa, and Thompson and MDM schemes have

simulated less CGMR. On 23 July, the orders of simulated area averaged CGMR (Fig. 27a) are according to the order of the schemes: MYDM>WDM6>NSSL-2>Lin>WSM6 schemes respectively. On 24 July, (Fig. 27b) the orders of simulated area averaged CGMR are according to the order of the schemes: MYDM>WDM6>WSM6>Lin>NSSL-2>MDM>TH schemes respectively. On 25 July, (Fig. 27c) the orders of simulated area averaged CGMR are according to the order of the schemes: MYDM>WDM6>WSM6> Lin>MDM> NSSL-2>TH schemes respectively. On 26 July, (Fig. 27d) the orders of simulated area averaged CGMR are according to the order of the schemes: MYDM> WSM6> WDM6> Lin>MDM>NSSL-2> TH respectively. Sharp spikes of graupel are found to be 325, 300 and 250 mg/kg at 500 hPa level during 24, 25 and 26 July respectively for MYDM scheme.

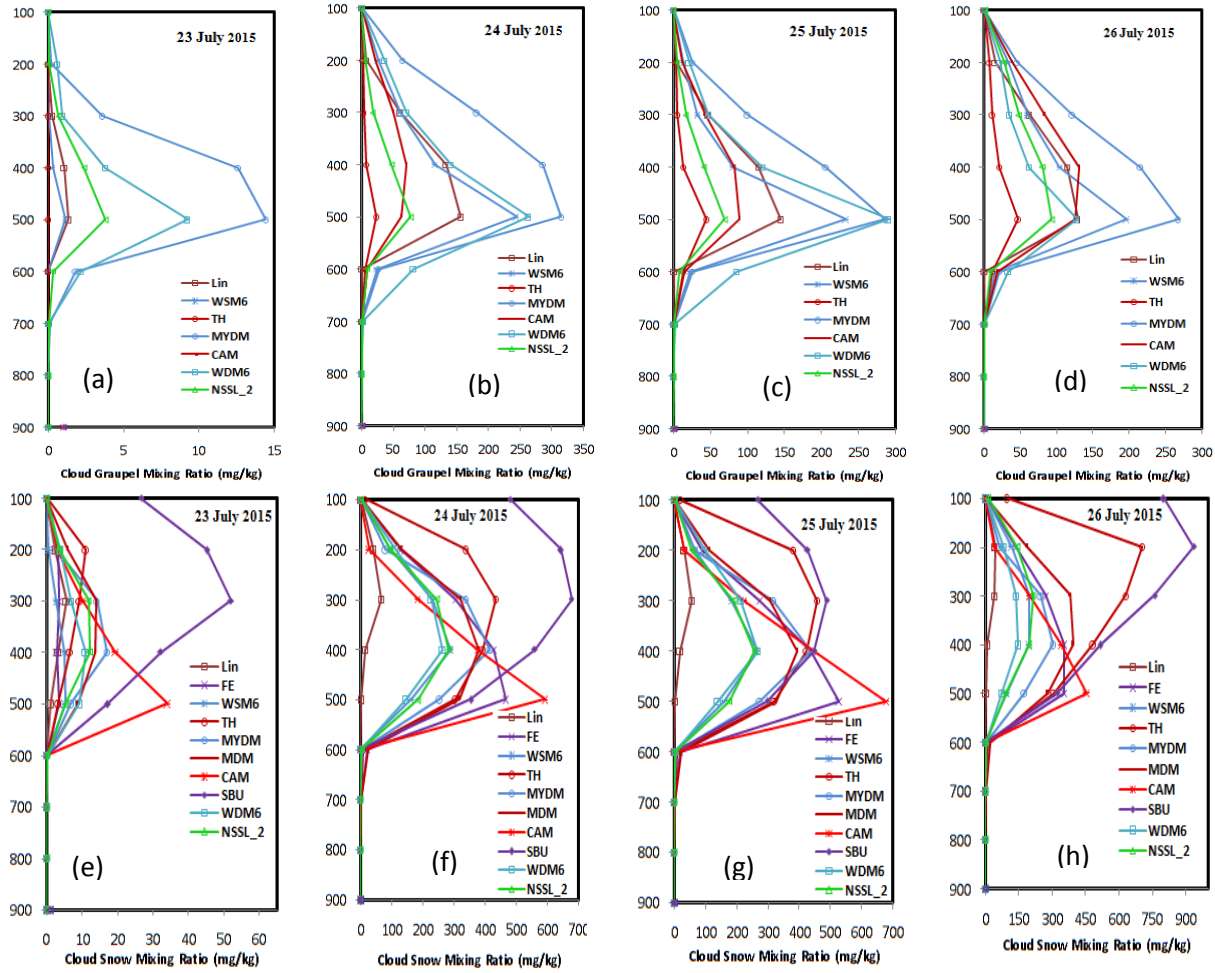

Fig. 27: Vertical profiles of time and space (a-d) Cloud graupel mixing ratio and (e-h) Cloud snow mixing ratio simulated by different MPs during 23-26 July 2015.

4.2.16 Cloud Snow Mixing Ratio (CSMR)

Area and time averaged vertical profiles of CSMR (mg/kg) using different MPs in combination with KF scheme during 23-26 July are shown in Fig. 27(e-h). The CSMR has

been simulated by Lin, FE, WSM6, Thompson, MYDM, MDM, CAM, SBU, WDM6 and NSSL-2 and the other MPs have not simulated CSMR in the troposphere. The area averaged CSMR has been simulated at 600-100 hPa level and is found maximum at 500-200 hPa during 23-26 July 2015. SBU and Lin schemes have simulated maximum and minimum CSMR during 23-26 July. Significant amount of CSMR has been simulated by SBU, Thompson, CAM, FE, MDM MYDM, NSSL-2 and Thompson MPs during 23-26 July. It is evident that substantial difference exists between the various MPs for the simulation of cloud snow. All MP schemes have exhibited a prominent spike containing much larger CSMR values between 500-200 hPa, and Thompson and MDM schemes have simulated less CSMR. On 23 July, the SBU scheme has generated the greatest amount of snow between 600 to 100 hPa. The CAM has simulated approximately half of the snow than that of SBU scheme, MYDM and another all MPs schemes have simulated approximately half of the snow than that of CAM scheme. The CAM has simulated almost near to the snow than that of SBU scheme, FE simulated almost near to snow that of CAM, MYDM, TH and MDM have simulated almost near to snow than that of FE scheme. Lin scheme has simulated less cloud snow mixing ratio than that of other schemes. The FE has simulated one third of the snow than that of CAM scheme, SBU and Thompson schemes have simulated almost near to snow that of FE. MDM has simulated almost near to snow than that of SBU and Thompson schemes. Lin scheme has simulated less cloud snow mixing ratio than that of other schemes. On 26 July, Thompson has simulated one third of CSMR than that of SBU. The CAM scheme has simulated half of CSMR than that of Thompson. MDM and FE schemes have simulated almost near to the CSMR than that of CAM. Lin scheme has simulated less cloud snow mixing ratio than that of other schemes.

4.3 Heavy rainfall during 30 August – 01 September 2015

4.3.1 Observed, TRMM and Model Simulated Rainfall for 30 August 2015

The observed and TRMM rainfall amounts over Bangladesh during 30 August - 1 September 2015 are presented in Fig. 28(a-f). The heavy rainfall is observed on 30 August (Fig. 28a) in the SE and NW region and light rainfall is found in the central to NE and SW regions of Bangladesh. Maximum rainfall is observed at Kutubdia, Dinajpur, Mymensingh, Sandwip and Sitakunda, and the amounts are 137, 96, 68, 57 and 52 mm respectively. TRMM (Fig. 28b) derived light rainfall all over the country on 30 August. Maximum rainfall is seen at Dinajpur, Sandwip, Sitakunda and Kutubdia, and the amounts are 44, 35, 33 and 32 mm respectively. It is seen that the distribution patterns of TRMM and observed rainfall are similar but TRMM derived rainfall is much lower than that of observed rainfall.

The rainfall amounts simulated using different MP schemes on 30 August 2015 are presented in Fig. 29(a-l). Kessler scheme has simulated heavy rainfall (Fig. 29a) in the S-SE and N-NE regions and light rainfall in the central to W-NW regions of Bangladesh. Maximum rainfall is simulated at Sylhet, Comilla, Teknaf, Cox's Bazar and Feni regions, and the amounts are 80, 74, 69, 66 and 66 mm respectively. Lin *et al.* and WSM3 schemes have simulated heavy rainfall (Fig. 29(b-c)) in the SE and NE regions of the country on that day and light rainfall is simulated at the central to W-NW regions. Maximum rainfall is simulated at Sylhet, Comilla, M. Court and Kutubdia regions, having the amounts 133, 69, 65 and 51 mm respectively and observed maximum is seen at Kutubdia, which indicates that the model simulated maximum rainfall is matched with the observed rainfall. Maximum rainfall is simulated by WSM3 scheme at Sylhet, Teknaf, Comilla and Cox's Bazar, where the amounts are 102, 73, 73 and 71 mm respectively. Ferrier scheme has simulated heavy rainfall in the SE and N-NE regions and light rainfall in the central to western regions (Fig. 29d). Maximum rainfall amounts simulated at Sylhet, Comilla, Cox's Bazar and Mymensingh are 110, 84, 70 and 64 mm respectively. The model simulated maximum rainfall position is matched with the observed rainfall position. WSM6 has simulated heavy rainfall in the S-SE and NE regions and light rainfall in the centre to W-NW regions (Fig. 29e). Maximum rainfall amounts simulated at Sylhet, Khepupara, Comilla and Cox's Bazar are 9 8, 85, 73 and 71 mm respectively. The model simulated maximum rainfall in the NE region is matched with the observed rainfall and minimum rainfall is also matched all through the country. The observed maximum rainfall position at NW region (Dinajpur) is not matched with simulated rainfall position.

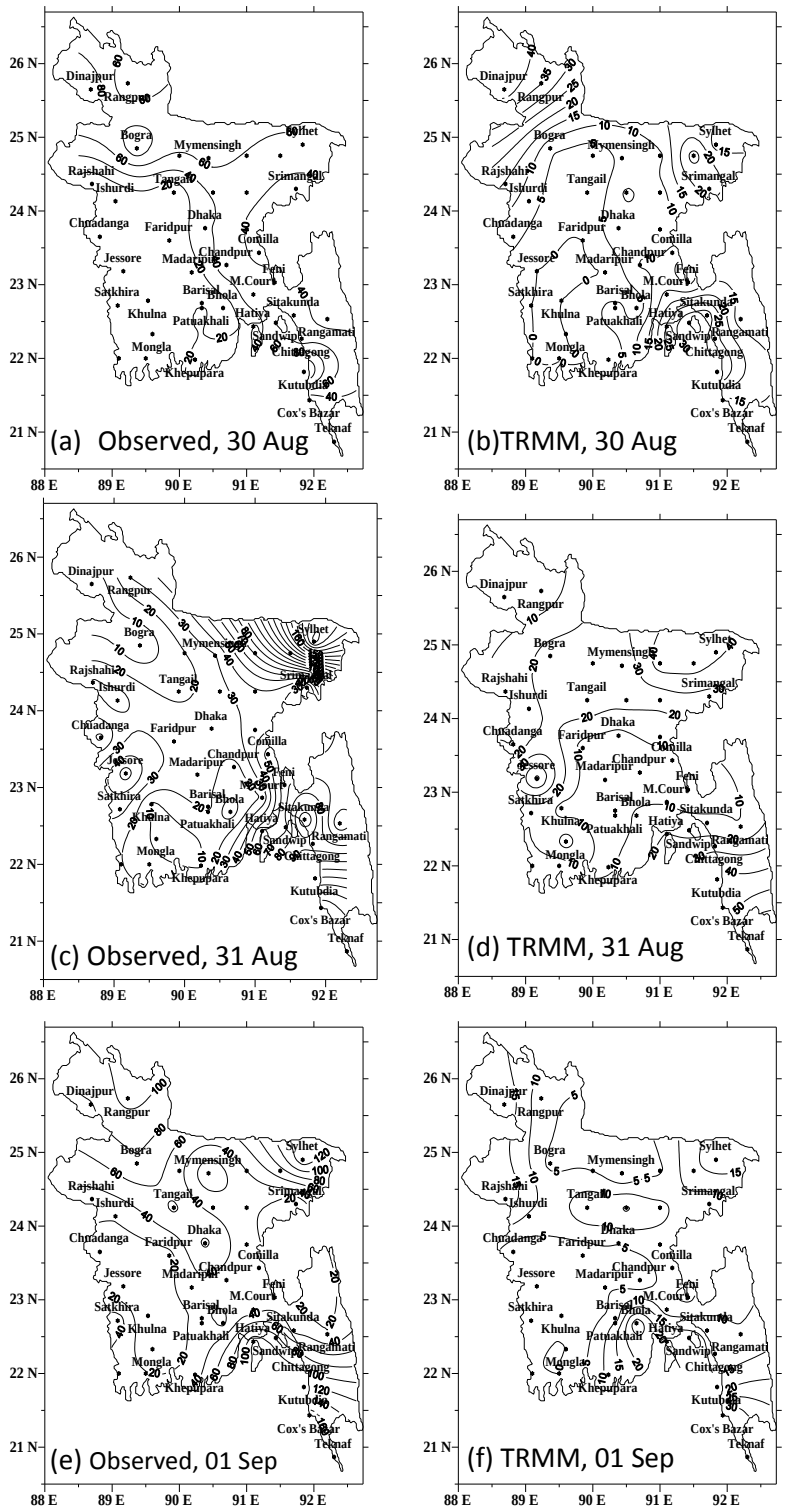

Fig. 28: Distribution of observed and TRMM rainfall during 30 August – 1 September 2015 over Bangladesh

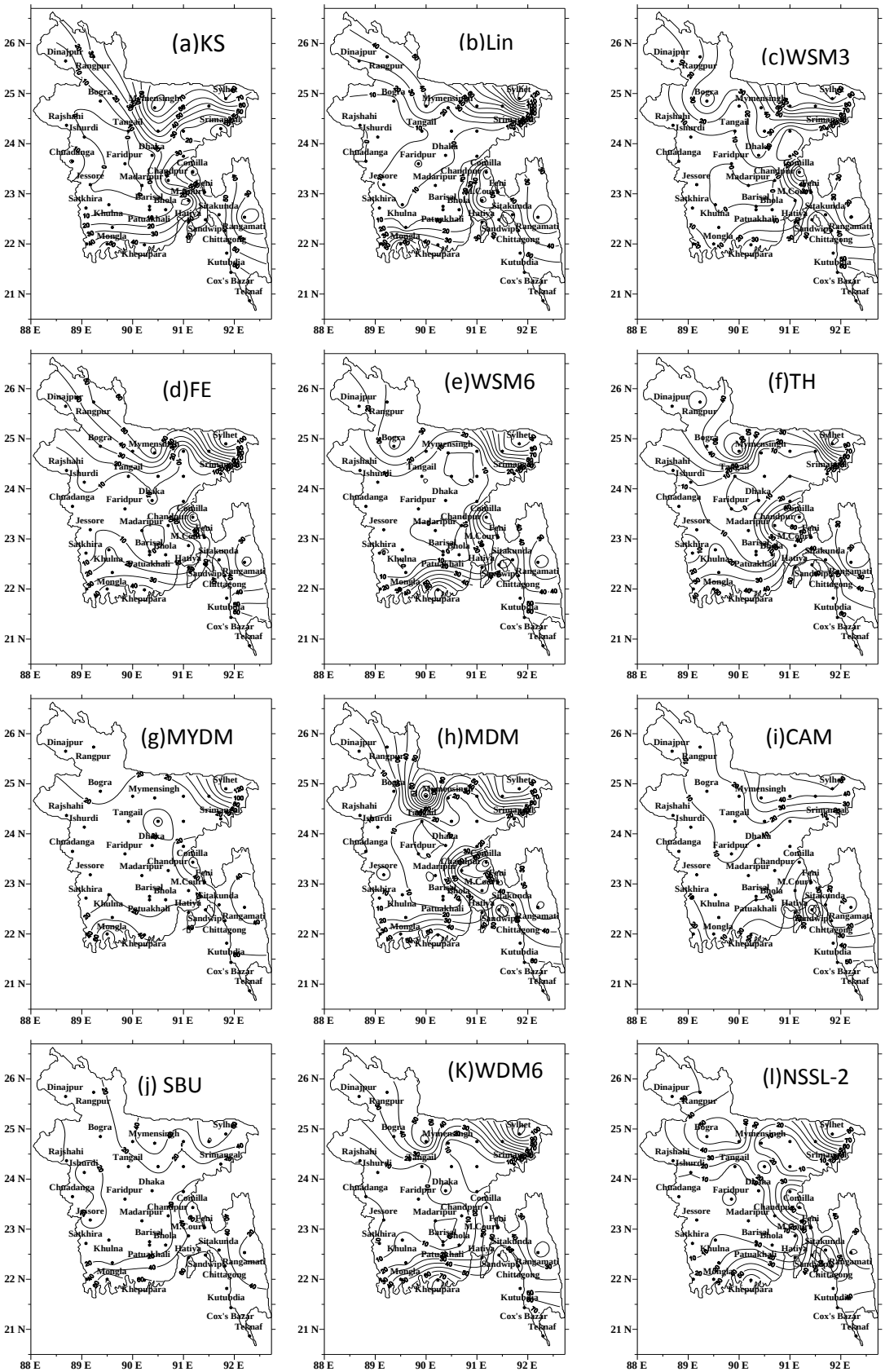

Fig. 29: Distribution of 24 hour model simulated station rainfall using different MPs of 30 August 2015 over Bangladesh.

Thomson scheme has simulated heavy rainfall in the S-SE, SW and NE regions and light rainfall occurred in the center to western regions (Fig. 29f). Maximum rainfall amounts simulated at Sylhet, Comilla, Teknaf and Cox's Bazar are 93, 80, 68 and 64 mm respectively, which indicates that the maximum rainfall position (except Dinajpur and Kutubdia) is matched with the observed maximum rainfall position. MYDM has simulated heavy rainfall in the NE regions and light rainfall is found all over the country (Fig. 29g). Maximum rainfall has been simulated at Sylhet, Teknaf, Comilla and Cox's Bazar and the amounts are 138, 74, 74 and 71 mm respectively on 30 August 2015. The model simulated maximum rainfall is almost in line with the observed rainfall at Sylhet. MDM scheme has simulated heavy rainfall in the N-NE and S-SE regions and light rainfall in the central to western regions (Fig. 29h) on 30 August. Maximum rainfall is found at Sylhet, Comilla, Teknaf, Khepupara and Cox's Bazar and the amounts are 100, 100, 77, 63 and 61 mm respectively, which indicates that the model simulated maximum rainfall is matched with the observed rainfall. CAM and SBU schemes have simulated heavy rainfall in the NE and SE regions and light rainfall in the western region (Fig. 29(i-j)). Maximum rainfall has been simulated at Teknaf, Sandwip, Sylhet, Cox's Bazar and Mymensingh is 72, 63, 57, 49 and 46 mm for CAM and at Comilla, Sylhet, Hatiya, Khepupara and Cox's Bazar and the amounts are 83, 63, 62, 62 and 55 mm respectively for SBU scheme. The model simulated maximum and minimum rainfall position is matched with observed rainfall for CAM and SBU schemes.

WDM6 and NSSL-2 schemes have simulated heavy rainfall in the SW, SE and NE regions and light rainfall in the centre to western regions (Fig. 29(k-l)). Maximum rainfall amounts simulated at Sylhet, Khepupara, Teknaf, Cox's Bazar and Sandwip are 113, 84, 78, 75 and 60 mm for WDM6 and at Chittagong, Khepupara, Sitakunda, Teknaf and Comilla are 75, 71, 69, 66 and 63 mm respectively for NSLL-2 scheme. The model simulated maximum rainfall is almost matched with the observed rainfall but maximum observed rainfall position at Kutubdia is shifted towards Chittagong. The simulated maximum rainfall is matched with the observed rainfall at Sylhet i.e. NE region for different microphysics schemes and the position of observed heavy rainfall in the NW region is not matched with the simulated rainfall.

4.3.2 Observed, TRMM and Model Simulated Rainfall for 31 August 2015

The heavy rainfall is observed on 31 August in the SE and NE region and light rainfall (Fig. 28c) is in all other regions of Bangladesh. Significant amount of rainfall is observed at Sylhet, Cox's Bazar, Teknaf, Kutubdia, Sitakunda and Chittagong and the amounts are 204, 160, 151, 120, 112 and 85 mm respectively on 31 August 2015. Maximum TRMM rainfall

(Fig. 28d) is seen at Teknaf, Jessore, Kutubdia and Sylhet and the amounts are 83, 54, 46 and 42 mm respectively. It is seen that the distribution patterns of TRMM and observed rainfall are nearly similar but TRMM derived rainfall is much lower than that of observed rainfall.

The rainfall amounts simulated using 12 different MPs coupling with KF scheme on 31 August 2015 are presented in (Fig. 30(a-l)). The Kessler, WSM3, WSM6, CAM and NSSL-2 schemes have simulated heavy rainfall in the S-SE and NE regions and light rainfall in the central to W-NW regions of Bangladesh. Maximum rainfall is simulated at Sandwip, Chittagong, Hatiya, Kutubdia and Sitakunda and the amounts are 175, 171, 177, 169 and 157 mm by Kessler (Fig. 30a), and the amounts at Sandwip, Sylhet, Cox's Bazar, Teknaf and Khepupara are 168, 152, 151, 143 and 128 mm simulated by WSM3 (Fig. 30c); rainfall amounts simulated by WSM6 at Sandwip, Chittagong, Sylhet, Hatiya and Cox's Bazar are 199, 176, 245, 186 and 173 mm (Fig. 30e), and the amounts simulated at Kutubdia, M. Court, Feni, Sitakunda and Chittagong are 163, 161, 143, 142 and 125 mm by CAM (Fig. 30i), whereas the amounts Sandwip, Chittagong, Feni, Sitakunda, Kutubdia are 172, 125, 170, 132 and 132 mm by NSSL-2 (Fig. 30l) schemes respectively. The simulated position of maximum rainfall in the SE region is matched with the observed rainfall.

Lin *et al.* Ferrier and MDM schemes have simulated heavy rainfall in the S-SE, NE and NW regions of the country on 31 August. Maximum rainfall is simulated at Sandwip, Sitakunda, Cox's Bazar, Sylhet and Chandpur and the amounts are 198, 185, 165, 156 and 131 mm by Lin et al. (Fig. 30b), the amounts simulated at Sandwip, Sitakunda, Sylhet, Cox's Bazar and Feni are 192, 179, 176, 166 and 157 mm by Ferrier (Fig. 30d) and the amounts simulated at Sandwip, Khepupara, Cox's Bazar, Teknaf and Chittagong are 195, 180, 168, 160 and 138 mm by MDM (Fig. 30h) respectively and the simulated heavy rainfall distribution pattern is matched with the observed maximum rainfall. Thomson and MYDM schemes have simulated heavy rainfall in the S-SE and NE regions and light rainfall in the centre to western region. Maximum rainfall has been simulated at Sandwip, Sitakunda, Cox's Bazar, Sylhet and Teknaf and the amounts simulated are 193, 171, 160, 165 and 158 mm by Thompson (Fig. 30f) whereas the amounts simulated at Sandwip, Sitakunda, Cox's Bazar, Kutubdia, Feni are 194, 208, 160, 187 and 167 mm respectively by MYDM (Fig. 30g) on 31 August 2015. The model simulated maximum rainfall is almost matched with the observed rainfall. SBU scheme has simulated heavy rainfall in the S-SE and NE regions and light rainfall occurred in the central towards west and NW regions (Fig. 30j). Maximum rainfall amounts simulated at

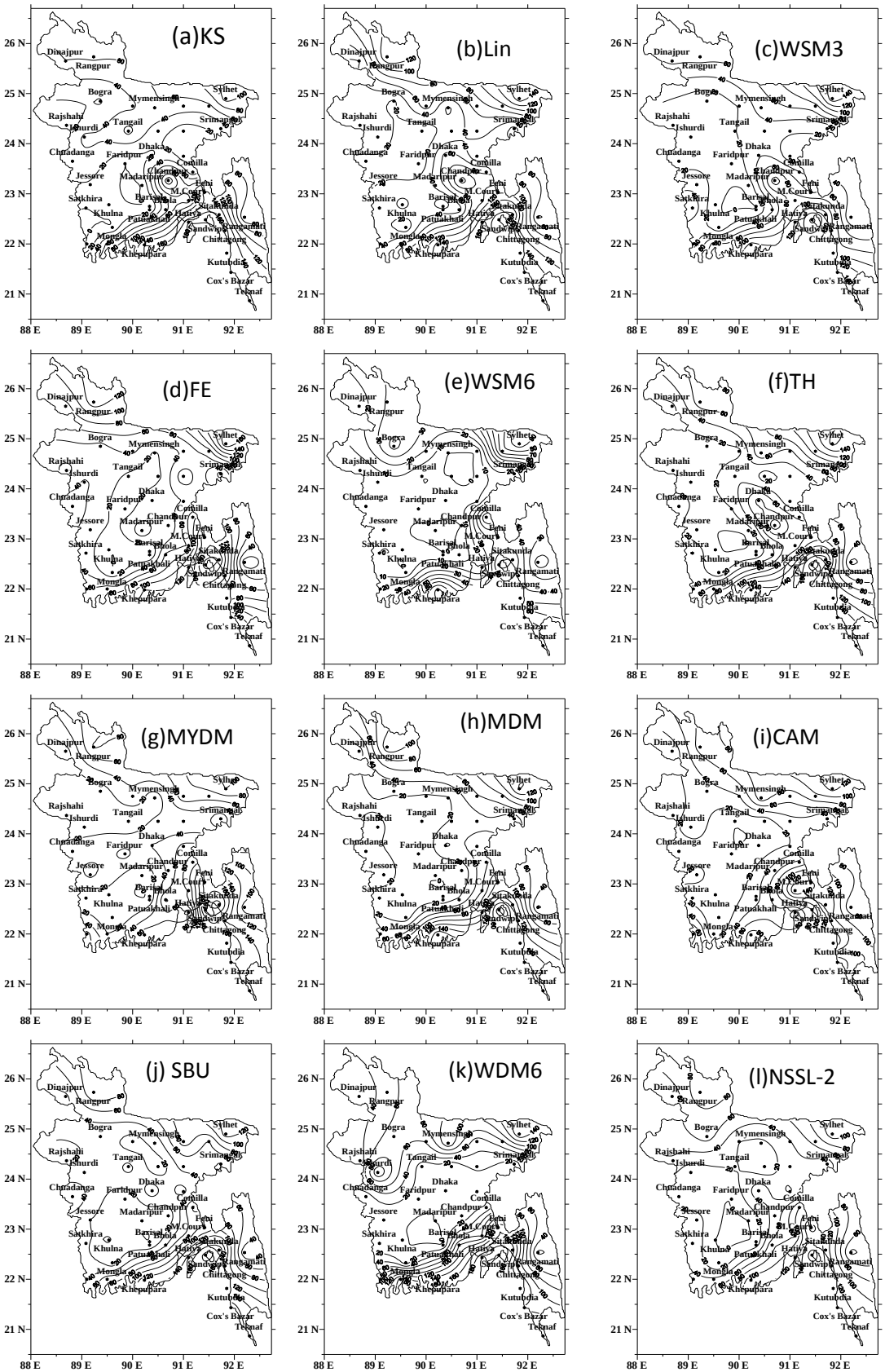

Fig. 30: Distribution of 24 hour model simulated station rainfall using different MPs of 31 August 2015 over Bangladesh.

Sandwip, Sitakunda, Cox's Bazar, Hatiya and Chittagong are 189, 178, 174, 147 and 115 mm respectively. WDM6 scheme has simulated heavy rainfall in the S-SE, West and NE region and light rainfall in the centre to other regions (Fig. 30k). Maximum rainfall simulated at Sandwip, Hatiya, Sitakunda, Feni and Sylhet is 201, 196, 170, 159 and 157 mm respectively. The model simulated maximum rainfall is matched with the observed rainfall as well as light rainfall also matched.

The model simulated heavy rainfall in the SE and NE regions of Bangladesh is almost matched with the observed rainfall for all MP schemes but almost all MPs also simulated heavy rain in the SW region on 31 August 2015. The simulated rainfall is also much higher than that of observed rainfall.

4.3.3 Observed, TRMM and Model Simulated Rainfall for 01 September

The heavy rainfall is observed in the SE, NE and NW regions and light rainfall in the centre to W-SW regions (Fig. 28e) of the country on 1 September. The amount of rainfall observed is 170, 158, 134, 119, 107 and 87 at Cox's Bazar, Teknaf, Sylhet, Kutubdia, Rangpur and Sandwip respectively. TRMM (Fig. 28f) derived light rainfall all over the country on that day. Maximum TRMM rainfall is seen at Cox's Bazar, Teknaf, Bhola and Hatiya is 39, 29, 29 and 20 mm respectively. It is seen that the distribution pattern of TRMM and observed rainfall are almost similar but TRMM derived rainfall is much lower than that of observed rainfall.

The rainfall simulated using different MP schemes coupling with KF scheme on 1 September 2015 is presented in Fig. 31(a-l). Kessler and Lin *et al*., schemes have been simulated heavy rainfall in the SE and NE regions and light rainfall in the central to W-NW and SW regions of Bangladesh. Significant amount of rainfall is being simulated at Teknaf, Kutubdia, Cox's Bazar, Chittagong and Sitakunda regions are 232, 227, 223, 160 and 155 mm by Kessler scheme (Fig. 31a), Teknaf, Kutubdia, Cox's Bazar, Chittagong and Sitakunda regions are 265, 352, 255, 189 and 169 mm respectively by Lin *et al*., scheme (Fig. 31b). The model simulated heavy rainfall in the region where the heavy rainfall was observed but the model simulated rainfall much higher than that of BMD observed rain. WSM3, Ferrier, WSM6, Thompson, MYMD and MDM schemes have been simulated heavy rainfall in the SE and NE regions and light rainfall in other regions of the country (Fig. 31(c-h)). Maximum rainfall has simulated are 231, 216, 184, 160 and 78 mm by WSM3 scheme,

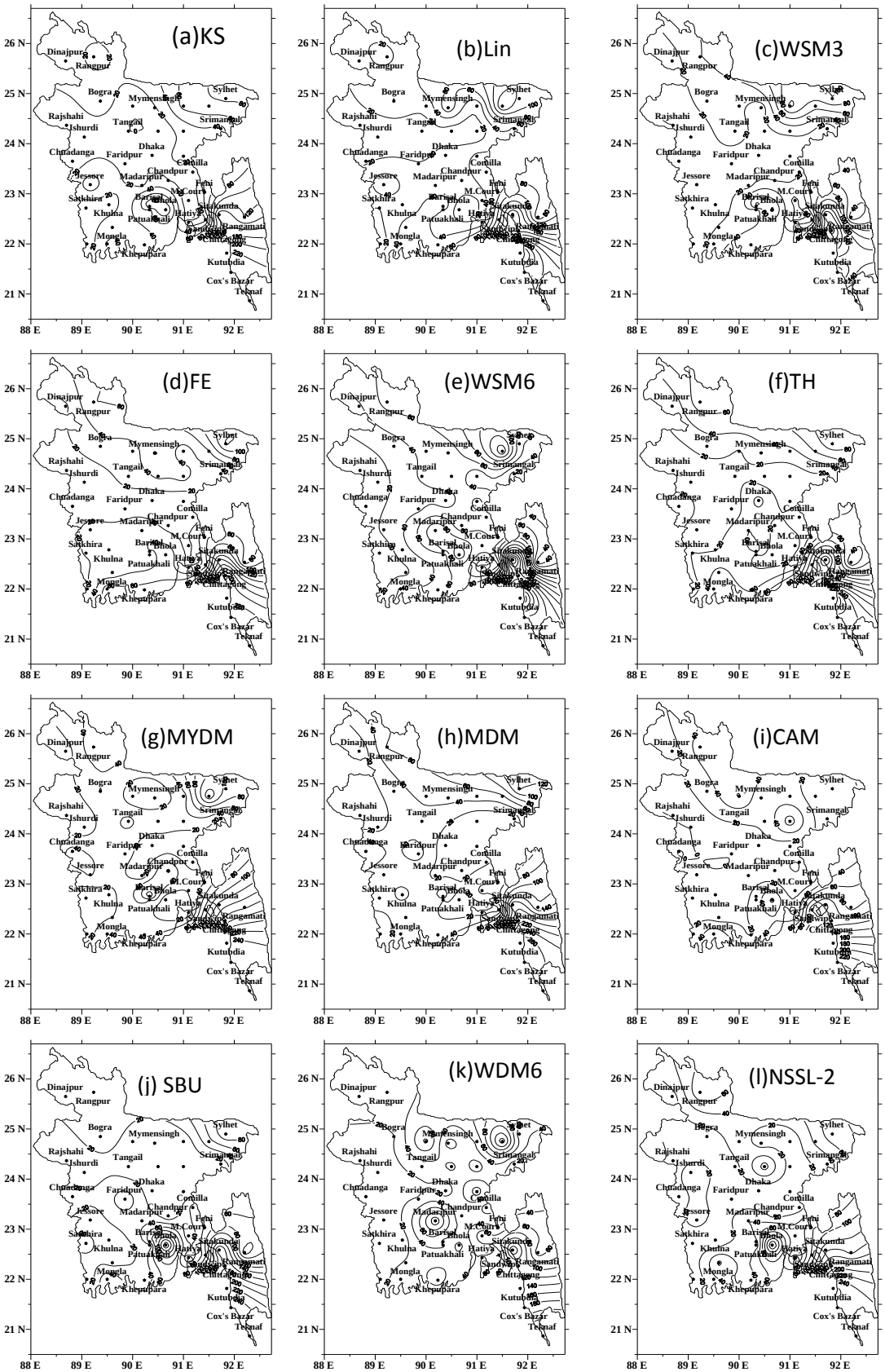

Fig. 31: Distribution of 24 hour model simulated station rainfall using different MPs of 1 September 2015 all over Bangladesh.

245, 231, 143, 209 and 143 mm by Ferrier scheme, 246, 229, 295, 362 and 250 mm by WSM6 scheme, 255, 121, 189, 321 and 250 mm by Thompson scheme, 260, 169, 128, 252 and 248 mm by MYDM scheme and 255, 216, 176, 280 and 258 mm by MDM scheme at Teknaf, Chittagong, Sitakunda, Kutubdia and Cox's Bazar respectively, which is matched with the observed maximum rainfall position. The model simulated maximum rainfall position in the SE region is matched with the observed rainfall position but the simulated rainfall in the NW region could not match with the observed heavy rainfall. CAM and WDM6 schemes have simulated heavy rainfall in the S-SE and NE regions and light rainfall in the central region to W-NW regions (Fig. 31(i & k)). Maximum rainfall is simulated 253, 242, 174 and 126 mm by CAM and 261, 180, 142 and 164 mm by WDM6 scheme at Teknaf, Cox's Bazar, Kutubdia and Sitakunda respectively. SBU and NSSL-2 schemes have simulated heavy rainfall in the SE region and light rainfall in the central to W-NW and SW regions (Fig. 31(j & l)). Maximum rainfall has simulated at Cox's Bazar, Teknaf, Kutubdia, Bhola and Chittagong regions is 259, 254, 223, 186 and 180 mm by SBU scheme and 250, 241, 266, 170 and 190 mm by NSSL-2 schemes respectively on 1 September 2015. The model simulated maximum rainfall in the SE region is matched with the observed rainfall and minimum rainfall is also matched all through the country.

The model simulated maximum rainfall position and amount is matched with the observed rainfall position and amount. All MPs except CAM have been simulated maximum rainfall in the SE and NE regions that is matched with the observed rainfall but the heavy rainfall in the NW region could not match by the simulation of rainfall for different MP schemes.

4.3.4 Area average rainfall during 30 August to 1 September 2015

Average observed rainfall of 35 BMD rainfall stations all over Bangladesh, model simulated by different MPs and TRMM rainfall during 30 August to 1 September 2015 are presented as in Fig. 32(a-d). Model simulated rainfall by different MPs, TRMM rainfall and heavy rainfall observed in the 5 SE stations during 30 August – 1 September 2015 are presented as in Fig. 32(e-h). On 30 August Thompson, MDM and SBU schemes have been simulated (Fig. 5a) almost similar average rainfall as observed from 35 Meteorological stations of all over Bangladesh and all other MP schemes have also simulated nearly equal rainfall and CAM has simulated less rainfall among the MP schemes. All MPs except CAM have simulated more rainfall than that of observed (Fig. 32b) in the SE region (i.e. heavy rainfall stations) of the country. TRMM derived rainfall is much lower than that of observed rainfall of all Bangladesh station average and also heavy rainfall stations (5 stations) in the SE region of the

country. On 31 August WSM3 and CAM schemes have simulated (Fig. 32c) almost similar average rainfall as observed from 35 Meteorological stations of all over Bangladesh and all other MP schemes have simulated higher rainfall and Lin *et al.* and WSM6 has simulated much higher rainfall among the MP schemes. WSM3 and CAM schemes have simulated almost same amount of rainfall and all other MPs simulated higher rainfall and WSM6 and WDM6 schemes (Fig. 32d) simulated much higher rainfall than that of observed rainfall in the SE region (i.e. heavy rainfall stations) of the country. TRMM derived rainfall is much lower than that of observed rainfall all over Bangladesh and also heavy rainfall stations (5 stations) in the SE region of the country.

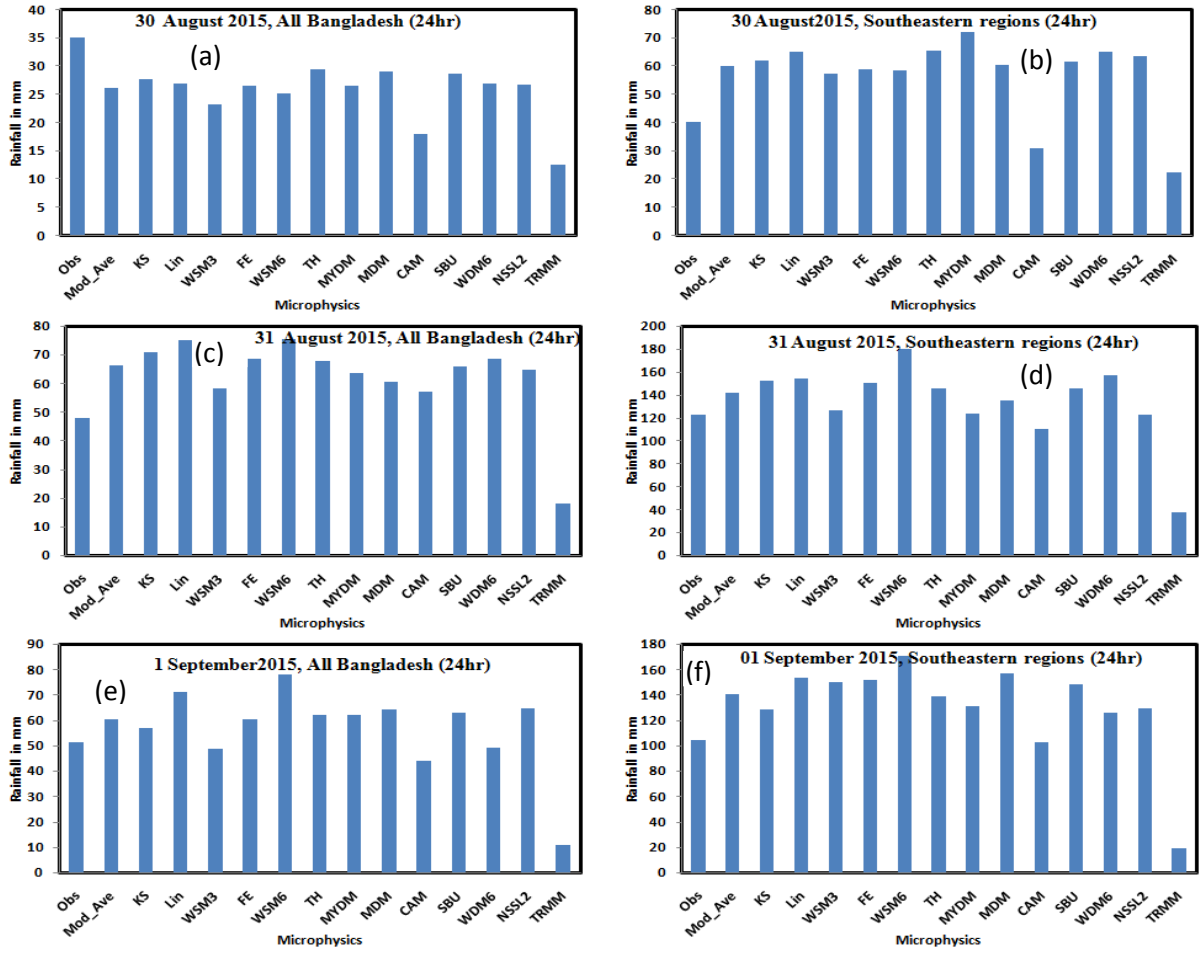

Fig. 32: Model simulated, TRMM derived and observed all Bangladesh stations average rainfall and also heavy rainfall stations (5 stations) in the SE region of the country during 30 August to 1 September 2015 using different MPs.

On 1 September WSM3, CAM and WDM6 schemes have simulated (Fig. 32e) almost similar average rainfall as observed from 35 Meteorological stations of all over Bangladesh and all other MP schemes have simulated higher rainfall and Lin *et al.* and WSM6 has simulated much higher rainfall among the MP schemes. CAM scheme has simulated almost same

amount of rainfall and all other MPs simulated higher rainfall and WSM6, MDM and SBU schemes (Fig. 32f) have simulated much higher rainfall than that of observed rainfall in the SE region (i.e. heavy rainfall stations) of the country. TRMM derived rainfall is much lower than that of observed rainfall all over Bangladesh and also heavy rainfall stations (5 stations) in the SE region of the country.

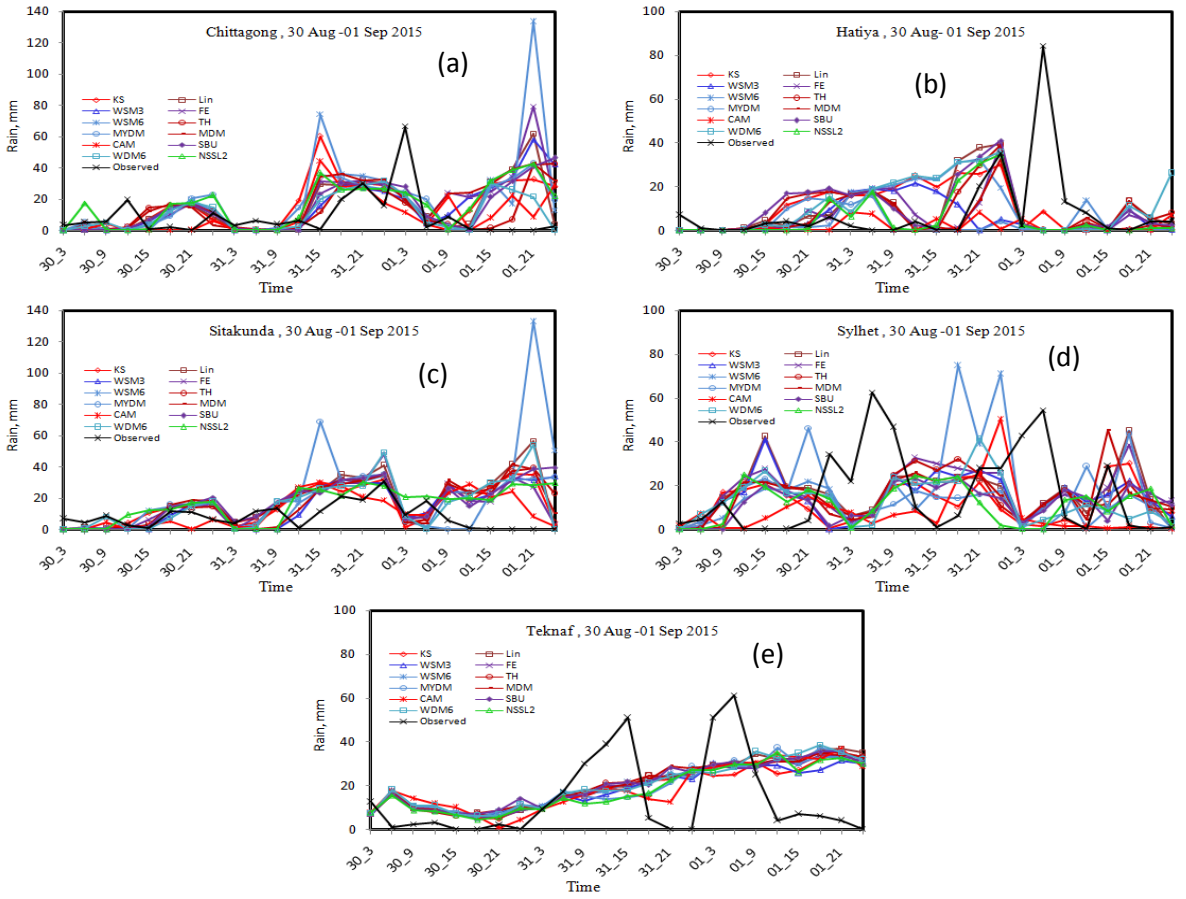

Fig. 33: 3-hourly observed and model simulated rain at (a) Chittagong, (b) Hatiya, (c) Sitakunda, (d) Sylhet and (e) Teknaf in the SE region using different MPs during 30 August- 1 September 2015.

4.3.5 Space and Time dependent Rain during 30 August-01 September 2015

3-hourly observed and model simulated rainfall at Cox's Bazar, Teknaf, Sandwip, Kutubdia and Chittagong and all above 5 stations in the SE region using different MPs coupling with KF scheme during 30 August to 1 September 2015 are presented in Fig. 33(a-f). At Chittagong all MPs have simulated 3 peaks but observation shows two peaks (Fig. 33a). All MPs have been simulated 1st peak 6 hours later and 2nd peak 12 hour earlier than that of observed. At Hatiya (Fig. 33b) the different MPs simulated peak of rainfall have found earlier than that of observed. At Sitakunda (Fig. 33c) the simulated peak of rainfall matched with the

observed peak except 1 September peak. At Sylhet (Fig. 33d) the model simulated 3 peaks of rainfall and from observation it is also found 3 peaks but model simulated 1st and 2nd peaks 6 hours later. At Teknaf (Fig. 6e) the time of 3-hourly simulated maximum rainfall is continuously increased but the model simulated rainfall is not matched with the observed peak of rainfall.

4.3.6 Vertical Velocity

The simulated position of maximum updraft has identified for different MP schemes every day during 30 August to 1 September 2015. Along the line of maximum updraft, vertical velocities (shaded) have plotted at 30 August for different MP schemes (Figure not shown). The maximum updrafts simulated times and position are different for different MP schemes. The maximum updrafts 6, 12, 17, 7, 14, 10, 14, 13, 3, 10, 11 and 9 ms^{-1} simulated by KS, Lin et al., WSM3, FE, WSM6, TH, CAM, MYDM, MDM, SBU, WDM6 and NSSL-2 schemes respectively at the times of 2400 UTC for all MP schemes except FE, SBU and NSSL-2. FE scheme has simulated maximum updraft at 2100 UTC, SBU at 1500 UTC and NSSL-2 at 2100 UTC.

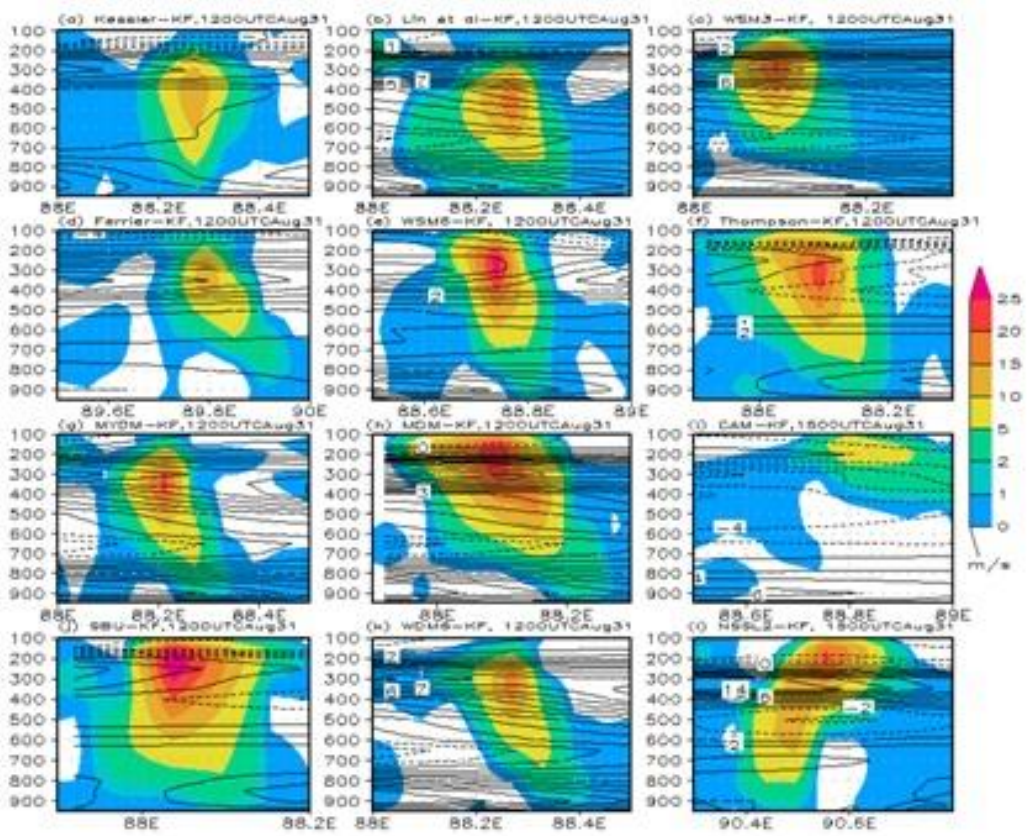

Fig. 34: WRF model simulated maximum vertical velocity (shaded) and vorticity (contour) along the line of maximum updraft using different MP schemes for 31 August 2015.

The maximum updraft is simulated at around 600-200 hPa by KS, Lin, WSM3, FE, WSM6, MYDM, Thompson and MDM schemes on 30 August. The updraft simulated is much less by CAM on this day. The updraft in the upper troposphere could be due to the latent heat release during glaciations and vapor deposition in all combination of MPs and KF scheme. The maximum updrafts 14, 18, 20, 14, 27, 23, 22, 22, 22, 5, 26, 18 and 16 m s^{-1} simulated by KS, Lin *et al*., WSM3, FE, WSM6, TH, MYDM, MDM, CAM, SBU, WDM6 and NSSL-2 schemes at times of 1200 UTC for all MP schemes except MDM and NSSL-2 and are presented in Fig. 34(a-l). The maximum updraft is simulated at around 700-200 hPa by KS, FE and CAM, 700-100 h Pa by WSM6, Thompson, MDM, SBU and NSSL-2 schemes on 31 August 2015. The updraft simulated is much less by CAM on this day. The maximum updrafts 11, 20, 17, 15, 22, 15, 24, 21,4,18, 14 and 18 m s^{-1} (Figure not shown) simulated by KS, Lin et al., WSM3, FE, WSM6, TH, MYDM, MDM, CAM, SBU, WDM6 and NSSL-2 schemes at times of 1200, 2100, 1200, 2400, 0900, 0900, 2400, 1200, 2400, 2400, 0900 and 2400 UTC respectively on 1 September 2015. The maximum updraft is simulated at around 700-200 hPa Lin *et al*., FE, WSM6, MYDM, MDM, SBU and NSSL-2. The updraft simulated is much less by KS, CAM and WDM6 on this day.

4.3.7 Vorticity

Along the line of maximum updraft, the vorticity (contour) have plotted for different MP schemes at 30 August (Figure not shown). The negative vorticity has simulated in the troposphere for all MPs except FE and WDM6 schemes. The positive vorticity has simulated in the lower to upper troposphere from 900-300 hPa levels and negative vorticity from 200-100 hPa levels by FE scheme on 30 August. WDM6 has simulated negative vorticity in the upper troposphere and positive vorticity in the lower to upper troposphere on this day. On 31 August, all MPs have simulated positive vorticity in the lower to upper troposphere except Kessler, Thompson and SBU schemes and are presented in Fig. 34(a-l). The positive vorticity has simulated in the lower to upper troposphere 900-200 hPa by Kessler scheme and positive vorticity from lower to middle troposphere and negative vorticity in the middle to upper troposphere by Thompson and SBU schemes. On 1 September positive vorticity has simulated in the lower to upper troposphere (Figure not shown) and negative vorticity from 200-100 hPa by KS, WSM3 and FE. Positive vorticity has simulated in the lower to middle troposphere and negative vorticity has simulated in the middle to upper troposphere by Lin *et al*., MYDM, MDM, CAM, SBU and NSSL-2 schemes. The other MP schemes have

simulated positive vorticity in the lower and upper troposphere and negative vorticity in the middle troposphere.

4.3.8 Relative Humidity (RH)

The RH (contour) is simulated along the line of maximum vertical velocity using different MPs on 30 August to 1 September 2015, when heavy rainfall observed in the SE region. All MPs coupling with KF scheme have simulated RH up to 100 hPa on 30 August to 1 September 2015 except KS scheme for 31 August. On 30 August all MPs coupling with KF scheme has simulated (Figure not shown) maximum RH >95% up to 300 hPa level where the vertical velocity and reflectivity is found maximum. On 31 August the maximum RH >95% is simulated for all MPs up to 400 hPa level (Fig. 35(a-l)) except KS, MDM, CAM and WDM6 where the vertical velocity and reflectivity is found maximum. On 01 September 2015 all MPs have simulated RH up to 100 hPa (Figure not shown) and maximum RH >95% is simulated for all MPs up to 400 hPa level except WSM3, MDM and WDM6 where the vertical velocity and reflectivity is found maximum.

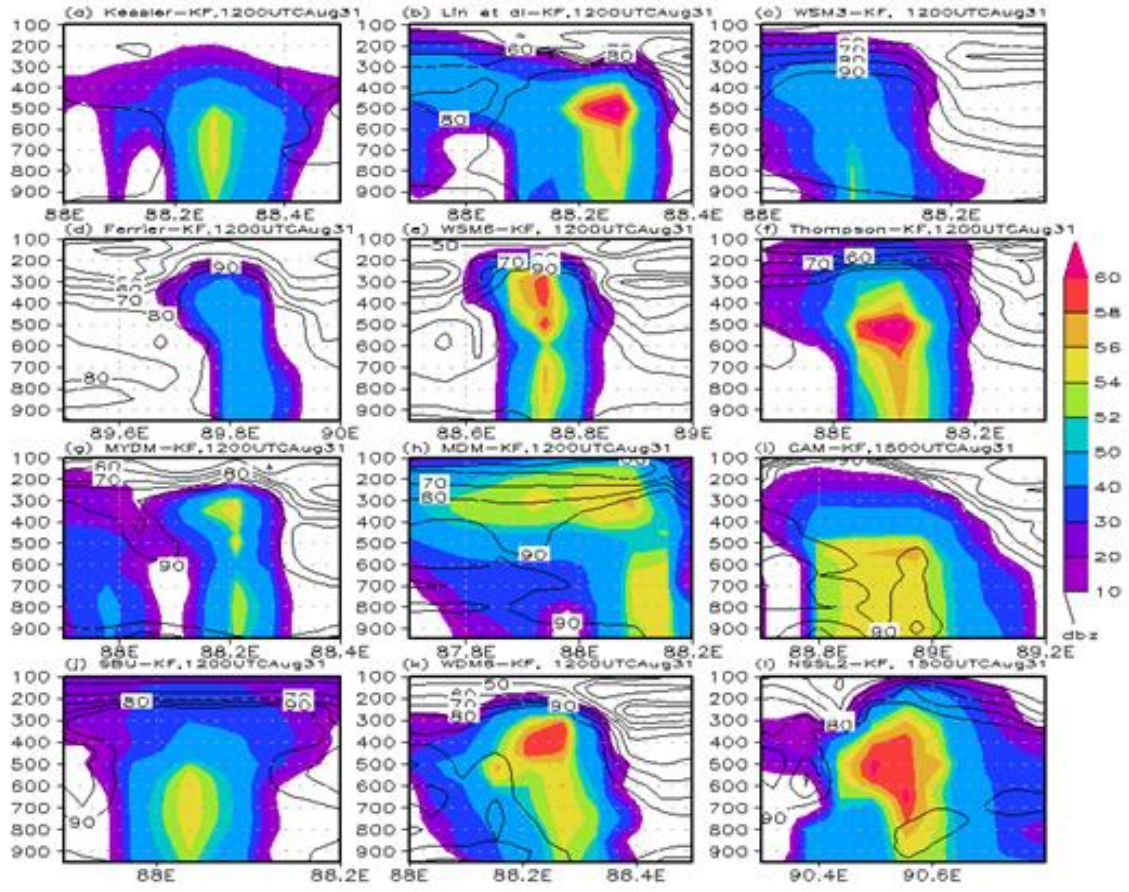

Fig. 35: WRF Model simulated reflectivity (shaded) and relative humidity (contour) using different MPs along the line of maximum vertical velocity on 31 August 2015.

4.3.9 Reflectivity

The reflectivity (shaded) has been plotted for the heavy rainfall event during 30 August to 1 September 2015 along the line of maximum vertical velocities using different MPs schemes. Lin, WSM3, WSM6, TH, MYDM, MDM, WDM6, SBU and NSSL-2 schemes have simulated reflectivity up to 150 hPa, Kessler, Ferrier and CAM schemes simulated reflectivity up to 200 hPa. Around 60 dBz reflectivity has simulated from 600-400 hPa by Lin *et al.,* WSM6 and WDM6 schemes on that day. On 31 August, WSM3, TH, SBU, WDM6 and NSSL-2 schemes have simulated reflectivity up to 100 hPa (Fig. 35(a-l)) and other schemes have simulated reflectivity up to 200 hPa. Lin et al., WSM6, Thompson, WDM6 and NSSL-2 schemes have simulated reflectivity around 60 dBz from 600-300 hPa on that day. The simulated reflectivity is much higher on 1 September than that of 30 and 31 August. Lin *et al*., WSM6 and WDM6 have simulated around 60 dBz reflectivity at different levels for 30 August to 1 September. Others have been simulated less reflectivity on those days.

4.3.10 Cloud Water Mixing Ratio (CWMR)

The CWMR (Shaded) has simulated using different MPs along the line of maximum vertical velocity on 30 August to 1 September 2015 and is presented for 31 August in Fig. 36(a-l). KS and WSM3 schemes have simulated CWMR up to 100 hPa and Lin et al., MYDM and SBU schemes up to 200 hPa, FE, WSM6, MDM, WDM6 and NSSL-2 schemes simulated up to 300 hPa and Thompson up to 400 hPa (Figure not shown) on 30 August. The CWMR is found to have maximum along the vertical line where vertical velocity and reflectivity are also maximum. Ferrier scheme has simulated maximum CWMR at 800-300 hPa, MYDM and SBU simulated maximum at 500-300 hPa level. KS and WSM3 schemes have simulated CWMR up to 100 hPa and FE, WSM6, Thompson, MYDM and SBU schemes have simulated up to 200 hPa and other schemes have simulated up to 300 hPa on 31 August. Ferrier scheme has simulated maximum CWMR at 900-200 hPa, Thompson, MYDM and SBU simulated maximum at 500-200 hPa level. KS, Lin et al., WSM3, FE, MYDM, SBU, WDM6 and NSLL-2 schemes have simulated CWMR up to 200 hPa (Figure not shown) and Thompson and MDM schemes have simulated up to 300 hPa and CAM scheme has simulated up to 500 hPa (Figure not shown) on 01 September. Ferrier scheme has simulated maximum CWMR at 900-200 hPa, MYDM has simulated at 700-300; SBU has simulated maximum at 500-200 hPa level on 1 September.

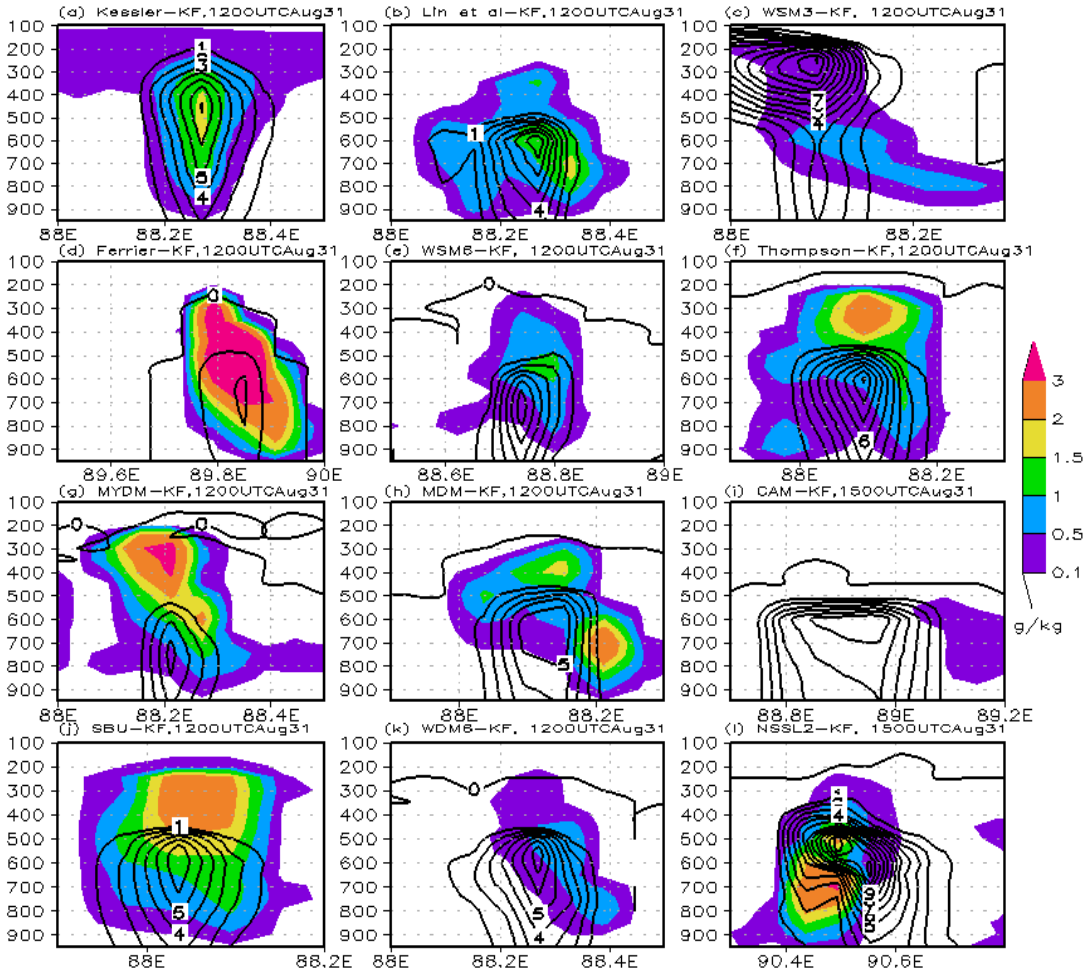

Fig. 36: WRF Model simulated CWMR (shaded, g/kg) and RWMR (contour, g/kg) using different MPs along the line of maximum vertical velocity on 31 August 2015.

The area average CWMR has plotted and analyzed in the SE region of the country using different MPs during 30 August to 1 September 2015 and are presented as in Fig. 37(a-c). On 30 August all MP schemes have simulated one maxima of CWMR from surface to 700 hPa except KS, WSM3 and FE schemes. The maximum is found at 800-700 hPa (Fig. 37a) level for all MPs schemes. The maximum CWMR simulated at 750 hPa 59mg/kg by CAM scheme on 30 August. On 31 August (Fig. 37b) and 1 September (Fig. 37c), the area average CWMR has been simulated two maxima. The first maxima are found at 750 hPa 74 mg/kg by CAM scheme and second maxima at 250 hPa level 100 mg/kg by Kessler scheme. The first maxima are found at 550 hPa 73 mg/kg by CAM scheme and second maxima at 120 hPa level 100 mg/kg by Kessler scheme on 1 September. The CAM scheme has simulated significantly higher CWMR than that of all other MPs from surface to 400 hPa level during the study period. The SBU scheme has simulated lower area average CWMR during 30 August to 1 September.

4.3.11 Rain Water Mixing Ratio (RWMR)

The RWMR (contour) has simulated along the line of maximum vertical velocity using different MPs during 30 August to 1 September 2015 and is presented for 31 August in Fig. 36(a-l). RWMR has simulated by WSM3 scheme up to 100 hPa and KS, WSM6, MYDM and NSSl-2 schemes up to 200 hPa, FE, Thompson and WDM6 schemes up to 300, MDM scheme up to 400 hPa, Lin et al. and SBU schemes up to 500 hPa on 30 August. The RWMR has found maximum along the vertical line where vertical velocity and reflectivity has also maximum. All MPs have been simulated maximum RWMR at 800-500 hPa except Kessler and WSM3 schemes. Kessler and WSM3 schemes have simulated maximum RWMR at 800-300 and 500-100 hPa level during 30 August 1 September.

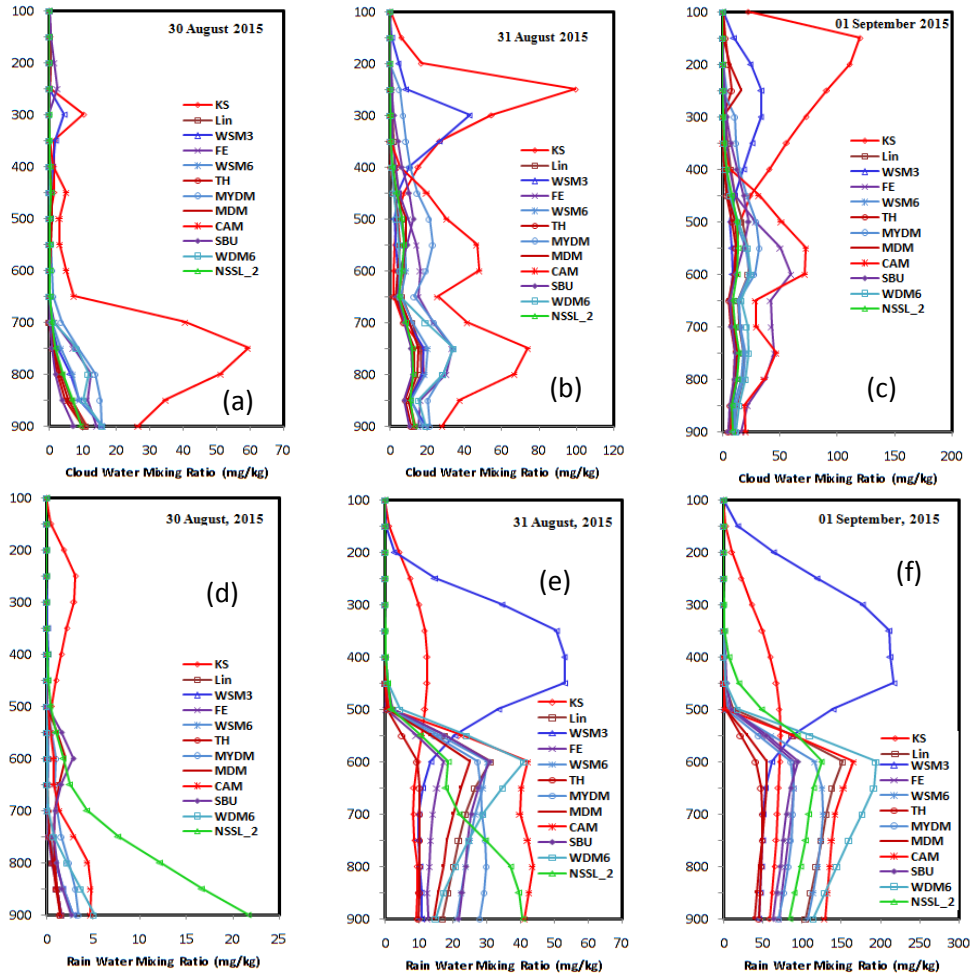

Fig. 37: Vertical profiles of time and space averaged (a-c) CWMR and (d-f) RWMR simulated by different MPs coupling with KF scheme during 30 August - 01 September 2015.

The maximum RWMR simulated by KS, Lin *et al.*, WSM3, Ferrier, WSM6, Thompson, MYDM, MDM, CAM, SBU, WDM6 and NSSL-2 are 5, 6, 10, 2, 4, 4, 5, 3, 4, 5, 5 and 5

mg/kg respectively. Kessler scheme has simulated maximum RWMR at 800-500 hPa and WSM3 simulated maximum RWMR at 300-200 hPa level on 30 August. The maximum RWMR simulated on 24 July by KS, Lin *et al.*, WSM3, Ferrier, WSM6, Thompson, MYDM, MDM, CAM, SBU, WDM6 and NSSL-2 are 7, 7, 12, 2, 6, 9, 4, 5, 6, 6, 7 and 13 mg/kg respectively. Kessler scheme has simulated maximum RWMR at 800-500 hPa and WSM3 has simulated double maximum of RWMR, one at 850-700 hPa and another maximum at 400-200 hPa level and NSSL-2 has simulated maximum at 700-500 hPa on 31 August. The maximum amount of RWMR has simulated by KS, Lin *et al.*, WSM3, Ferrier, WSM6, Thompson, MYDM, MDM, CAM, SBU, WDM6 and NSSL-2 are 7, 7, 10, 2, 5, 5, 5, 5, 16, 6, 6 and 12 mg/kg respectively on 1 September.

The area average RWMR have plotted and analyzed using different MPs during 30 August to 1 September 2015 in the SE region of the country and are presented as in Fig. 37(e-h). The RWMR has simulated by all MP schemes up to 500 hPa level except KS and WSM3 schemes, where KS and WSM3 simulated up to 100 hPa level during the heavy rainfall period 30 August to 1 September. Significant amount of RWMR has been simulated by all MPs during 31 August and 1 September. Highest amount of RWMR has been simulated by NSSL-2, CAM and WDM6 schemes in the lower troposphere on 30, 31 August and 1 September respectively. The simulated area average RWMR are NSSL-2>CAM> WDM6>MYDM schemes respectively on 30 August (Fig. 37e). On 31 August (Fig. 37f) the simulated area average RWMR are CAM>WDM6>NSSL-2>MYDM>WSM6>SBU>Lin> FE>WSM3>KS>TH respectively. The simulated RWMR on 1 September are as follows: WDM6> CAM>Lin>WSM6>NSSL-2>MYDM>FE>SBU>KS>WSM3>MDM>TH schemes respectively (Fig. 37g). This suggests that the amount of rain simulated depends on RWMR in the lower to middle troposphere.

4.3.12 Cloud Ice Mixing Ratio

Area and time average vertical profile of CIMR (mg/kg) has simulated using different MPs during 30 August to 1 September and are presented in Fig. 38(a-c). The area average CIMR has been found at 550-100 hPa level and maximum at 300-150 hPa during 30 August to 1 September 2015. MYDM scheme has simulated significantly higher amount of CIMR than that of other MP schemes (Fig. 38a) during 30 August to 1 September. It is evident that substantial difference exists between the various cloud ices. The MYDM profile has exhibited a prominent spike containing much larger CIMR values between 300-150 hPa and TH scheme has simulated less CIMR during 30 August to 1 September. On 30 August the

simulated area average CIMR are MYDM> MDM> WSM6> WDM6> NSSL-2> Lin> SBU> CAM> Thompson schemes respectively. The simulated area average CIMR are MYDM> WDM6> WSM6> MDM> NSSL-2> Lin> CAM> SBU> TH schemes respectively during 31 August to 1 September (Fig. 38(b & c)).

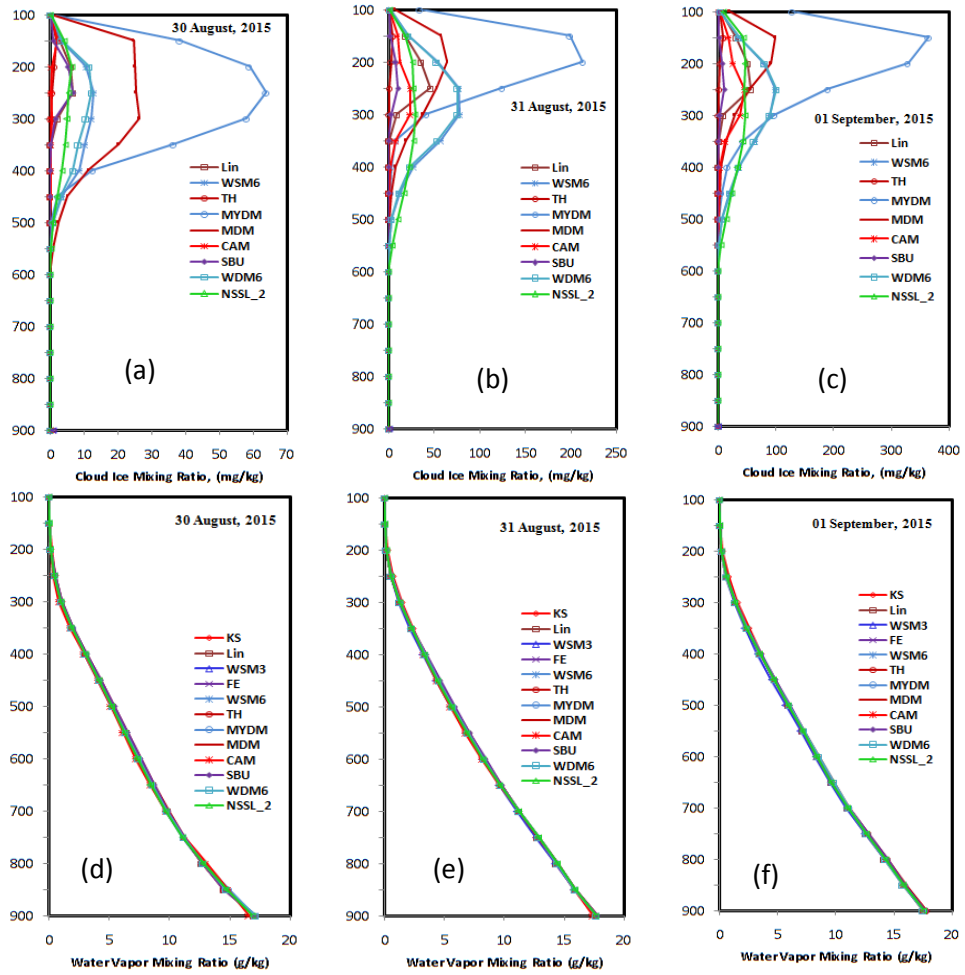

Fig. 38: Vertical profiles of time and space averaged (a-c) CIMR and (d-f) WVMR simulated by different MPs coupling with KF scheme during 30 August - 01 September 2015.

4.3.13 Water Vapor Mixing Ratio

Space and time average vertical profiles of WVMR are constant during 30 August to 1 September 2015 for different MPs schemes and are shown in Fig. 38(d-f). The patterns of water vapor profile are similar up to 100 hPa level for all MP schemes during the study period. All MP schemes have been simulated almost same amount of WVMR and decreased continuously from surface to 150 hPa level during 30 August to 1 September 2015.

4.3.14 Cloud Graupel Mixing Ratio (CGMR)

The simulated area and time average vertical profile of CGMR (mg/kg) for different MPs during 30 August to 1 September 2015 are presented in Fig. 39(a-c)). The CGMR has simulated by Lin, WSM6, Thompson, MYDM, CAM, WDM6 and NSSL-2 and the other MPs have not simulated CGMR. The area average CGMR has simulated at 600-250 hPa on 30 August and 700-100 hPa level on 31 August and 1st September and has found maximum at 550-300 hPa on 30 August and 550-200 hPa during 30 August to 1 September 2015. Lin et al., MYDM and WSM6 schemes have simulated maximum CGMR on 30, 31 August and 1 September respectively and Thompson scheme simulated minimum CGMR during the period.

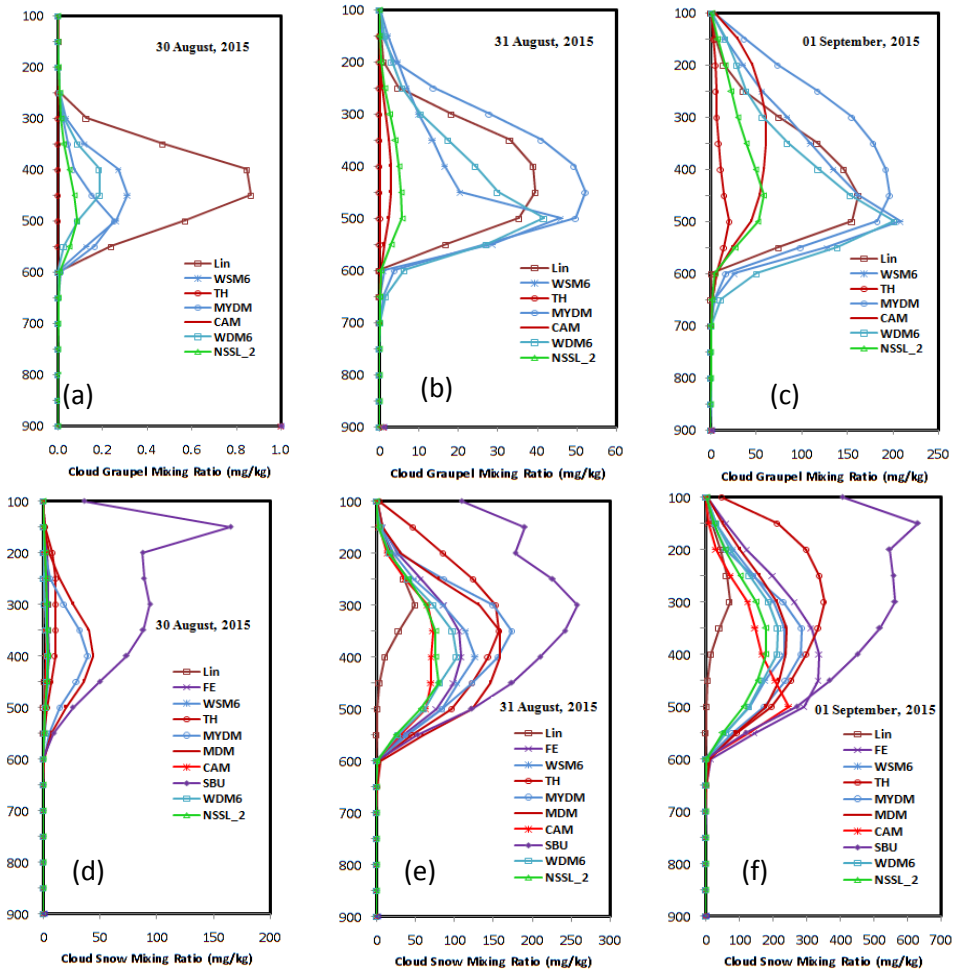

Fig. 39: Vertical profiles of time and space (a-c) cloud graupel mixing ratio and(d-f) Cloud snow mixing ratio simulated by different MPs during 30 August - 01 September.

It is evident that substantial difference exists between the various MPs for the simulation of cloud graupel. All MP schemes has exhibited a prominent spike containing much larger CGMR values between 550-250 hPa and Thompson and CAM schemes has simulated less

CGMR. On 30 August the simulated area average CGMR (Fig. 39a) are Lin> WSM6> MYDM> WDM6> NSSL-2>CAM> TH schemes respectively. On 31 August (Fig. 39b) the simulated area average CGMR are MYDM> WSM6> WDM6> Lin> NSSL-2> CAM> Thompson schemes respectively. On 1 September (Fig. 39c) the simulated area average CGMR are WSM6> WDM6>MYDM> Lin> NSSL-2> CAM> Thompson schemes respectively. Sharp spike of graupel are found 0.87 mg/kg at 450 hPa for Lin scheme, 52 mg/kg at 450 for MYDM scheme and 209 mg/kg at 500 hPa level for WSM6 scheme during 30 August to 1 September respectively.

4.3.15 Cloud Snow Mixing Ratio

The simulated area and time average vertical profile of CSMR (mg/kg) for different MPs during 30 August to 1 September are shown in Fig. 39(d-f). The CSMR has simulated by Lin, FE, WSM6, TH, MYDM, MDM, CAM, SBU, WDM6 and NSSL-2 schemes and the other MPs have not simulated CSMR. The area average CSMR has simulated at 600-100 hPa level and found maximum at 500-100 hPa during 30 August to 1 September 2015. SBU and Lin *et al*. schemes have simulated maximum and minimum CSMR during the study period. Significant amount of CSMR has simulated by all MPs during 30 August to 1 September. It is evident that substantial difference exists between the various MPs for the simulation of cloud snow. All MP schemes has exhibited a prominent spike containing much larger CSMR values between 500-100 hPa and Lin and CAM schemes has simulated less CSMR. On 30 August (Fig. 39d), the SBU scheme has generated the greatest amount of snow between 450 to 100 hPa. The MDM has simulated approximately half of the snow than that of SBU scheme, TH and all MPs schemes have simulated approximately half of the snow than that of MDM scheme. The CSMR has simulated SBU>MDM> MYDM>TH>NSSL-2>CAM> WDM6>WSM6> FE and Lin schemes on 30 August (Fig. 39d), SBU> WDM6> TH> MDM> WSM6>FE>MYDM>NSSL-2>CAM and Lin schemes on 31 August (Fig. 39e) and SBU>FE>TH>MYDM>CAM>MDM>WSM6>WDM6>NSSL-2 and Lin *et al.*, schemes on 1 September (Fig. 39f) 2015.

Chapter V

CONCLUSIONS

On the basis of the present study, following conclusions can be drawn:

- In the present study, the Weather Research and Forecast (WRF-ARW v3.5.1) model has been used to simulate the heavy rainfall events of 23-26 June, 23-26 July and 30 August to 1 September 2015 in the monsoon over Bangladesh. The model vertical coordinate is terrain following hydrostatic pressure and the horizontal grid is Arakawa C-grid staggering. The model has different microphysics options but in this research 12 microphysics schemes are used for the simulation of heavy rainfall events in the monsoon season. The 12 MPs are Kessler (KS), Lin *et al.* (Lin), WSM3-class simple ice (WSM3), Ferrier (FE), WSM6, Thompson (TH), MYDM, MDM, CAM V5.12-Moment 5 class (CAM), Stony Brook University (SBU), WDM6 and NSSL 2-moment (NSSL2) schemes. The model has integrated by using initial and lateral boundary conditions (LBCs) from NCEP-FNL analysis at six hourly intervals. Surface layer is treated using Monin-Obukhov and planetary boundary layer (PBL) is treated with Yonsei University scheme. Kain-Fritsch scheme has been used coupling with 12 different MP schemes for the simulation of heavy rainfall in the monsoon season.
- All MPs have simulated maximum rainfall in the central to SE regions but observed rainfall is found in the SE region on 24 June 2015. The model simulated maximum rainfall is found to match with the observed rainfall at Bhola but the maximum rainfall position at Chandpur is shifted towards SE region i.e. Chittagong on 25 June. The position of simulated maximum rainfall is matched with the observed rainfall position at Sylhet i.e. NE region for different MPs but observed heavy rainfall position at Chittagong is shifted towards Sitakunda-Feni region on 23 July 2015. The simulated maximum rainfall position is matched with the observed rainfall at Sylhet i.e. NE region for different MPs but the observed heavy rainfall position in the NW region has not matched with the simulated rainfall on 30 August 2015 but the simulated rainfall is much higher than that of observed rainfall. The position and amount of model simulated maximum rainfall are found to match with the position and amount of observed rainfall on 31 August 2015. The heavy rainfall in the NW

region could not match with the simulated rainfall for different MP schemes on 1 September 2015.

- All MPs have simulated almost similar average rainfall all over the country and SE region on 23, 25 and 26 June, 24 July and 31 August – 1 September 2015. All MPs have simulated higher average rainfall than that of observed average of all Bangladesh rainfall on 23 July and less rainfall on 24 June, 26 July and 30 August. All Bangladesh station averaged rainfall suggests that among 12 MPs, TH, SBU, WSM6 and WDM6 during 23-26 June, MDM, Lin, SBU, KS and TH schemes during 23-26 July and WSM3, WDM6, CAM, MDM and MYDM schemes during 30 August to 1 September have simulated almost similar amount of rainfall as observed during the study period of 2015. The model has also simulated similar amounts of rainfall in the heavy rainfall area of 5 stations in the SE region by SBU, WDM6, Lin, TH and WSM6 schemes on 23-26 June, KS, Lin, WDM6, MDM and SBU schemes on 23-26 July and CAM, NSSL-2, MYDM and WSM3 schemes during 30 August to 1 September 2015. TRMM derived rainfall is much lower than that of observed rainfall all over Bangladesh and southeastern region during the period. The time of 3-hourly simulated maximum rainfall during 23-26 June, 23-26 July and 30 August to 1 September 2015 are almost found to match with the observed maximum rainfall except some anomalies. During 30 August to 1 September 2015, at Teknaf the time of 3-hourly simulated maximum rainfall is continuously increased but the model simulated rainfall is not matched with the observed peak of rainfall.
- The maximum updraft has been identified for different MP schemes every day during 23-26 June, 23-26 July and 30 August to 1 September 2015 when heavy rainfall is observed in the SE region of Bangladesh. The maximum updraft is found as high as 20 ms^{-1} in the upper troposphere by using Lin *et al.*, WSM3, MYDM, MDM and WDM6 schemes at around 600-200, 400-100 and 600-200 hPa for the heavy rainfall events of 23-26 June, 23-26 July and 30 August to 1 September 2015 respectively. The updraft in the upper troposphere could be due to the latent heat release during glaciations and vapor deposition.
- Positive and negative vorticity have been simulated in the lower to middle troposphere and middle to upper troposphere respectively along the line of maximum vertical velocity by Lin *et al.*, MYDM, MDM, CAM, SBU and NSSL-2 schemes. The other MP schemes have simulated positive vorticity in the lower and upper troposphere and negative vorticity in the middle troposphere.

- All MPs have simulated maximum RH in the upper troposphere along the line of maximum vertical velocity during 23-26 June, 23-26 July and 30 August to 1 September 2015.
- The reflectivity has been simulated maximum around 60dBz along the line of maximum vertical velocity for all heavy rainfall events by different twelve different MPs.
- The maximum amount of area and time averaged vertical profiles of cloud water mixing ratio have been simulated by CAM and FE at 500 and 600 hPa during 23-26 June, 23-26 July 2015 respectively and KS and CAM at 300-100 hPa during 30 August to 1 September 2015. The CWMR is found to have maximum value along the vertical line where vertical velocity and reflectivity are also maximum.
- The highest amount of area and time averaged RWMR have been simulated by CAM, NSSL-2 and WDM6 schemes up to 600 hPa during 23-26 June, CAM, NSSL-2, WDM6, MYDM, SBU and WSM3 schemes up to 500 hPa during 23-16 July and NSSL-2, CAM and WDM6 schemes in the lower troposphere during 30 August -1 September respectively. It is also found that the MP schemes have simulated higher RWMR in the lower to middle troposphere the rain also simulated higher.
- Space and time averaged vertical profiles of WVMR are constant and similar up to 100 hPa level for different MPs schemes during 23-26 June, 23-26 July and 30 August to 1 September 2015.
- Area and time averaged vertical profiles of CIMR using different MPs have been simulated at 600-100 hPa level and is found maximum at 300-200 hPa during 23-26 June, 23-26 July and 30 August to 1 September 2015. The MYDM profile has exhibited a prominent spike containing much larger CIMR values between 300-150 hPa. It is evident that substantial difference exists between the various cloud ices**.**
- Area and time averaged vertical profiles of CGMR using different MPs have been simulated at 700-100 hPa level and is found maximum at 600-300, 500-200 and 500-200 hPa by WDM6, MYDM and WSM6 during 23-26 June, 23-26 July and 30 August to 1 September 2015 respectively.
- The simulated area and time averaged vertical profiles of CSMR for different MPs have been simulated at 600-100 hPa level and is found maximum at 500-100 hPa by SBU, MDM and MYDM schemes during 23-26 June, 23-26 July and 30 August to 1 September 2015.

REFERENCE

Ahmed, R., 1989: Probabilistic estimates of rainfall extremes in Bangladesh during the pre-monsoon season, Indian Geogr J. 64, 39–53

Alam, M. M. 2014: Impact of cloud microphysics and cumulus parameterization on simulation of heavy rainfall event during 7–9 October 2007 over Bangladesh, J. Earth Syst. Sci. 123, 2, 259–279

Alexander, L.V., X. Zhang, T.C. Peterson, J. Caesar , B. Gleason , A.M.G. Klein Tank, M. Haylock, D.Collins , B. Trewin, F. Rahimzadeh , A. Tagipour, R. K. Kumar, J. Ravedekar , G. Griffiths , L. Vincent , D. B. Stephenson, J. Burn , E. Aguilar , M. Brunet , M. Taylor , M. New, P. Zhai, M. Rusticucci, J. L. Vazquez-Aguirre 2006: Global observed changes in daily climate extremes of temperature and precipitation. J Geophy Res 111 (DO5109). doi:10.1029/ 2005JD006290

Anderson, D., and Coauthors, 2007: Seasonal forecasting system 3. ECMWF Tech. Memo. 503, 58

Arakawa, A., and W. H. Schubert, 1974: Interaction of a cumulus cloud ensemble with the large-scale environment, Part I. J. Atmos. Sci., 31, 674–701.

Awan, N. K., H. Truhetz, and A. Gobiet, 2011: Parameterization induced error characteristics of MM5 and WRF operated in a climate mode over the Alpine region: An ensemble-based analysis. J. Climate, 24, 3107–3123.

Bashar, M. K., 1987: Study of Potential Evapo-transpiration and Consumptive use of Water for Different Crops over Bangladesh, Project report, Rajshahi Univ. Eng. Technol., Rajshahi.

Bhanu, K. O. S. R. U., Suneetha, P., Rao, R.S. and Kumar, S. M., 2012: "Simulation of Heavy Rainfall Events during Retreat Phase of Summer Monsoon Season over Parts of Andhra Pradesh", International Journal of Geosciences, 3, 737-748

Bhowmik, S. K. R. and V. R. Durai, 2008: "Multi-model ensemble forecasting of rainfall over Indian monsoon region", Atmósfera 21, 3, 225-239.

Biasutti M, S.E. Yuter, C.D. Burleyson, A.H. Sobel 2012: Very high resolution rainfall patterns measured by TRMM precipitation radar: seasonal and diurnal cycles. Clim Dyn 39:239–258. doi:10.1007/s00382-011-1146-6

BMD, 2000: Mean Monthly Rainfall Data of Bangladesh, Bangladesh Meteorological Department, Agargaon, Dhaka.

Bukovsky, M. S., and D. J. Karoly, 2009: Precipitation simulations using WRF as a nested regional climate model. J. Appl. Meteor. Climatol., 48, 2152–2159.

Chatfield, R. B., H. Guan, A. M. Thompson, and H. G. J Smit, 2007: Mechanisms for the intraseasonal variability of tropospheric ozone over Indian Ocean during the winter monsoon, J. Geophys. Res., 112, D10303

Chen, G. T. J., and C. C Yu., 1988: Study of low-level jet and extremely heavy rainfall over northern Taiwan in the Mei-Yu season, Monthly weather review 116, 4, 884-891.

Chen, G. T. J, C. C. Wang, and D. T. W. Lin, 2005: Characteristics of low-level jets over northern Taiwan in Mei-Yu season and their relationship to heavy rain events, Monthly weather review 133,1, 20-43.

Chen, Y. L, and J. Li. 1995: Large-scale conditions favorable for the development of heavy rainfall during TAMEX IOP 3, Monthly weather review 123, 10, 2978-3002.

Chen, J. Y., and Y. Sun, 2002: Hydrolysis of lignocellulosic materials for ethanol production, a review, Bi ore source technology 83, 1, 1-11.

Chiew, F. H. S., 2006: Estimation of rainfall elasticity of stream flow in Australia. Hydrol Sci J 51(4):613–625

Chowdhury M. R., 2003: The El Nino-Southern Oscillation (ENSO) and seasonal flooding – Bangladesh, Theoretical and Applied Climatology **76**: 105–124.

Das, S., R. Ashrit, G.R. Iyengar, S.M. Mohandas, D. Gupta, J.P. George, E. N. Rajagopal, and S.K. Dutta:2008: "Skills of different mesoscale models over Indian region during monsoon season: Forecast errors", J. Earth Syst. Sci. 117, 5, 603–620.

Das, S., M. M. Rahman, and J. Singh, 2012: "Simulation of Seasonal Monsoon rainfall over the SAARC Region by Dynamical Downscaling using WRF Model", SMRC Report No-42,1-38.

Deardorff, J. W., 1972: Parameterization of the planetary boundary layer for use in general circulation models, Mon. Wea. Rev., 100, 93–106.

Ding, Y., 1992: Summer monsoon rainfalls in China. J. Meteor. Soc. Japan, 70, 373–396.

Dudhia, J., 1989: Numerical study of convection observed during the winter monsoon experiment using mesoscale two-dimensional models, J. Atmos. Sci., 46, 3077-3107.

Ek, M. A. A., K. E. Mitchell, Y. Lin, E. Rogers, P.Grundmann, V. Koren, G. Gayno, and J. D. Tarpley, 2003: Implementation of Noah land surface model advances in the National Centers for Environmental Prediction operational mesoscale Eta model, Journal of Geophysical Research, 108, D22, 8851, doi:10.1029/2002 JD003296

Ferrier, B. S., W.K. Tao, and J. Simpson, 1995: A double moment multiple phase four-class bulk ice scheme, Part II: Simulations of convective storms in different large-scale environments and comparisons with other bulk parameterizations. J. Atmos Sci., 52, 1001-1033.

Ferretti, Rossella, et al, 2000: Analyses of the precipitation pattern on the Alpine region using different cumulus convection parameterizations." Journal of Applied Meteorology 39, 2, 182-200.

Fritsch, J. M. and C. F. Chappell, 1980: Numerical Prediction of Convective Driven Mesoscale Pressure Systems, Part I: Convective Parameterization, J.Atoms.sci.37, 1722- 1733.

Fujinami H, D. Hatsuzuka , T. Yasunari , T. Hayashi, T. Terao , F. Murata, M. Kiguchi, Y. Yamane , J. Matsumoto, M.N Islam , A. Habib 2011: Characteristic intraseasonal oscillation of rainfall and its effect on interannual variability over Bangladesh during boreal summer. Int J Climatol 31:1192–1204. doi:10.1002/joc. 2146

Gadgil, Sulochana, M. Rajeevan, and Ravi Nanjundiah, 2005: Monsoon prediction-Why yet another failure? Current science 88, 9, 1389-1400

Groisman PY, T.R. Karl, D.R .Easterling, R.W. Knight, P.F. Jameson, K.J. Hennessy, R. Suppiah, C.M. Page, J. Wibig, K. Fortuniak, V.N. Razuvaev, A. Douglas, E. Forland, P.M. Zhai 1999: Changes in the probability of heavy precipitation: important indicators of climatic change. Clim Change 42:243–283

Hirose M, R .Oki, S. Shimizu, M. Kachi, T. Higashiuwatoko 2008: Finescale diurnal rainfall statistics refined from eight years of TRMM PR data. J Appl Meteorol Climatol 47:544–561. doi:10. 1175/2007jamc1559.1

Hong, S. Y., and J. O. J. Lim, 2006: The WRF Single Moment 6-Class Microphysics Scheme (WSM6), J Korean Meteorol. Soc., 42, 2, 129-151.

Hong S.Y., Y. Noh and J. Dudhia 2006: A new vertical diffusion package with an explicit treatment of entrainment processes. Mon. Wea. Rev., 134, 2318-2341.

Hong, S. Y., J. Dudhia and S. H. Chen, 2004: A Revised Approach to Ice Microphysical Processes for the Bulk Parameterization of Clouds and Precipitation, Mon. Wea. Rev., 132, 103-120.

Hong, Song-You, and Hua-Lu Pan, 1996: Nonlocal boundary layer vertical diffusion in a medium-range forecast model, Monthly weather review 124, 10, 2322-2339

Hoskins BJ, M.J. Rodwell 1995: A model of the Asian summer monsoon: 1. The Global-Scale. J Atmos Sci 52, 1329–1340

https://www.google.com/search?q=Formation+of+Different+Hydrometeors&client

http://my.athenet.net

IPCC (2007) Climate Change 2007: The physical science basis, Summary for policymakers, Contribution of the Working Group I to the Fourth Assessment Report of the Intergovernmental Panel on Climate Change. Cambridge University Press, Cambridge

Iwashima T, R.Yamamoto, Y. Sakurai 2002: Long-term trends of extremely heavy precipitation intensity in Japan in recent 100 years, Recent Res Devel Meteorol 1, 1–9

Kain J. S., 2004: The Kain-Fritsch convective parameterization: An update. J. Appl. Meteor., 43, 170-181.Lin, Y.-L., R.D. Farley, and H. D. Orville, 1983: Bulk parameterization of the snow field in a cloud model. J. Climate Appl. Meteor., 22, 1065-1092.

Kain, J. S. and J. M. Fritsch, 1993: Convective parameterization for mesoscale models: the Kain-Fritsch scheme, the representation of cumulus convection in numerical models, Meteo. Monogr, No. 46 Amer. Meteor. Soc., 165–170.

Kain J. S. and J. M. Fritsch 1990: A one-dimensional entraining/detraining plume model and its application in convective parameterization. J. Atmos. Sci., 47, 2684-2702.

Karl TR, Knight RW 1998: Secular trends of precipitation amount, frequency and intensity of the United States. Bull Am Meteorol Soc 79:223–241

Karmakar S and A .Khatun 1995: Variability and probabilistic estimates of rainfall extremes in Bangladesh during the southwest monsoon season. Mausam 46(1):47–56

Kessler, E., 1969: On the distribution and continuity of water substance on atmospheric circulation. Meteorol. Monogr., 10, 32, 84.

Khaladkar, R. M., S.G. Narkhedkar, and P. N. Mahajan, 2007: "Performance of NCMRWF Models in Predicting High Rainfall Spells During SW Monsoon Season -A Study

for Some Cases in July 2004", ISSN 0252-1075 IITM Research Report No. RR-116,1-21.

Khairoutdinov, M., and Y. Kogan, 2000: A new cloud physics parameterization in a large-eddy simulation model of marine stratocumulus, Monthly weather review 128, 1, 229-243.

Kotroni, V., and K. Lagouvardos, 2001: Precipitation forecast skill of different convective parameter-ization and microphysical schemes: application for the cold, Geophysical research letters 28, 10, 1977-1980.

Kim, H. W., and D. K, Lee, 2006: An observational study of mesoscale convective systems with heavy rainfall over the Korean Peninsula. Wea. Forecasting, **21**, 125–148.

Kuo, Y.-H., and G. T.-J. Chen, 1990: The Taiwan Area Mesoscale Experiment (TAMEX): An overview. Bull. Amer. Meteor. Soc., 71, 488–503.

Leung, L. R., Y.-H. Kuo, and J. Tribbia, 2006: Research needs and directions of regional climate modeling using WRF and CCSM. Bull. Amer. Meteor. Soc., 87, 1747–1751.

Li, J., and Y. L. Chen, 1998: Barrier jets during TAMEX. Mon. Wea. Rev., 126, 959–971.

Lin, Y., and B. A. Colle, 2011: A new bulk microphysical scheme that includes riming intensity and temperature-dependent ice characteristics, Monthly Weather Review 139, 3, 1013-1035.

Lin, Y.L., R. D. Farley, and H. D. Orville, 1983: Bulk parameterization of the snow field in a cloud model, J. Climate Appl. Meteor., 22, 1065-1092.

Mansell, E. R., C. L. Ziegler, and E. C. Bruning, 2010: Simulated electrification of a small thunderstorm with two-moment bulk microphysics. J. Atmos. Sci., 67, 171–194, doi:10.1175/2009JAS2965.1.

McCumber, M., W. -K. Tao, J. Simpson, R. Penc and S. -T. Soong, 1991: Comparison of ice-phase microphysical parameterization schemes using numerical simulations of tropical convection, Journal of Applied Meteorology 30, 985-1004.

Milbrandt, J. A. and M. K. Yau 2005: A multi moment bulk microphysics parameterization. Part I: Analysis of the role of the spectral shape parameter. Journal of the Atmospheric Sciences, 62, 9, 3051-3064.

Milbrandt, J. A., and M. K. Yau, 2006: A multimoment bulk microphysics parameterization. Part IV: Sensitivity experiments, Journal of the atmospheric sciences 63, 12, 3137-3159.

Mlawer, E. J., S. J. Taubman, P. D. Brown, M. J. Lacono and S. A. Clough, 1997: Radiative transfer for inhomogeneous atmosphere: RRTM, a validated correlated-k model for the longwave, J. Geophys. Res., 102(D14), 16663-16682.

Morrison, H., G. Thompson, and V. Tatarskii, 2009: Impact of cloud microphysics on the development of trailing stratiform precipitation in a simulated squall line: Comparison of one-and two-moment schemes, Monthly Weather Review 137, 3, 991-1007.

Murata F, T. Terao, T. Hayashi, H. Asada, J. Matsumoto 2008: Relationship between atmospheric conditions at Dhaka, Bangladesh, and rainfall at Cherrapunjee, India. Nat Hazards 44:399–410. doi:10.1007/s11069-007-9125-2

Neale, Benjamin M., et al., 2012: Patterns and rates of exonic de novo mutations in autism spectrum disorders, Nature, 485, 7397, 242-245.

Ohsawa, T., T. Hayashi, Y. Mitsuta, J. Matsumoto, 2000: Intraseasonal variation of monsoon activities associated with the rainfall over Bangladesh during the 1995 summer monsoon season. J Geophys Res Atmos 105, 29445–29459

Ose, T., 1998: Seasonal change of Asian summer monsoon circulation and its heat source. J Meteor Soc Japan 76, 1045–1063

Pleim, J., 2007: A combined local and non-local closure model for the atmospheric boundary layer. Part II: Application and evaluation in a mesoscale meteorological model, J.Applied Meteor. Climatology, 46, 1396–1409.

Ranadhur, R. P. S., Pal, K. and Joshi, P.C., 2009: Impacts of Satellite-Observed Winds and Total Precipitable Water on WRF Short-Range Forecasts over the Indian Region during the 2006 Summer Monsoon, Weather and Forecasting, 24, 1706-1731.

Rodrigo F. S., 2002: Changes in climate variability and seasonal rainfall extremes: a case study from San Fernando (Spain), 1821–2000, Theor Appl Climatol 72, 3, 193–207

Romatschke U. and R.A. Houze 2011: Characteristics of precipitating convective systems in the South Asian monsoon. J Hydrometeorol 12:3–26. doi:10.1175/2010jhm1289.1

Routray, A., U. C. Mohanty, D. Niyogi, S. R. H. Rizvi and K. K. Osuri, 2010: Simulation of heavy rainfall events over Indian monsoon region using WRF-3DVAR data assimilation system, Meteorol Atmos Phys, 106, 107–125.

Schumacher, R. S., and R. H. Johnson, 2005: Organization and environmental properties of extreme-rainproducing mesoscale convective systems. Mon. Wea. Rev., **133**, 961–976.

Shin, H. H., and S. Y Hong, 2011: Intercomparison of Planetary Boundary-Layer Parametrizations in the WRF Model for a Single Day from CASES-99, Boundary-Layer Meteorol, 139, 261–281

Skamarock, W. C., J. B. Klemp, J. Dudhia, D. O. Gill, D. M. Barker, W. Wang, and J. G. Powers, 2008: A description of the Advanced Research WRF version 3. NCAR Tech. Note 4751STR, 113

Su BD, T Jiang, W.B. Jin, 2006: Recent trends in observed temperature and precipitation extremes in the Yangtze River basin, China. Theor Appl Climatol 83, 139–151

Suppiah R. and K Hennessy 1998: Trends in seasonal rainfall, heavy rain days, and number of dry days in Australia 1910–1990. Int J Climatol 18:1141–1155

Tripoli, G. J., and W. R. Cotton, 1980: A numerical investigation of several factors contributing to the observed variable intensity of deep convection over south Florida, Journal of Applied Meteorology 19, 9, 1037-1063.

Vitrat, F., and F. Molteni, 2009: Dynamical Extended-Range Prediction of Early Monsoon Rainfall over India, Monthly Weather Review, 137, 1480-1492.

Wang, W., and N. L. Seaman, 1997: A comparison study of convective parameterization schemes in a mesoscale model, Monthly Weather Review 125, 2, 252-278.

Xie SP, Xu HM, N.H. Saji, Y.Q. Wang, W.T. Liu 2006: Role of narrow mountains in large-scale organization of Asian monsoon convection. J Clim 19:3420–3429

Xukai, Z., and R. Fumin, 2015: Changes in regional heavy rainfall events in China during 1961-2012, Advances in Atmospheric Sciences 32, 5, 704

Zhang, Q., K. H. Lau, Y. H. Kuo, and S. J. Chen, 2003: A Numerical study of a mesoscale convective system over the Taiwan Strait. Mon. Wea. Rev., 131, 1150–1170.

Conference Presentation

S. U. Haney, M. M. Alam and M. A. E. Akhter, 2017: Sensitivity of Microphysics for the Simulation of Heavy Rainfall during 30 August to 1 September 2015 over Bangladesh using High Resolution WRF-ARW Model, Presented at the National Conference on Physics – 2017, Bangladesh Physical Society, Atomic Energy Centre, Dhaka, 5-7 January 2017.

Sumi Umme Haney, M. M. Alam and M. A. E. Akhter 2016: Sensitivity of Microphysics for the Simulation of Heavy Rainfall during 23-26 June 2015 over Bangladesh using High Resolution WRF-ARW Model, Presented on the Conference on Weather Forecasting and Advances in Physics: Bangladesh Perspective, Khulna University of Engineering & Technology, Khulna, 20 May 2016.

Sumi Umme Haney, M. M. Alam, M. A. E. Akhter, 2016: Sensitivity of Microphysics for the Simulation of Heavy Rainfall during 23-26 July 2015 over Bangladesh Using High Resolution WRF-ARW Model, Presented at International Conference on Physics-2016, Bangladesh Physical Society, Dhaka, 10-12 March 2016.